SPRINGER BRIEFS IN MATERIALS

Mariusz Holtzer
Marcin Górny
Rafał Dańko

Microstructure and Properties of Ductile Iron and Compacted Graphite Iron Castings

The Effects of Mold Sand/Metal Interface Phenomena

Springer

SpringerBriefs in Materials

More information about this series at http://www.springer.com/series/10111

Mariusz Holtzer · Marcin Górny
Rafał Dańko

Microstructure and Properties of Ductile Iron and Compacted Graphite Iron Castings

The Effects of Mold Sand/Metal Interface Phenomena

Springer

Mariusz Holtzer
AGH University of Science
and Technology
Kraków
Poland

Rafał Dańko
AGH University of Science
and Technology
Kraków
Poland

Marcin Górny
AGH University of Science
and Technology
Kraków
Poland

Translated by Piotr Paliwoda

ISSN 2192-1091 ISSN 2192-1105 (electronic)
SpringerBriefs in Materials
ISBN 978-3-319-14582-2 ISBN 978-3-319-14583-9 (eBook)
DOI 10.1007/978-3-319-14583-9

Library of Congress Control Number: 2015934042

Springer Cham Heidelberg New York Dordrecht London
© The Author(s) 2015
This work is subject to copyright. All rights are reserved by the Publisher, whether the whole or part of the material is concerned, specifically the rights of translation, reprinting, reuse of illustrations, recitation, broadcasting, reproduction on microfilms or in any other physical way, and transmission or information storage and retrieval, electronic adaptation, computer software, or by similar or dissimilar methodology now known or hereafter developed.
The use of general descriptive names, registered names, trademarks, service marks, etc. in this publication does not imply, even in the absence of a specific statement, that such names are exempt from the relevant protective laws and regulations and therefore free for general use.
The publisher, the authors and the editors are safe to assume that the advice and information in this book are believed to be true and accurate at the date of publication. Neither the publisher nor the authors or the editors give a warranty, express or implied, with respect to the material contained herein or for any errors or omissions that may have been made.

Printed on acid-free paper

Springer International Publishing AG Switzerland is part of Springer Science+Business Media (www.springer.com)

Contents

Symbols and Abbreviations

A	Surface area (m^2)
a_i	Activity of element (–)
d_a	The average, arithmetic grain size of the sand matrix (mm)
d_g	The average geometric grain size of the sand matrix (mm)
D_L	Diffusion coefficient in the liquid iron (m^2/s)
d_L	The average, logarithmic grain size of the sand matrix (mm)
D_o	Diffusion coefficient (m^2/s)
d_p	The average pore opening between sand grains (m)
F	The force applied to the particles (N)
g	Acceleration is due gravity (m/s^2)
G	Gibbs energy (J/mol)
H	Enthalpy (J/mol)
h	Heat transfer coefficient ($W/(m^2\ K)$)
h	Metallostatic head height (m)
H_f	Latent heat of fusion (J/kg)
K	Equilibrium constant (–)
k	Thermal conductivity (W/(m K))
P	Permeability ($m^4/N\ s$)
P_{dyn}	Dynamic pressure (Pa)
P_{exp}	Expansion pressure (Pa)
P_f	Friction pressure (Pa)
P_{gas}	Gas pressure (Pa)
PI_{chem}	Chemical penetration index (–)
P_{met}	Metallostatic pressure (Pa)
P_γ	Capillarity pressure (Pa)
Q	Activation energy (J/mol)
R	Gas constant (R = 8.3147 kJ/deg)
r	The radius of the gas bubble (m)
S	Entropy (J/mol K)
S_t	Grain-specific surface (cm^2/g)

t	Temperature (°C)
T	Temperature (K)
t	Time (s)
T_L	Liquidus temperature (K)
T_S	Solidus temperature (K)
v	Speed of movement of the particle (m/s)
V	Velocity with which the metal hits the mold (m/s)
γ	Specific gravity of the material particles (N/m^3)
γ_i	Activity coefficient (–)
η	Dynamic viscosity of the liquid ($N\ s/m^2$)
θ	Contact angle between the molten metal and the material used for mold (–)
ρ	Density of metal (kg/m^3)
σ	The surface tension of the liquid metal (N/m)
ADV	Acid demand value
CE	Carbon equivalent
CGI	Compacted graphite cast iron
EDS	Energy-dispersive X-ray spectroscopy
FA	Furan resin
FGI	Flake graphite cast iron
FNB	Furan no-bake
LDASC	Low-density alumina-silicate ceramic
LOI	Loss on ignition (%)
MW	Molecular weight
PF–FA resin	Phenol-formaldehyde–furfuryl alcohol
PTS acid	p-toluenesulfonic acid
REE	Rare earth elements
R–FA resin	Resorcinol–furfuryl alcohol
SGI	Spheroidal graphite cast iron
UF–FA resin	Urea-formaldehyde–furfuryl alcohol, resin
UF–PF–FA resin	Urea-formaldehyde–phenol–furfuryl alcohol
VOC	Volatile organic compounds
WDS	Wavelength-dispersive X-ray spectroscopy
()	Component of the slag phase, (CaO)
[ ]	Component of the metal phase, [C]
{ }	Gas, {CO}
(s)	Solid, $Fe_{(s)}$
(l)	Liqiud, $Fe_{(l)}$
(g)	Gas, $H_2O_{(g)}$

Introduction

The widespread use of cast components in technologically advanced industrial equipment (automotive, wind energy, aerospace) force the centers, constituting a scientific base for the casting industry, to pay attention to all the factors of the casting process, which condition receiving of the castings that meet the requirements of their customers. The current state of technology for preparation and processing of liquid metal, the quality evaluation of materials, and preparation of the mold must be enriched with the results of the basic phenomena after filling the mold with molten metal, during the crystallization process and cooling of the casting. This includes the thermodynamically very complex mold/metal and metal/air interaction in the mold cavity. Suppressing these issues may lead to adverse changes in the surface layer microstructure, the formation of surface porosity, or burns of molding sand to the casting. Each of these treated separately does not create conditions for optimizing the manufacturing process. Therefore, the synergy of experience on the part of the constructor, metallurgist, specialist in the field of molding sand and reclamation and knowledge of the physicochemical phenomena occurring on the interface mold/metal is a guarantee for good casting.

The monograph presents the authors' own research and analysis of the literature, which allow to look at processes for making high-quality cast iron castings from the perspective of the synergy of many factors, including those associated with obtaining and evaluating the following properties: high-quality spheroidal graphite (SGI) and compacted/vermicular graphite (CGI) cast iron, the quality of molding and core sands, the impact on the quality of the recycling process of the quartz matrix of the prepared molding sand, in terms of impact on the castings surface layer.

The problem of interaction between molding sand and the metal and its impact on the quality of castings have been studied by a group of researchers for many years. The work of such authors as: J.M. Svoboda (Process Metallurgy International. Inc. Illinois, USA), H.G. Levelink (Metaalinstituut TNO, Delft, The Netherlands), I. Riposan and M. Chisamera (Politehnica University of Bucharest, Romania), D.M. Stefanescu and S. Boonmee (The Ohio State University, USA), T.S. Piwonka and L. Winardi (University of Alabama USA), and R.L. Naro (ASI International, Inc. Cleveland USA) should be mentioned.

This monograph is the result of years of research the authors conducted at the Faculty of Foundry Engineering, AGH University of Science and Technology in Cracow, Poland, on spheroidal graphite and vermicular graphite cast iron, physical chemistry of metallurgical and foundry processes, the development of new, environmentally friendly binders for molding sands and cores, the assessment of the properties, and the quality of molding sand and cores. A wide range of work on the recycling of molding sand resulted in the development and implementation of custom solutions for industrial equipment and methodology for assessing the performance and quality of molding sands and cores with the reclaimed sand. The primary research on the effects of the matrix of reclaimed molding sand allowed the mechanism of the appearance of the effect of degenerated surface layer of the casting and the extent of this phenomenon depending on the type of hardener to resin used and the application of protective coatings to be explored. The presented data make it possible to assess the impact of the presence of a degenerate surface layer on the mechanical and plastic properties of the casting or its corrosion resistance.

The authors, in addition to the results of their own research and scientific research, largely benefited from the extensive literature in this area, as evidenced by numerous references listed at the end of each chapter.

This work was carried out within the framework of the *Testing the mechanism of reaction of products of the thermal destruction of binders on the surface layer of the high quality cast iron* research project, number UMO-2011/03/B/ST8/05,869, financed by the Polish National Science Centre (NSC) (2012–2014).

The authors hope that the monograph and the obtained research results will rouse interest in the subject, rather scantily represented in the world literature, through presenting materials on the needs for synergy of engineering and metallurgical processes associated with the manufacture of high-quality castings. The research presented in this book does not cover the entire complex of the scientific issues disclosed, and can serve as inspiration to conduct wider research in this important area by the scientific communities of colleges and industrial research institutions.

Kraków, Poland

Mariusz Holtzer
Marcin Górny
Rafał Dańko

Chapter 1
The Influence of Mold/Metal Interactions on the Castings Microstructure—Bibliographical Research

Mariusz Holtzer

Abstract The phenomena on the mold/metal interface largely determine the microstructure of the casting surface layer, quality of the surface and casting performance characteristics (mechanical properties, wear resistance, corrosion resistance, etc.). Processes that occur here are of particular importance in the case of cast iron with vermicular or spheroidal graphite performed in sand molds (graphite degradation and graphite depletion). It is assumed that the direct cause of graphite degradation, resulting in a layer of flake graphite, is the Mg depletion at the surface layer of the casting and the main reason (although not the only) for the decrease of the Mg concentration is the reaction of sulfur and oxygen. To explain this phenomenon, Fe–Mg, Mg–S, Mg–O and Fe–S systems have been discussed. Performed thermodynamic calculations have shown that the magnesium and sulfur and oxygen reactions in liquid iron occur in the gas phase, wherein the thermodynamic reaction of Mg vapors with oxygen gas is more privileged than with the sulfur vapors. To clarify the mechanism of the formation of the surface layer on the casting Stefanescu et al. developed a thermo-diffusion model 2-D. However, this model does not take the kinetic agent and the degree of undercooling during solidification of the casting into account, which affects the amount of primary austenite formed, which may also result in a reduction of the Mg concentration. To reduce the degree of transition of sulfur from molding sand to casting surface layer, the use of protective coatings for molds and cores, containing desulfurization ingredients such as CaO, MgO, talc, or Mg-FeSi, which binds sulfur and supplements magnesium at the same time is preferred.

The surface quality of castings is as important as its bulk properties. Surface quality is ultimately the product of physical and chemical interactions occurring between the molding material and the cast metal in liquid state as well as during solidification and subsequent cooling in the mold. The surface layer of a casting has, in most cases, a microstructure and associated properties that are different than those in the bulk of the casting. The casting surface exhibits some roughness, which commonly depends

© The Author(s) 2015

M. Holtzer et al., *Microstructure and Properties of Ductile Iron and Compacted Graphite Iron Castings*, SpringerBriefs in Materials,
DOI 10.1007/978-3-319-14583-9_1

on the molding materials used in the casting process. The average roughness increases with the metallostatic height and decreases with higher sand fineness and pouring temperature [1]. The microstructure underneath the casting surface is different compared to the bulk microstructure in terms of the amount of graphite, graphite morphology and matrix structure. The properties of the casting skin may differently affect the mechanical properties of the casting. As the thickness of the casting decreases, the relative effect of the skin on the mechanical properties increases. In the case of spheroidal graphite cast iron (SGI) and compacted graphite cast iron (CGI) made into sand molds, the phenomenon of changing the shape of spheroidal or vermicular graphite into the flake graphite takes place in the casting skin (it is so called graphite degradation[1]). The result is a reduction in the mechanical properties—tensile strength, fatigue strength. Moreover, a phenomenon of graphite depletion can also occur in the top layer of castings with spheroidal and vermicular graphite (graphite depletion[2]—lower percentage of graphite than that of the bulk) underneath the casting surface, and a pearlitic/ferritic rim[3] may also appear (pearlitic rim appears as a band of pearlite underneath the casting surface). The presence of ferrite decreases, and the presence of the perlite may deteriorate the machinability. This abnormal surface layer becomes most critical for thin wall castings, where it could occupy more than 10 % of the total thickness. In heavy section castings, the prolonged solidification allows more time for the metal-mold interaction leading to an abnormal surface layer. The surface layer defect can occur with any molding technique, but each type presents individual characteristics with other factors affecting the end result. Sulfur, supplied by the mold and cores, oxygen (especially if a turbulent flow occurs), water—bearing materials, the reaction between magnesium and sulfur or oxygen, causing dross formation, were found as important causes of graphite degeneration in the surface layer of SGI and CGI castings.

Additionally, the reaction product (insulated inclusions or slag aggregates) could have negative effects on casting performance and machinability. While holding magnesium-treated ductile iron in the ladle or automatic pouring device, two different processes could take place: (a) vaporization of magnesium having a high partial pressure and reaction; (b) adsorption and diffusion of oxygen into liquid metal and the reaction of oxygen with magnesium dissolved in the metal. These two processes give different types of reaction products. Defects in the casting skin include a degradation graphite shape, high temperature reaction products, porosity and exogenous inclusions from a reaction of the surface slag/mold of the SGI casting with molding sand or even non-reacted sand particles. Casting skin can have, for example, a negative influence on the mechanical properties or decreased machinability of thin wall castings.

---

[1]Graphite degradation (degeneration) refers to the area where graphite exhibits lower nodularity (including compacted and flake graphite) than the bulk.

[2]Graphite depletion refers to a zone with less graphite when compared to the bulk microstructure.

[3]Ferritic and pearlitic rims refer to the predominated matrix structure at the casting skin. The ferritic rim is referred to when ferrite is the predominated phase. The pearlitic rim is then the complementary of the ferritic rim [2].

1.1 The Formation of the Casting Skin Depleted or Enriched with Graphite

The formation mechanism of the casting skin is rather complex. Several mechanisms were proposed. The proposed mechanisms include Mg depletion through oxidation or reaction with sulfur, and carbon enrichment or depletion in the surface layer due to reactions with molding materials.

Both pearlite formation areas and graphite depletion run by the same mechanism, which is associated with the casting skin decarburization [3–7].

Reisenre [8] suggests that this phenomenon is caused by a chemical reaction of the carbon contained in the cast iron with moisture and oxygen present in the mold.

The direct reaction of carbon (C) with hydrogen (H) which generate hydrocarbons (C_xH_y) is less likely than the reaction of C with water vapor. These reactions may be as follows (1.1) and (1.2):

$$[C] + \frac{1}{2}O_{2(g)} \rightarrow CO_{(g)} \tag{1.1}$$

$$[C] + H_2O_{(g)} \rightarrow CO_{(g)} + H_{2(g)} \tag{1.2}$$

The chemical reactions can lead to the carbon depletion of the casting skin. These reactions of course are more pronounced in the green sand, due to the natural moisture content. The decarburized layer may appear as a ferrite area (ferritic rim) or as a graphite depleted area.

The cause of the occurrence of pearlite areas, unlike the ferrite areas, is carburized casting skin. Sulfur also has an effect on creating pearlite or ferrite areas. An insufficient sulfur content favors the formation of type D graphite which in turn promotes matrix ferritization. Increasing the concentration of sulfur causes the creation of the A type graphite, which contributes to matrix pearlitization.

Stefanescu et al. [5] suggested the following mechanisms of the formation of pearlite areas:

- oxidation of the carbon contained in the liquid metal by oxygen or water vapor present in the mold atmosphere, thereby reducing the number of nuclei for ferrite nucleation and increasing the A1 transformation temperature.
- carburizing subsurface by carbon resulting from the molding sand. Calculations done in the diffusion of atoms from the mold and the obtained thickness of the perlite area are approximately consistent with the microscopic observations.

1.2 Degradation of the Graphite

All the proposed mechanisms of this phenomenon are based on the assumption that there would be a Mg subsurface cast layer depletion. This causes the degradation of graphite as a result of the transformation: spheroidal graphite → vermicular

graphite → flake graphite. Two reactions are given as a reason for the Mg depletion of the cast surface layer (1.3) and (1.4):

$$[Mg] + [S] = MgS_{(s)} \tag{1.3}$$

$$[Mg] + [O] = MgO_{(s)} \tag{1.4}$$

These processes take place in the vicinity of the wall of the mold. Large undercooling at the mold/metal interface favors solidification of austenite dendrites that reject magnesium at the solidification front. This results in low Mg and flake graphite structure close to the mold/metal interface with a high nodularity zone further inside.

It is believed that the cast iron with vermicular graphite (CGI) is more likely to create a degenerated casting skin than spheroidal graphite cast iron (SGI) and gray cast iron (FGI). This is due to the fact that CGI contains less Mg, respectively, which makes them more susceptible to the depletion of Mg. SGI has a higher concentration of Mg and typically has a thinner layer of degenerated graphite. However, in FGI there is only a trace amount of Mg, thus the difference in magnesium concentration in the surface layer and the depth of the casting is small. Flake graphite appears virtually the entire cast volume.

Based on the assumption that the main cause of graphite degradation is the casting skin depletion in Mg; it can be assumed that in order to minimize the thickness of the surface layer of degenerated graphite, you must minimize the amount of Mg entering the reactions (1.3) and (1.4) and reduce undercooling on the mold wall.

The phenomenon of the degeneration of graphite in cast iron is a major problem for foundries, which use molding or core sands prepared from ingredients containing sulfur (e.g. molding sand with furan resin hardened with sulfonic acids, or the molding sand with phenolic resins hardened with acids containing sulfur), which are becoming more and more popular in cast iron foundries.

The thickness of the casting skin where changes in the shape of graphite or decrease in its concentration may occur depends on many factors: the cooling rate, pouring temperature, the binder used, protective coatings applied, the content of Mg and inoculant [9].

1.3 Selected Phase Systems Analysis

1.3.1 The Fe–Mg System

Solubility of Mg in Fe is possible only at high pressures and temperatures. Below 1000 °C, Mg does not dissolve in Fe. The solubility of Mg in the liquid iron is also small and a temperature of 1600 °C at a pressure of 0.1 MPa, it is referred to as 0.059 % mass [10–12].

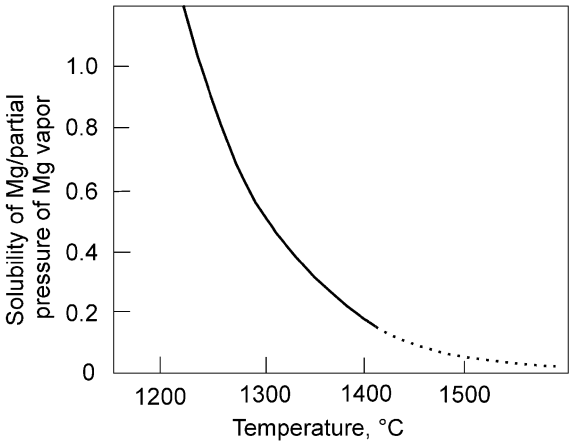

Fig. 1.1 The solubility of Mg in the liquid carbon-saturate iron alloys depending on the temperature of the metal [13]

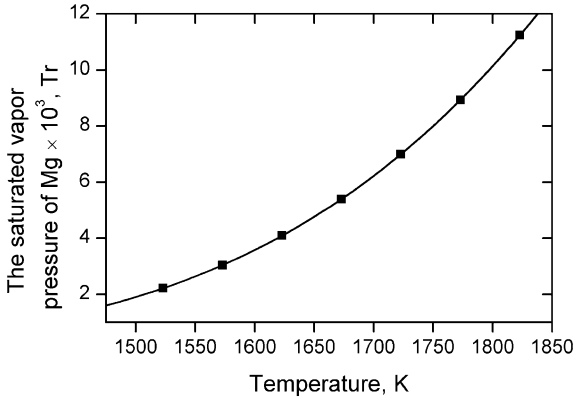

Fig. 1.2 The dependence of a saturated vapor pressure of magnesium on the temperature

Magnesium vapor solubility in carbon-rich melts is proportional to the partial pressure of magnesium vapor over the melt (Fig. 1.1). The solubility is reduced by carbon at high temperatures and increased at low temperature, due to the opposing effects of the relative stability of iron and magnesium carbides and the relative atomic size of iron and magnesium [11–14].

The temperature dependence of a saturated vapor pressure of magnesium is given by (Fig. 1.2) [12]:

$$\log P_{Mg} = 12.79 - 1.41 \log T - \frac{7550}{T} \tag{1.5}$$

where P_{Mg} is in Torr (0.1 MPa = 760 Tr), and T is in degree Kelvin.

The process of Mg dissolution in liquid iron takes place according to the following reaction (1.6) [15]

$$Mg_{(g)} = [Mg] \tag{1.6}$$

The equilibrium constant K for this reaction is:

$$K = \frac{a_{Mg}}{P_{Mg}} = [\%Mg] \cdot \frac{\gamma_{Mg}}{P_{Mg}}$$

where: γ_{Mg} magnesium activity coefficient, dependent on the alloy composition.

At 1873 K the Gibbs energy of solution of the magnesium in liquid iron ΔG^{o}_{1873} = 58,700 J/mol and K_{1873} = 0.023.

The reaction of vaporization of liquid magnesium can be expressed as:

$$Mg_{(l)} = Mg_{(g)} \tag{1.7}$$

The Gibbs energy of vaporization of the liquid magnesium as a function of temperature is:

$$\Delta G^{o} = -RT \cdot \ln K = RT \cdot \ln P_{Mg} = 129,700 - 94.3\ T\ \frac{J}{mol}$$

The Gibbs energy as a function of temperature for the dissolution of liquid magnesium in liquid iron:

$$Mg_{(l)} = [Mg]$$

$$\text{is: } \Delta G^{o} = 247{,}100 - 125.75\,T\ \frac{J}{mol}$$

The equilibrium constant K for this reaction as a function of temperature can be expressed as (Fig. 1.3):

$$\ln K = 15.13 - \frac{29,735}{T} \tag{1.8}$$

1.3.2 The Fe–S System

Phase FeS_x appears in pure iron or low-alloy steels with a certain concentration of sulfur, which has a relatively narrow range of homogeneity region from $FeS_{1.00}$ to $FeS_{1.14}$. Therefore, the solubility of sulfur in the iron is associated with the secretion of $FeS_{1.00}$. Gibbs energy of FeS formation from iron and sulfur vapor, is calculated based on the combinations of two equations:

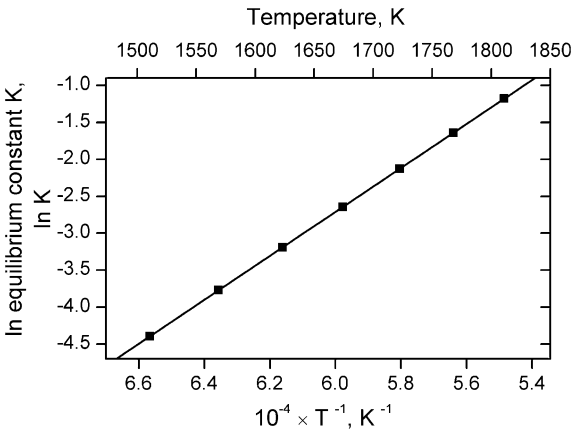

Fig. 1.3 Temperature dependence of the equilibrium constant for the solubility of liquid magnesium in liquid iron

$$H_{2(g)} + \frac{1}{2}S_{2(g)} = H_2S_{(g)}$$

$$Fe_{(s)} + H_2S_{(g)} = FeS_{(s)} + H_{2(g)}$$

$$Fe_{(s)} + \frac{1}{2}S_{2(g)} = FeS_{(s)} \tag{1.9}$$

within the temperature range of 25–911 °C (Fe_α)

$$\Delta G^o = -150{,}250 + 52.55 \cdot T \ \frac{J}{mol} \tag{1.10}$$

within the temperature range of 911–988 °C, i.e. the FeS melting point:

$$\Delta G^o = -150{,}900 + 53.30 \cdot T \ \frac{J}{mol} \tag{1.11}$$

FeS and iron form eutectic Fe + FeS (contents 31 % mass S). Iron and sulfur form a continuous liquid solution over the whole range above liquidus temperature (Fig. 1.4), in contrast to the iron and oxygen, where saturation occurs and the oxide phase is separated, when the oxygen concentration exceeds the amount of Fe given in the equation:

$$\log(\%O)\text{sat.} = -\frac{6320}{T} + 2.734 \tag{1.12}$$

The solubility of sulfur in the solid iron is virtually zero (in Fe_α at a temperature of 900 °C the solubility of sulfur is 0.02 % mass, and in Fe_γ at 920 °C is 0.011 % mass, while at a temperature of 1400 °C in Fe_δ is 0.16 % mass)

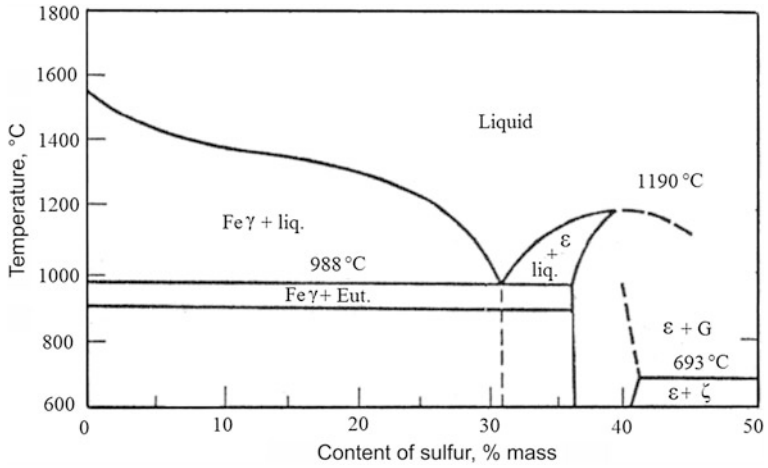

Fig. 1.4 The Fe–S phase diagram [39]

$$\log\,[S]_{\gamma} = -\frac{4700}{T} + 1.52 \tag{1.13}$$

The enthalpy of dissolution S_2 in Fe_{α} equals to 77.3 kJ/mol, and in Fe_{γ} is 60.1 kJ/mol.

Therefore, when the sulfur-containing liquid iron is cooled and sulfur is precipitated until when the iron reaches the temperature of 988 °C, and then eutectic precipitates at the grain boundaries.

FeS has an unlimited solubility in liquid iron, as opposed to MnS (solubility 0.2 % mass).

Diluted solutions of sulfur in the liquid iron show a strong negative deviation from a perfect solution due to the high mutual affinity of the two elements. The Gibbs energy of solution for sulfur in liquid iron at the 1 % mass standard state can be represented as:

$$\frac{1}{2}S_{2(g)} = [S]_{1\%} \tag{1.14}$$

$$\Delta G^{o} = -135{,}060 + 23.43 \cdot T\ \frac{J}{atom[S]} \tag{1.15}$$

the equilibrium constant for this reaction is:

$$\log K = -\frac{7063}{T} + 1.22 \tag{1.16}$$

In the dilute standard state, the activity can be expressed as:

$$a_{[S]} = \gamma_S \cdot [\%S] \tag{1.17}$$

and the equilibrium constant for the reaction:

$$\log K = -\frac{6534}{T} + 0.966 \tag{1.18}$$

Similarly, the Gibbs energy of formation of solution of oxygen gas in the liquid iron is always negative:

$$\frac{1}{2}O_{2(g)} = [O]_{1\%} \tag{1.19}$$

$$\Delta G^o = -117{,}111 - 2.89 \cdot T \ \frac{J}{atom[O]} \tag{1.20}$$

and the equilibrium constant for the reaction:

$$\log K = \frac{6116}{T} + 0.15 \tag{1.21}$$

The addition of another element decrease or increases the sulfur content of the melt, changes the sulfur activity coefficient, dissolved in the iron: increase (C, Si, Al) or decrease (Cr, Mn, Cu) (Fig. 1.5).

Up to about 0.05 % mass of the sulfur solutions in iron practically meet Henry's Law (Henry's activity coefficient ≈1).

1.3.3 The Mg–O System

Magnesium has a high affinity to oxygen and sulfur. At the liquid iron temperature, magnesium's reaction with oxygen can be carried out according to the two schemes [14, 16, 17]:

Scheme 1: The assumption that magnesium in the form of vapors react with oxygen gas:

$$\begin{array}{lll} (1) & Mg_{(g)} + [O]_{1\%} = MgO_{(s)} & \Delta G_1^o = -613{,}000 + 207.4 \cdot T \ \frac{J}{mol} \\ & & \log K_1 = \frac{32{,}015}{T} - 10.83 \\ (2) & \frac{1}{2}O_{2(g)} \rightarrow [O]_{1\%} & \Delta G_2^o = -117{,}111 - 2.89 \cdot T \ \frac{J}{atom[O]} \\ \hline (3) & Mg_{(g)} + \frac{1}{2}O_{2(g)} = MgO_{(s)} & \Delta G_3^o = \Delta G_1^o + \Delta G_2^o \end{array} \tag{1.22}$$

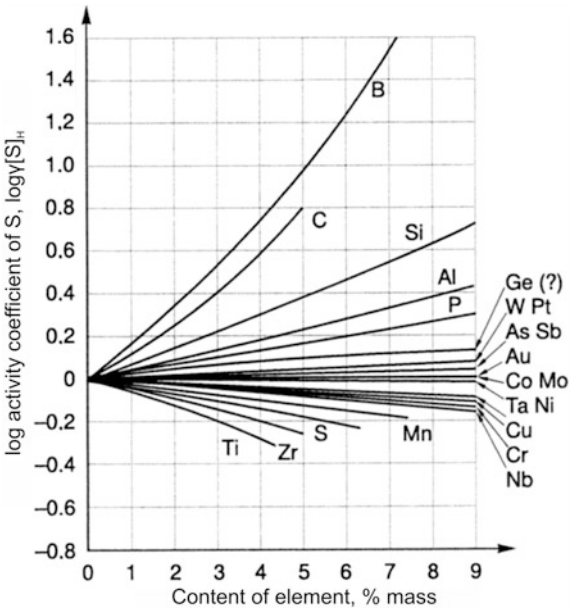

Fig. 1.5 Effect of the components of the melt on the activity coefficient of sulfur $\gamma_{[S]H}$ at a temperature of 1873 K [40]

$$\mathbf{\Delta G_3^o = -730{,}111 + 204.5 \cdot T}\ \frac{J}{mol} \qquad \text{(range 1263}-\text{2273 K)}$$

$$\log K_3 = \log \frac{a_{MgO_{(s)}}}{P_{Mg} \cdot P_{O_2}^{\frac{1}{2}}} = \frac{38{,}132}{T} - 10.68$$

Scheme 2: The assumption that magnesium dissolved in the iron [Mg] reacts with oxygen dissolved in the iron [O]:

$$\begin{array}{lll}
(4) & \frac{1}{2}O_{2(g)} \rightarrow [O]_{1\%} & \Delta G_4^o = -117{,}111 - 2.89 \cdot T\ \frac{J}{atom[O]} \\
(5) & Mg_{(g)} \rightarrow [Mg] & \Delta G_5^o = -136{,}175 + 67.46 \cdot T\ \frac{J}{atom[O]} \\
(6) & Mg_{(g)} + \frac{1}{2}O_{2(g)} = MgO_{(s)} & \Delta G_6^o = -730{,}111 + 204.5 \cdot T\ \frac{J}{mol} \\
\hline
(7) & [Mg] + [O]_{1\%} = MgO_{(s)} & \Delta G_7^o = \Delta G_6^o - \Delta G_5^o - \Delta G_4^o
\end{array} \qquad (1.23)$$

$$\mathbf{\Delta G_7^o = -476{,}825 + 139.93 \cdot T}\ \frac{J}{mol} \qquad \text{(range 1263}-\text{2273 K)}$$

$$\log K_7 = \log \frac{a_{MgO_{(s)}}}{[\%Mg] \cdot [\%O] \cdot \gamma_{Mg} \cdot \gamma_O} = \frac{24{,}903}{T} - 7.31$$

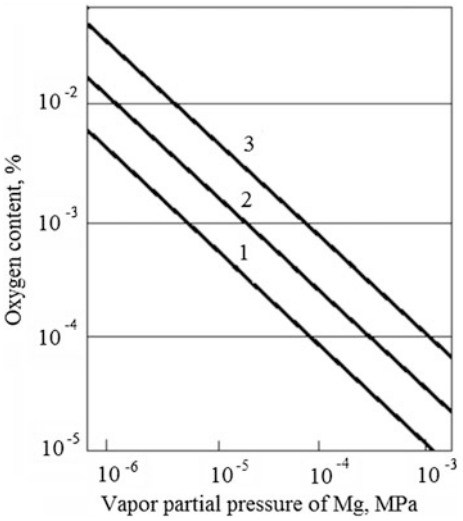

Fig. 1.6 The dependence of the solubility of oxygen in liquid iron on magnesium vapor partial pressure at *1*—1550 °C, *2*—1600 °C, *3*—1650 °C [40]

where activity coefficients γ_{Mg} and $\gamma_O \rightarrow 1.0$ for diluted solutions of Mg and O dissolved in iron.

Due to the high affinity of magnesium to oxygen, the treatment of liquid iron alloys with magnesium leads to a significant reduction in the oxygen activity of the melt (Fig. 1.6). The $P_{Mg} = 0.1$ MPa (1 atm), $\gamma_{Mg} = 1$ i $a_{MgO} = 1$ activity of oxygen is $a_o = 0.13 \times 10^{-10}$ at a temperature of 1200 °C and $a_o = 0.56 \times 10^{-6}$ at 1600 °C.

1.3.4 The Mg–S System

Mg also has a high affinity to sulfur. For the $P_{Mg} = 0.1$ MPa, $\gamma_s = 5$ and $a_{MgS} = 1$, we obtain a concentration of sulfur in a magnesium solution: $[S] = 0.11 \times 10^{-6}$ to 1200 °C, and $[S] = 0.50 \times 10^{-3}$ to 1600 °C.

At the liquid iron temperature, the reaction of magnesium and sulfur, as well as oxygen, can be carried out according to the two schemes [data come from: 14, 19]:

Scheme 1: The assumption that magnesium in the form of $Mg_{(g)}$ vapors reacts with sulfur vapor $S_{(g)}$:

$$(8)\quad Mg_{(g)} + [S]_{1\%} = MgS_{(s)} \qquad \Delta G_8^o = -483{,}300 + 208.2 \cdot T \ \frac{J}{mol}$$

$$\log K_8 = \frac{25{,}242}{T} - 10.87$$

$$(9)\quad \frac{1}{2}S_{2(g)} \rightarrow [S]_{1\%} \qquad \Delta G_9^o = -135{,}060 + 23.43 \cdot T \ \frac{J}{atom} \qquad (1.24)$$

$$\log K_9 = \frac{7{,}054}{T} - 1.22$$

$$(10)\quad Mg_{(g)} + \frac{1}{2}S_{2(g)} = MgS_{(s)} \qquad \Delta G_{10}^o = \Delta G_8^o + \Delta G_9^o$$

$$\mathbf{\Delta G_{10}^o = -618{,}360 + 231.63 \cdot T} \ \frac{J}{mol} \qquad \text{(range 1263–1973 K)}$$

$$\text{klog } K_{10} = \log \frac{a_{MgS_{(s)}}}{P_{Mg} \cdot P_{S_2}^{\frac{1}{2}}} = \frac{32{,}295}{T} - 12.10$$

Scheme 2: The assumption that magnesium dissolved in the iron [Mg] reacts with sulfur dissolved in the iron [S]:

$$(11)\quad \frac{1}{2}S_{2(g)} \rightarrow [S]_{1\%} \qquad \Delta G_{11}^o = -135{,}060 - 23.43 \cdot T \ \frac{J}{atom}$$

$$\log K_{11} = \frac{6535}{T} - 0.964$$

$$(12)\quad Mg_{(g)} \rightarrow [Mg] \qquad \Delta G_{12}^o = -136{,}175 + 67.46 \cdot T \ \frac{J}{mol} \qquad (1.25)$$

$$(13)\quad Mg_{(g)} + \frac{1}{2}S_{2(g)} = MgS_{(s)} \qquad \Delta G_{13}^o = -618{,}360 + 231.63 \cdot T \ \frac{J}{mol}$$

$$(14)\quad [Mg] + [S]_{1\%} = MgS_{(s)} \qquad \Delta G_{14}^o = \Delta G_{13}^o - \Delta G_{12}^o - \Delta G_{11}^o \ \frac{J}{mol}$$

$$\mathbf{\Delta G_{14}^o = -347{,}125 + 187.60 \cdot T} \ \frac{J}{mol} \qquad \text{(range 1263–1973 K)}$$

$$\log K_{14} = \log \frac{a_{MgS_{(s)}}}{[\%Mg] \cdot [\%S] \cdot \gamma_{Mg} \cdot \gamma_S} = \frac{18{,}129}{T} - 9.80$$

where activity coefficients γ_{Mg} and $\gamma_S \rightarrow 1.0$ for diluted solutions of Mg and S dissolved in iron.

Table 1.1 lists the Gibbs energy values calculated for the two proposed schemes of reaction of magnesium and oxygen, magnesium and sulfur in the temperature range 1573–1823 K.

Gibbs energy (ΔG^o) is negative in all the considered cases. However, the Gibbs energy is more negative for systems in which the elements react with each other in a gaseous state (reactions 3 and 10). For this reason, the reactions of magnesium vapor with oxygen gas, and magnesium vapors with sulfur vapor are thermodynamically

Table 1.1 The Gibbs energy for the reactions of magnesium with oxygen and magnesium with sulfur extending according to schemes (1) and (2)

Temperature (K)	1573	1623	1673	1723	1773	1823
ΔG°_{3}, J/mol $Mg_{(g)} + ½O_{2(g)} = MgO_{(s)}$	−408,433	−398,208	−387,983	−377,758	−367,533	−357,308
ΔG°_{7}, J/mol $[Mg] + [O]_{1\ \%} = MgO_{(s)}$	−256,621	−249,621	−242,622	−235,622	−228,623	−221,623
ΔG°_{10}, J/mol $Mg_{(g)} + ½S_{2(g)} = MgS_{(s)}$	−254,006	−242,425	−230,843	−219,262	−207,680	−196,099
ΔG°_{14}, J/mol $[Mg] + [S]_{1\ \%} = MgS_{(s)}$	−52,030	−42,650	−32,270	−23,890	−14,510	−5,130

Table 1.2 The difference in Gibbs energy of MgO and MgS formation (magnesium, sulfur and oxygen in gaseous form)

Temperature (K)	1573	1623	1673	1723	1773	1823
ΔA^{o} (J/mol)	−154,458	−155,815	−157,173	−158,530	−159,888	−161,245

Table 1.3 The difference in Gibbs energy of MgO and MgS formation (magnesium, sulfur and oxygen in solution)

Temperature (K)	1573	1623	1673	1723	1773	1823
ΔA^{o} (J/mol)	−204,685	−207,068	−209,452	−211,835	−214,219	−216,602

more favored. These calculations also show that the reaction of magnesium with oxygen, relative to the reaction of magnesium with sulfur is also more thermodynamically favored. Due to the greater affinity of magnesium to oxygen than to sulfur, after the introduction of Mg to the liquid metal iron oxides are formed first, and sulfides next.

Assuming that the standard state for the sulfur and oxygen in an infinitely dilute solution, expressed in % mass, the difference between the affinity of Mg to oxygen and Mg to sulfur in solution (expressed as $\Delta A^{o} = \Delta G^{o}$ formation of MgO $- \Delta G^{o}$ formation of MgS):

- sulfur, oxygen and magnesium are in a gaseous state (Table 1.2):

$$\begin{aligned}\Delta A^{o} &= (-730{,}111 + 204.5 \cdot T) - (-618{,}360 + 231.63 \cdot T) \\ &= \mathbf{-111{,}751 - 27.15 \cdot T}\ \mathrm{J/mol}\ (\text{range } 1363\text{–}1973\ \mathrm{K})\end{aligned}$$

- sulfur, oxygen and magnesium are in solution (Table 1.3):

$$\begin{aligned}\Delta A^{o} &= (-476{,}825 + 139.93 \cdot T) - (-347{,}125 + 187.60 \cdot T) \\ &= \mathbf{-129{,}700 - 47.67 \cdot T}\ \mathrm{J/mol}\ (\text{range } 1363 - 1973\ \mathrm{K})\end{aligned}$$

Table 1.4 Values of the equilibrium constant K for the reactions with the participation of Mg, S and O (reactions 1.23 and 1.25) [14 + author's own research]

Equilibrium constant K for reaction	1573 K	1623 K	1673 K	1723 K	1773 K	1823 K
$\log K_7 = 24{,}903/T - 7.31$	3.3×10^8	1.1×10^8	3.8×10^7	1.4×10^7	5.4×10^6	2.2×10^6
$\log K_{14} = 18{,}129/T - 9.80$	53.10	23.44	10.86	5.27	2.66	1.39

As it is apparent from Table 1.2, the difference of Gibbs energy of the solid formation of MgO and MgS from gaseous components is negative and becomes slightly lower with the increasing temperature. This means that the affinity of magnesium to oxygen is greater than the affinity of magnesium to sulfur. The case of solid formation of MgO and MgS from the components forming solution with Mg (Table 1.3) is similar.

The high activity of Mg in the Fe–C alloys saturated carbon with respect to sulfur and oxygen dissolved in the melt ultimately leads to lowering their surface activity. The creation of new phases, such as, e.g. MgO and MgS, helps reduce the work necessary to form crystal nuclei and reduces the degree of alloy undercooling. The increase of the alloy surface tension is observed even with a small addition of Mg, due to occurring reactions—desulfurization and deoxidation (removal of surface active elements) and a reduction in the surface activity of these elements (Table 1.4). A further increase in the amount of magnesium input into the cast iron leads to a reduction in the alloy surface tension due to the high surface activity of the element [18].

1.4 Loss of Magnesium in the Melt by Reaction with Oxygen and Sulfur

A magnesium treated liquid metal in SGI is highly reactive with its surrounding gases or the solid environment (mold). The negative effects of these interactions can be Mg-fading and consequent spherical graphite shape degeneration in the surface. Additionally, the reaction products (insulated inclusions or aggregated into slag) could have negative effects on casting performance and machinability.

When the liquid ductile iron is held in the ladle two processes can take place: (a) evaporation of magnesium, which has a high partial pressure (b) adsorption and diffusion of the oxygen in the melt, followed by reaction of oxygen with magnesium dissolved in the liquid metal [19].

Magnesium, after the introduction of the liquid cast iron, first reacts with oxygen, next with sulfur before the conditions for the graphite spheroidization process are made. Depending on the sulfur content, the amount of Mg is necessary to ensure full spheroidization may vary from 0.02 to 0.06 % mass. The lower the temperature of the spheroidization treatment is, the smaller the rate of magnesium loss.

The oxygen which reacts with Mg may be derived from metal, but in the case of iron material containing more than 3 % of carbon, it is unlikely (this can occur e.g. in the case of long withholding of the molten metal at a high temperature, large amounts of steel scrap in the charge, moisture, from the feed and atmosphere, etc.). Typical dissolved oxygen contents in the liquid metal at a temperature of 1693 K are [20]:

- in SGI: 50–140 ppb;
- in CGI: 140–300 ppb;
- in FGI: 300–1500 ppb.

where 1 ppb = 0.001 ppm.

The total amount of oxygen in the iron is comprised of the dissolved oxygen and the oxygen bound in the oxide.

oxygen total = dissolved oxygen + oxygen bound in oxides

The amount of dissolved oxygen decreases with the decreasing temperature, while the total amount of oxygen is constant. i.e. the amount of oxygen bound in the oxide increases with the decreasing temperature. While the amount of oxygen dissolved in the liquid cast iron does not depend on the type of furnace (the melting process), it has an impact on the total amount of oxygen. This means that the amount of bound oxygen in the oxide changes. Iron melted in a cupola furnace contains more oxygen, and thus more than cast iron melted in an induction furnace [21].

The presence of oxygen in the liquid cast iron is secondary and is rather the result of long-term retention, pouring, a turbulent flow of metal through the gating system, the liquid metal in contact with the oxygen in the mold cavity and the dissociation of the water vapor during heating of the mold [22].

The resulting MgO has a low density and low solubility in iron. Therefore, the MgO particles tend to float in the ladle onto the surface of the molten metal during pouring and accumulate on the upper surface of the casting. They can also be introduced into the interior of the casting as harmful non-metallic inclusions. The low temperature of molten metal favors the formation of these impurities in the form of dross.

Magnesium as a powerful desulfurizing element forms magnesium sulfide MgS (T_m = 2500 K), a compound with low density and poor wettability, almost insoluble in the liquid iron alloys, which tends to float on the surface of liquid iron and contaminate it [23]. MgS is relatively short-lasting and reacts with oxygen to form MgO and release sulfur, which re-enters into the liquid iron and reacts with Mg. Such a cyclic deoxidation and desulfurization continuously reduces the amount of the efficient Mg needed for spheroidization. You should make every effort to remove MgS from the surface of iron after the spheroidization in the ladle and before inoculation and pouring metal into a mold.

When the amount of sulfur and oxygen in the iron output is low, then the introduction of 0.018 % mass Mg is sufficient to obtain graphite in the spheroidal form. However, in reality the indicated Mg level to ensure effective spheroidization should be such that the full spheroidization, residual Mg measured was 0.03–0.07 % mass.

Wherein the amount of the residual comprises total Mg content, i.e. also in the form of the associated MgO, MgS and $MgSiO_3$.

If the amount of residual Mg is too large (e.g., greater than 0.06 %), it may have a high risk of carbide formation, porosity, and slag. This risk increases with the increase in the rate of solidification (small sections of castings can promote the formation of carbides) and low density of graphite nodules. It is therefore necessary to carried out an efficient inoculation treatment after spheroidizing one, leading to a high density of graphite nodules which minimize chilling tendency.

1.5 Graphite Degradation Mechanisms

Several mechanisms were proposed to explain the phenomenon of the graphite casting surface layer degradation. All of them are based on the assumption that the cause of this phenomenon is to reduce the concentration of Mg in the surface layer of the casting as a result of the reaction of Mg and S, and Mg with O. As demonstrated above, the original oxygen content of the liquid cast iron is very low. The second source of oxygen, affecting the formation of the surface layer on the casting may be the mold atmosphere, and in the case of the green sand—water, which decomposes under the influence of heat [8, 24]. Additionally, the catalysts and binders for molding sands and cores can be an additional source of sulfur. These include molding sands with furfuryl and urea-formaldehyde resins, which the sulfonic acids with the addition of sulfuric acid are used for hardening (see Chap. 2).

A skin forms during solidification after pouring the mold Mg treated cast iron. Defects in this skin include a degenerate graphite shape, high temperature reaction products, porosity and exogenous inclusions from a reaction of surface slag/dross with molding sand. The effect of casting skin on mechanical properties has been documented in the literature. A clear reduction in tensile and yield strength that occur in both ductile and compacted graphite iron was shown [7, 9, 25, 26].

In order to verify that magnesium reacts with sulfur and/or oxygen diffusing from the mold Stefanescu et al. [5] developed a model of Mg diffusion (model 1-D), which allowed the cast to anticipate areas poor in Mg. In this model the following assumptions were considered: (1) on the mold/metal interface Mg concentration decreases as a result of reaction with oxygen, and sulfur, (2) has no liquid convection in the area, (3) the initial residual amount of Mg is 0.019 %, (4) the diffusion coefficient of Mg in the liquid cast iron was adopted as a permanent, (5) the diffusion time was taken as solidification time using a simulation software (adopted 70 s). Diffusion Eq. (1.26) for the solute is in the form (as Fick's 1st law):

$$\mathrm{D} \cdot \frac{\partial^2 C}{\partial x^2} = \frac{\partial \mathrm{C}}{\partial \mathrm{t}} \tag{1.26}$$

where: D—diffusion coefficient of Mg in liquid Fe; C—composition, x—distance, t—time of diffusion.

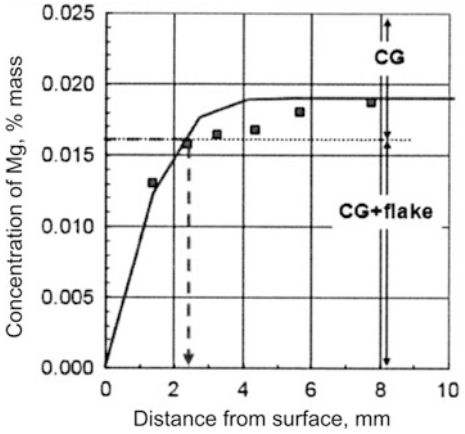

Fig. 1.7 Comparison of experimental data (*squares*) and diffusion model prediction (*solid line*) in CGI casting [2]

Calculations made on the basis of this model confirmed the validity of diffusion theory to explain the phenomenon of degradation of the surface layer of graphite in cast.

The size of the diffusion coefficient D_o of magnesium in the liquid iron at a temperature of 1623 K is 1.49×10^{-8} m^2/s [2, 27].

Figure 1.7 show the comparison of measured and calculated, usage model 1-D, Mg level in casting skin of CGI. Both predict a degenerated graphite skin thickness of about 2.3 mm, which agrees well with the observation by Stefanescu et al. [5]. However, the diffusion model 1-D, although it explains many experimental results, it is not checked with regard to the explanation of all observations and have a number of limitations.

1.5.1 New Contributions to the Theory of Casting Skin Formation

The new 2-D thermal-diffusion model was developed with the following assumptions [4]:

- The thermal field was simulated concomitantly with the diffusion field providing the temperature distribution at all time-steps. The solidification time was evaluated directly from thermal field.
- Diffusivity as a function of temperature and of the liquid/solid state of the iron was used.
- The initial Mg level was taken as 0.02 % mass.
- A Mg sink at the mold/metal interface was assumed.
- Liquid convection in the casting was ignored.

- The critical Mg level for graphite degradation was assumed to be 0.015 % mass.
- The iron was eutectic composition with a solidification range 1135–1144 °C.

Assuming that the diffusion and thermal conductivity are not a function of position, i.e. the molding sand transfer Eq. (1.27) has the form:

$$\frac{\partial C}{\partial t} = D \cdot \left(\frac{\partial^2 C}{\partial x^2} + \frac{\partial^2 C}{\partial y^2} \right) \tag{1.27}$$

And heat transport Eq. (1.28):

$$\frac{\partial T}{\partial t} = k \cdot \left(\frac{\partial^2 T}{\partial x^2} + \frac{\partial^2 T}{\partial y^2} \right) \tag{1.28}$$

The heat flux at the interface mold/casting is described by the following equation:

$$h \cdot A \cdot (T - T_{mold}) = V \cdot \rho \cdot \Delta H_f - V \cdot \rho \cdot \frac{\partial T}{\partial t} + k \cdot A \cdot \frac{\partial T}{\partial t}$$

When the system temperature is within the range of solidification ($T_S < T < T_L$), we receive (1.29):

$$h \cdot A \cdot (T - T_{mold}) = -V \cdot \rho \cdot \frac{\partial T}{\partial t} + k \cdot A \cdot \frac{\partial T}{\partial t} \tag{1.29}$$

h heat transfer coefficient (W/(m^2 K))
A surface area (m^2)
ρ density (kg/m^3)
H_f latent heat of fusion (J/kg)
V volume (m^3)
k thermal conductivity (W/(m K))

Assuming the solubility of Mg in solid iron as 0.17 at %, Mg diffusion in the liquid iron was adopted at $D_L = 1.49 \times 10^{-8}$ m^2/s at 1350 °C. The magnesium diffusion coefficient (D_o) is 4.35×10^{-7} m^2/s and the activation energy (Q) equal to 44.9×10^3 J/mol. Mg diffusion in the solid iron is taken as a constant equal to $D_S = 1.0 \times 10^{-11}$ m^2/s. Then, the diffusion of Mg in the range liquidus-solidus is expressed by the formula (1.30):

$$D_{S/L} = D_S \cdot \frac{(T - T_S)}{(T_L - T_S)} + D_L \cdot \left[1 - \frac{(T - T_S)}{(T_L - T_S)} \right] \tag{1.30}$$

where T_L—liquidus temperature, T_S—solidus temperature.

This model is specifically for Mg depletion and does not take solidification kinetics effects into account. Therefore, this model cannot be used to clarify the effect of the protective coating.

The thickness of the surface layer is affected by the pouring temperature, since the duration of the Mg diffusion is longer at a higher temperature and deeper depletion of Mg is expected (casting skin is thicker). Another factor influencing the thickness of the surface layer is the initial Mg content. Reducing the initial amount of Mg exponentially increases the thickness of the casting skin (with a lower initial content of Mg that will form a thicker layer depleted with Mg). It turns out that in the case of SGI (a typical Mg content 0.04 % mass) a casting skin should be thinner than in CGI (a typical Mg content is 0.02 % mass).

1.5.2 Kinetic Effects Solidification

The previous considerations dealing with the creation of the flake graphite layer at the casting-mold interface were based on the phenomenon of depletion of the surface layer of the casting in Mg. Mampaey et al. [28] demonstrated that in the skin formed on the gray cast iron castings graphite type D appeared, in the depths of casting—graphite type A. As in gray cast iron there is not Mg, the formation of the skin can be attributed to the influence of solidification kinetics (e.g. larger undercooling at the interface). The main reason of skin formation, in this case, can be solidification with the separation of primary austenite at the interface of the mold/casting. With the increase of undercooling and/or a reduction in the carbon equivalent, the amount of primary austenite increases. Other factors that affect the amount of primary austenite at the boundary phase are thermal conductivity and inoculation.

The Effect of Carbon Equivalent (CE)[4]
Recent work by Boonmee and Stefanescu [3] and Qing et al. [19] have shown that the carbon equivalent significantly affects the thickness of surface layer depleted of graphite. It was shown that layer thickness decreases with increasing carbon equivalent.

Effect of Inoculation
The application of the FeSi protective coating reduces undercooling, due to the modifying activity. The result is forming a smaller amount of the primary austenite, and thinner casting skin is consequently formed.

[4]Carbon Equivalent, CE = C + 0.30Si + 0.36P, where Si and P are silicon and phosphorus, respectively.

Effect of Thermal Conductivity
The application of the inactive protective coating of high thermal conductivity to the mold increases undercooling at the interface mold/cast, and thus the increase in the thickness of the casting skin, i.e. a protective coating which reduces the cooling rate, thereby reducing the undercooling should promote the formation of a thin surface layer.

1.5.3 Summary of the Casting Skin Formation Mechanisms

Boonmee [4] developed two parallel mechanisms formed on the casting surface layer containing degraded graphite relative to the rest of the casting based on:

- austenite layer growth (influence of solidification kinetics);
- magnesium depletion (by reaction with oxygen or sulfur).

The kinetics of solidification influences the formation of the surface layer by changing the size of undercooling at the interface mold/metal, which leads to a change in the quantity of primary austenite. An example is the use of protective coatings with high thermal conductivity, which favors the formation of thicker outer layers. On the other hand, a mechanism of Mg depletion dominates for castings with a long solidification time (large castings). Generally it can be said that high undercooling favors the formation of a thicker layer of primary austenite and limits the oxidation of magnesium and vice versa.

The mechanism based on the oxidation of Mg controls the formation of the surface layer at low cooling rates. However, at high cooling rate, the controlling step is the formation of austenite layers at the interface mold/casting. 2-D thermal-diffusion model is based on the phenomenon of Mg oxidation and should therefore be assessed only for the area of low cooling rate.

1.5.4 Conclusions Regarding the Casting Surface Layer Formation Mechanisms

The surface layer formation mechanism developed by Stefanescu and Boonmee takes not only the chemical reactions occurring at the interface mold/cast into account, but also the effect of casting solidification kinetics:

- decarbonising the casting surface layer is responsible for the depletion of the graphite and the formation of ferrite rims. The decarbonisation process is favored by the presence of moisture and higher pouring temperatures. On the other hand, carburization of the surface layer causes the formation of pearlite rims.
- degradation of the graphite can be explained by either a depletion of the surface layer of magnesium as a result of chemical reactions with components of the mold and the atmosphere inside the mold, or an increase in the amount of

austenite in the surface layer (large undercooling at the interface mold/metal promotes the growth of dendrites of austenite, that reject Mg at the solidification front) [29]. As a result, the amount of Mg is reduced, and flake graphite structure is formed near the interface mold/metal, and there are areas with a high degree of spheroidization in the depth of the casting.

- given the above mechanisms, reducing the formation of surface layer on the casting may be obtained either by minimizing the extent of the depletion layer of Mg or decreasing undercooling at the mold wall.

1.6 The Reaction of Magnesium with Sulfur in the Mold

The effect of sulfur on the formation of skin on cast iron was described by Martin and Karsaya already in 1979 [30]. The developed theory assumed that under high temperature, p-toluenesulfonic acid (PTSA) is used as a catalyst so that furfuryl and phenolic resins generate SO_2, which is responsible for the reaction of Mg–S in cast iron. Complete dissociation of sulfur-containing catalyst components occurs practically at the temperature of liquid magnesium. It was found that the S/Mg ratio of 0.5 in the middle of the mold increased to above 2.5 on the surface of the casting.

Sulfur dioxide resulting from the thermal decomposition of PTSA is adsorbed at the metal surface, after it has dissociated into atoms, which allows diffusion into molten metal and/or will be reduced by iron to form dissolved FeS and FeO. Both these products will react with Mg in solution in the iron melt. The direct reaction of magnesium with oxygen and sulfur is also possible. The entire process can be written as follows:

$$CH_3C_6H_4SO_3H\ (\text{PTSA}) + HOH\ (\text{water steam}) = C_6H_5CH_3\ (\text{toluene}) + H_2SO_4 = C_6H_5CH_3\ (\text{toluene}) + \{SO_2\} + \{H_2O\}$$

$$\begin{gathered}\{SO_2\} = 2[O] + [S] \\ 3[Fe] + \{SO_2\} = [FeS] + 2[FeO] \\ [Mg] + [FeS] = (MgS) = [Fe] \\ [Mg] + [FeO] = (MgO) + [Fe] \\ \text{and/or} \\ [Mg] + [O] = (MgO) \\ [Mg] + [S] = (MgS)\end{gathered}$$

As a result of the reaction the concentration of Mg in the surface layer reduces, and consequently, degeneration of the nodular graphite follows. This process continues until the complete solidification of the surface layer of the casting. Also, other reactive elements such as rare earth or Mn can react with sulfur to form the corresponding sulfides [31, 32].

Wherein the degree of degeneration of graphite depends inter alia on the residual magnesium content and applied protective coating. There is more graphite degeneration in the surface layer of the casting (thickness of the degenerated surface layer is 280–530 μm) with a lower content of magnesium, less than 0.03 % mass Mg_{res}., typical of CGI, when protective coatings are not used, as compared to a higher magnesium content of 0.04–0.05 % mass Mg_{res}., used in SGI (the thickness of the degenerated surface layer is 185 μm) [32].

One should also pay attention to the possibility of accumulation of sulfur obtained in the process of mechanical reclamation of molding sand with resins hardened with a catalyst containing sulfur, which leads to an increase in the thickness of the degraded graphite layer [31, 33–35]. Therefore, one should avoid using 100 % reclaimed sand. Insufficient molding sand refreshment can cause an increase in the sulfur content to 0.3–0.5 % mass of the matrix prepared on the basis of the reclaimed sand. The solution to this problem would be to use thermal reclamation.

The occurrence of the phenomenon of flake graphite in SG iron castings may also take place in the case of classical green sand and coal dust. Then the source of sulfur is coal dust and the molding sand returning from the circulation is enriched in sulfur.

1.7 The Reaction of Magnesium with Oxygen in the Mold

The occurrence of Mg depletion in the surface layer of the cast was also found in molding sand with water glass, which do not contain sulfur. Therefore, it appears that the main reason for reducing the concentration of Mg is its reaction with oxygen. Tinebar [36] found that the application of the molding sand with binders containing water causes the vermicular or flake graphite to appear on the surface of the ductile iron castings. The reason for this is the oxidizing atmosphere, made in the mold by moisture.

Oxidation of magnesium takes place mainly in the liquid state and mushy state when the diffusion rate is high. The most likely reactions are:

$$\text{(a)} \quad [Mg] + \{CO_2\} \rightarrow (MgO) + \{CO\}$$
$$\text{(b)} \quad [Mg] + \{H_2O\} \rightarrow (MgO) + \{H_2\}$$
$$\text{(c)} \quad [Mg] + \frac{1}{2}\{O_2\} \rightarrow (MgO)$$

The lowest value (most negative) a Gibbs energy of creating (ΔG) has the (b) reaction. However, this reaction can only take place if there is moisture in the system. Therefore, in the dry molding sand, containing no water (such as molding sand with water-glass) the most likely to be considered is the (c) reaction.

When the Mg concentration in the liquid iron surface layer decreases due to the formation of MgO, an additional portion of Mg is provided in the bath depth of the as a result of diffusion. The process is diffusion controlled.

Using a higher temperature of pouring, it is expected that it will create a thicker skin. This is a result of the longer time of reaction and higher diffusion rate of oxygen. For the same reason thick castings walls, which solidify for longer time, will have a thicker skin [3, 37].

An inactive protective coating should reduce the flow of oxygen from the mold. Also, the thermal conductivity of the coating material plays an important role.

When silica sand (SiO_2) is used as a matrix it is capable of further reactions, e.g.:

$$2MgO_{(s)} + SiO_{2(s)} \rightarrow Mg_2SiO_{4(s)} \text{ (magnesium orthosilicate)}$$
$$MgO_{(s)} + SiO_{2(s)} \rightarrow MgSiO_{3(s)} \text{ (magnesium silicate)}$$

1.8 The Role of the Protective Coating in the Formation of a Casting Surface Layer

Boonmee and Stefanescu [4] and Chisamera et al. [32] suggest that it would be advantageous to apply coatings containing desulfurization agents such as CaO or MgO for the reduction in transition of sulfur from the molding sand to casting. Desulfurization of liquid iron by CaO according to Voronova takes place according to the reactions [38]:

$$(CaO) + [S] \rightarrow (CaS) + [O]$$
$$(CaO) + [S] + [C] \rightarrow (CaS) + CO$$
$$(CaO) + [S] + \frac{1}{2}[Si] \rightarrow (CaS) + \frac{1}{2}(SiO_2)$$
$$2(CaO) + [S] + \frac{1}{2}[Si] \rightarrow (CaS) + \frac{1}{2}(2CaO \cdot SiO_2)$$

Therefore, the CaO-containing a coating should reduce the thickness of the surface layer of the casting when in the mold material sulfur is present. The use of a protective coating of CaO in the case of mold made from molding sand bonded with phenol resins or urea-furfuryl resins significantly limited the thickness of the surface layer on the casting. However, if the molding sand with binders not containing sulfur (e.g. with water glass) thus protective coating with CaO acts neutrally. But even in this case, the application of a CaO protective coating produces a thicker surface layer than when this coating is not used. This is due to the higher thermal conductivity of the CaO protective coating than clean sand (with no coating) [3].

Operation of the MgO protective coating is different from the CaO coating. This is due to the fact that from the thermodynamical point of view the process of MgO creating is privileged, i.e. MgO is an inefficient desulfurization agent than CaO. In addition, MgO has a very high thermal conductivity, which causes the thickness of the surface layer to increase as compared with the molding sand, just as if no protective coating was applied.

The best results, both in terms of reduction of the thickness of the casting skin and increasing the degree of spheroidization in the interior of the casting were obtained when the protective coating contains active Mg. A fine-grained FeSi–CaMgRE alloy was used (similarly as for the spheroidization) or in the form of a mechanical mixture of fine-grained Mg FeSi75 alloy, where the mixture was more effective than aforementioned alloy [32].

It should be understood that the oxides contained in the protective coatings MgO or (CaO + MgO + talc) operate mainly as sulfur neutralizers, which pass from the mold, due to the desulfurization reaction. In contrast, the Mg–FeSi protective coating fulfills a dual role: sulfur binder, and also a magnesium supplement which reacted with sulfur or oxygen at the mold/casting interface; which increases the potential for spheroidization iron prior to solidification. This is particularly important in the case of thick casting solidification.

Recommendations for reducing the formation of a degenerated surface layer on castings made with molding sand hardened with PTS acid are as follows [32]:

- sulfur content in molding sand should be less than 0.15 % mass (or even <0.07 % mass);
- limit the amount of acid PTS used, preferably less than 50 % mass in relation to the resin;
- limit the use of reclaimed sand, usually less than 70 % mass;
- use well maintained and calibrated mixers;
- use an effective grain recovery classification system;
- use a mixture of phosphoric acid with PTS acid, but be aware that this may lead to a P transition to casting;
- lower the pouring temperature, usually below 1350 °C (depending on the weight of the casting and the wall thickness);
- apply a desulfurizing protective coating such as CaO–MgO-talk or special Fe–Si coatings containing Mg;
- use a mixture of PTS acid with xylenesulfonic acid and benzenesulfonic acid as a catalyst.

References

1. Stefanescu DM, Giese SR, Piwonka TS, Lane AM (1996) Cast iron penetration in sand molds. Part I: Physics of penetration defects and penetration model. AFS Trans 104:1233–1248
2. Boonmee S (2013) Ductile and compacted graphite iron casting skin – evaluation, effect on fatigue strength and elimination. Doctor Dissertation, The Ohio State University
3. Boonmee S, Stefanescu DM (2013) Casting skin management in compacted graphite iron. Part I: Effect of mold coating and section thickness. Trans AFS 121:435–448
4. Boonmee S, Stefanescu DM (2013) Casting skin management in compacted graphite iron. Part II: Mechanism of casting skin formation. Trans AFS 121:449–459
5. Stefanescu DM, Wills S, Massone J, Duncan F (2008) Quantification of casting skin in ductile and compacted graphite irons and its effect on tensile properties. Int J Metalcast (Fall 2008): 7–26
6. Boonmee S, Stefanescu DM (2010) Casting skin of compacted graphite iron. Part II: Influence on tensile mechanical properties. AFS Trans 118:217–222
7. Boonmee S, Moran MK, Stefanescu DM (2011) On the effect of the casting skin on the fatigue properties on CG iron. Trans AFS 119:421–430
8. Reisner HO (1962) Some aspects of the formation and structure of a skin on iron castings and a method used to obviate its occurrence. The British Foundryman September:362–369
9. Boonmee S, Stefanescu DM (2011) The mechanism of formation of casting skin in CG iron and its effect on tensile properties. Key Eng Mater 457:11–16
10. Mazurov EF et al (1977) Teoria mietalurgiczeskich procesov. Izd. Metallurgia, Moskwa, pp 32–45
11. Massalski TB (1996). In: Cahn RW, Haasen P (eds) Physical metallurgy, structure and stability of alloys, Vol 1. North-Holland, Amsterdam
12. Zhang X, Han Q, Chen D (1991) Dissolution equilibrium of magnesium vapor liquid iron. Metall Trans B 22B:918–921
13. Speer MC, Parlee NAD (1972) Dissolution and desulfurization reactions of magnesium vapor in liquid iron alloys. AFS Cast Met Res J 8(3):122–128
14. Modrzyński A (2000) Thermodynamic and kinetic analysis of the system: liquid saturated alloy (Fe-C) – vapour of Mg. Solidification of Metals and Alloys 2(44):239–248
15. Katz S, Landefeld C F (eds) (1988) Foundry processes. Their chemistry and physics. Plenum Press, New York, London
16. Knacke O et al (1991) Thermochemical properties of inorganic substances. Springer, Berlin
17. Chapman MW (2009) Insoluble oxide product formation and its effect on coke dissolution in liquid iron. Doctor thesis, University of Wollogong
18. Czikel J (1959) Beitrag zum problem der graphitkristallisation in eisen-kohlenstoff-legierungen. Gieserei Tech Wiss Beih 11(25):1385–1393
19. Qing J, Lekakh S, Richards V (2013) No-bake S-containing mold-DI metal interactions: consequences and potential application. AFS Trans 121:409–418
20. Seutens F (2010) Industrial applications of the oxygen activity measurement in cast iron. In: 4° Congreso Latinoamericano de Fundicion, Buenos Aires, 27 October 2010
21. Elmquist I, Orlenius J, Dioszegi A (2007) Influence of melting process on oxygen content in gray iron. AFS Trans 115:625–635
22. Verdes B, Chira J, Virgolici M, Moise V (2012) Thermal stability of fayalite system formation at the interface between steel and mould. U.P.B. Sci Bull Series B 74(2):257–268
23. Katz S (2004) Slag's effects on cast iron production. AFS Trans 112:945–957
24. Matijasevic S, Gomez-Gallardo B, Wallace J (1974) Ferrite surface layers on gray iron castings. AFS Trans 82:571–622
25. Starkey MS, Irving PE (1982) A Comparison on the fatigue strength of machined and as cast surfaces of SG iron. Int J Fatigue 4(3):129–136
26. Labrecque C et al (2008) Comparative study of fatique endurance limit for 4 and 6 mm thin wall ductile iron castings. Int J Metalcast 2:7–17

27. Woehlbier F (1978) Diffusion and defect data. Trans Tech Publications, Rockport, MA 17 (1–4):216–222
28. Mampaey F, Li PY, Wettnick E (1993) Variation of gray iron strength along the casting diameter. Trans AFS 101:3–56
29. Goodrich GM, Lobenhofer RW (2002) Effect of cooling rate on ductile iron mechanical properties. Trans AFS 110:1003–1032
30. Martin F, Karsay S (1979) Localized flake graphite structure as a result of a reaction between molten ductile iron and some components of the mold. AFS Trans 87:221–226
31. Xiaogan H, Jin X, Xuqi D, Yaoke W (1992) Nodular iron surface deteriration due to PTSA in resin. AFS Trans 100:9–15
32. Chisamera M, Ivan N, Riposan I, Stan S (2014) Iron casting skin management in No-Bake mould – effects of magnesium residual level and mould coating. In: 71st World Foundry Congress, Bilabo, Espania, 19–21 May 2014
33. Dańko R, Holtzer M, Górny M, Żymankowska-Kumon S (2013) Effect of reclamation on the skin layer of ductile iron cast in furan molds. J Mater Eng Perform 22(11):3592–3600
34. Holtzer M, Górny M, Dańko R, Żymankowska-Kumon S (2013) Impact in the quality of moulding sand with furan resin on the formation of the skin layer of ductile iron castings. In: EUROMAT 2013: European Congress and Exhibition on Advanced Materials and Proces, Sevilla, Espania, 8–13 September 2013
35. Dańko R, Górny M, Holtzer M, Żymankowska-Kumon S (2014) Influence of the furan moulding sand on the ductile iron casting surface quality. In: 71 WFC: World Foundry Congress, Advanced Sustainable Foundry, Bilbao, 19–21 May 2014
36. Tinebar JP, Wilson SJ (1993) Nobake chemical binder systems: Their effect on microstrutural and physical properties of ductile iron. Trans AFS 101:169–174
37. Duncan FC, Kroker J (2011) A new test casting to evaluate skin formation in CGI. Trans AFS 119:10–023
38. Voronova NA (1983) Desulfurization of hot metal by magnesium. The International Magnesium Association, Dayton
39. Coudurier L, Hopkins DW, Wilkomirsky I (eds) (1985) Fundamentals of metallurgical processes. Pergamon Press, New York
40. Bodsworth G, Bell HB (1973) Physical chemistry of iron and steel manufacture. Longman, London
41. Alcock CB, Itkin VP, Horrigan MK (1984) Vapor pressure of the metallic elements. Canadian Metallurgical Quartely 23:309–313

Chapter 2
Molds and Cores Systems in Foundry

Mariusz Holtzer and Rafał Dańko

Abstract Sand binding systems can have a significant impact on the nature of the casting skin formation. In particular, the binder containing elements such as S, O and N may adversely affect the structure of the layer. As in the case of spheroidal graphite cast iron (SGI) and compacted graphite cast iron (CGI) main factor causing the degeneration of graphite in the surface layer of the casting is sulfur, therefore these binding systems (binder) which contain sulfur have been thoroughly discussed here. The following are sand mold technologies: furan, acid catalyzed, phenolic, acid catalyzed, hot box, warm box and Shell (Croning) process. Sand molding with the use of furfuryl resins technology is presented in detail due to their widespread use in casting both cast iron and cast steel. To reduce the thickness of the surface layer, which may be the adverse effect of sulfur on the degeneracy of the graphite, S content in molding sand should be less than 0.15 % mass, and even below 0.07 % mass. Sand binding systems can have a significant impact on the nature of casting skin formation. In the case of green sand, moisture promotes the formation of the ferritic rim (Reisener, Br Foundryman 55:362–369, 1962; Matijasevic et al. Trans AFS 82:571–622, 1974; Narasimha and Wallace, AFS Trans 83:531–550, 1975). Research carried out for sand mold with sodium silicate and phenolic urethane has shown that SGI and CGI castings made in the first sand mold is pearlitic rim occurred, and in the second sand mold this occurrence is not found (Boonmee and Stefanescu, Foundry Trade J 186:225–228, 2012). Regarding the effect of the molding sand on the nature of the casting skin formation, they can be divided into molding sand: with binders containing sulfur (i.e. furfuryl alcohol and urea-formaldehyde resin) and the molding sand that are not bound with binders not containing sulfur (i.e. phenol-urethane resin). From the point of view of the top layer the sulfur-containing molding sand is much more important, due to its adverse effect on the formation of spheroidal graphite.

© The Author(s) 2015

M. Holtzer et al., *Microstructure and Properties of Ductile Iron and Compacted Graphite Iron Castings*, SpringerBriefs in Materials,
DOI 10.1007/978-3-319-14583-9_2

2.1 The Influence of Sulfur on the Casting Skin Formation

Studies have shown that sulfur is a primary factor causing graphite degeneration at the metal-mold interface [1–7]. Sulfur originating from SO_2 dissociation and from metal surface diffusion into molten metal form sulfides of the following reactive elements: Mg, rare earth elements (REE) and Mn without being suffice not time for new nodulizing elements to reach the surface by diffusion from adjoining metal layers. To reduce the thickness of the surface layer, which may be the adverse effect of sulfur on the degeneracy of the graphite, the sulfur content should not exceed 0.15 % mass for cold-setting resins using regenerated sand [7]. Therefore, among others, the reclaimed sand weight should be less than 70 % mass and should be used as an acid catalyst blend phosphoric acid with p-toluenesulfonic acid (PTSA). However, in this case, the phosphorus pick-up may take place and its segregation on the surface of ductile iron casting.

Similarly, the amount of sulfur in the lustrous carbon producer in clay sand molding material should be limited to 1 % mass, with a maximum of 0.1 % mass in the molding sand. In highly susceptible areas, such as the metal surrounding a thin corner of the sand, the limiting sulfur content may be lower, less than 0.07 % mass.

Generally, sulfur is considered to be a major contribution to the problem, but in many cases sulfur is not the only element in the mold causing flake graphite [7].

2.2 The Influence of Oxygen on the Casting Skin Formation

Existing or generated oxidizing gases in the mold cavity may be another important factor for graphite degeneration in the surface layer of the ductile iron castings. Dissolved oxygen will react with Mg or MgS to form MgO. Water bearing no-bake binder systems such as: ester-cured phenolic, furan no-bake and an inorganic no-bake binder exhibited a more prominent flake or vermicular graphite structure at the mold/metal interface versus the non water binder systems such as phenolic-urethane no bake (cold box) and alkyd oil [8, 9].

2.3 The Influence of Nitrogen on the Casting Skin Formation

Nitrogen is under suspicion as one of the elements promoting flake graphite. Nitrogen may derive from the metal or binder used for molding sand or core (e.g., furan resin). In treated ductile iron the effect of nitrogen is much less pronounced as it is purged from the system through Mg-treatment. Therefore, the main sources of nitrogen are binders containing a large amount of this element. Nitrogen has a profound effect on the frequency and severity of the pinholes. The influence of nitrogen on the structure is visible as matrix results (more pearlite or/and carbide

incidence), but disputed as the influence on graphite morphology. Nitrogen has a limited effect on the degeneration of graphite in the surface layer. Organic resins decompose below the liquid iron temperature to generate ammonia (NH_3), which is an important source of both N_2 and H_2.

Molds may be classified in two large families

- **lost molds** (single use molds): These are specially made for each casting and are destroyed after pouring. The molds are generally made of sand, and are chemically bonded, clay-bonded, or even unbonded. Investment casting can also be included in this family;
- **permanent molds** (multi use molds): These are used for gravity and low-pressure casting, pressure die-casting, and centrifugal casting. The molds are typically metallic.

2.4 Molding with Clay-Bonded Sand (Green Sand)

Green sand is the most common molding process. Green sand is generally not used to make cores. Green sand is the only process that uses a moist sand mix. The mixture is made up of about 85–95 % silica (or olivine or zircon) sand; 5–10 % bentonite clay; 3–9 % carbonaceous materials such as sea coal, petroleum products, corn starch or wood flour; and 2–5 % water [10, 11].

The clay and water act as a binder, holding the sand grains together. The carbonaceous materials burn off when molten metal is poured into the mold, creating a reducing atmosphere which prevents the metal from oxidizing as it solidifies. In the case of cast steel castings—the molding sand only contains bentonite, cereal binder and water. The introduction of carbonaceous materials could cause carburization of the surface layer of the casting. Most carriers of lustrous carbon (sea coal, lignite) contain sulfur, which may cause graphite degradation. Therefore, the sulfur content in carbonaceous materials should be limited [12].

2.5 Molding and Core-Making with Chemically-Bonded Sand

There are many different types of chemical binders. They are divided into two main types: organic and inorganic. Chemical binding systems are primarily used for core-making. Cores require different physical characteristics than molds; therefore, the binding systems used to make cores may be different from those used for molds. This means that the binding system used must produce strong, hard cores that will collapse to allow removal after the casting has hardened. Therefore, cores are typically formed from silica sand (and occasionally olivine, zircon or chromite sand), and strong chemical binders. The sand and binder mix is placed in a core-box

where it hardens into the desired shape and is removed. Hardening, or curing, is accomplished with a chemical or catalytic reaction or by heat.

Although a wide variety of resin binder processes are currently used, they can be classified into the three general categories:

- *Cold-setting processes* (*No-bake systems*) The curing of cold-setting sands is effective at ambient temperature. The process begins when the last component of the formulation has been introduced into the mix.
- *Gas-hardened processes* (*Cold-box system*) In these processes, curing takes place by injecting a catalyst or a hardener in a gaseous form.
- *Hot curing processes* In these processes, curing takes place by heating the sand-resin mix or, more often, by allowing it to come into contact with the heated pattern equipment.

The selection of the process and type of binder depends on the size and number of cores or molds required, production rates, and equipment.

Cold-setting processes include the following processes: phenolic-acid catalyzed, furan-acid catalyzed, polyurethane (phenolic isocyanate), resol-ester (alkaline phenolic ester hardened), alkyd oil-unbaked, ester silicate, cement.

Gas-hardened processes include the following processes: cold-box (amine hardened phenolic urethane), resol-ester (alkaline phenolics methyl formate hardened), SO_2 hardened furan resins, SO_2 hardened epoxy/acrylic (free radical curing), CO_2 hardened sodium silicate (water glass), CO_2 hardened alkaline phenolic.

Hot curing processes include the following processes: hot-box, phenolic and/or furan based, warm-box, Shell (Croning), linseed oil, alkyd oil-baked.

Another way to categorize binders is by the elementary classification of "organic" and "inorganic."

The ester catalyzed silicate no-bake and the CO_2-gassed systems are classic foundry examples of inorganic core binders.

Due to the issues discussed in the monograph on the impact of developments on the border mold/metal in the performance of cast iron with spheroidal graphite and vermicular graphite, especially on the surface layer cast in terms of changes in the structure and the amount of graphite, only those sand mold technologies which may cause the greatest changes in the microstructure of the surface layer and yet are widely used in practice will be discussed in detail. These include:

- furan, acid catalyzed,
- phenolic, acid catalyzed,
- hot box,
- warm box,
- Shell (Croning) process.

2.5.1 Furan, Acid Catalyzed

Sulfonic acid cured furan no-bake (FNB) binders are based upon furfuryl alcohol (FA). Furan resins are made from furfuraldehyde or, more commonly, from furfuryl alcohol, both of which are obtained from agricultural waste products.

These binders are commonly used for the molding and core-making of medium and large sized parts, for small and medium batch production and for all alloy types. Only certain types are used for steel casting, as cracks, fins or pinholes may occur. The process allows for good flexibility in application and properties. FNB binders provide excellent mold and core strength, cure rapidly and allow the sand with which they are used to be reclaimed at fairly high yields.

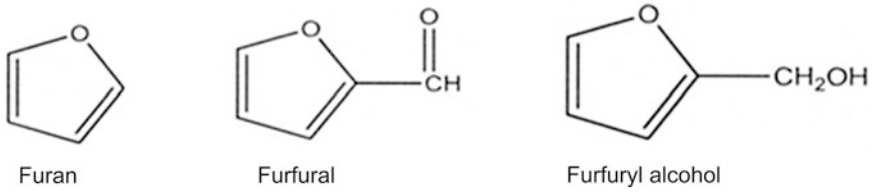

It is a simple two-part binder system made up of an acid catalyst and a reactive furan-type resin. The addition of an acid catalyst to a furan resin causes an exothermic polycondensation, which hardens the binder. The FNB's condensation reaction produces water, which tends to slow the cure rate (dehydration). The bond producing reaction is the further polymerization of these chaines with cross-linking.

The FNB curing mechanism is shown in Fig. 2.1.

In the presence of strong acids, prepolymers of furfural and furfuryl alcohol form polymer films that serve as binders. The curing rate is directly proportional to

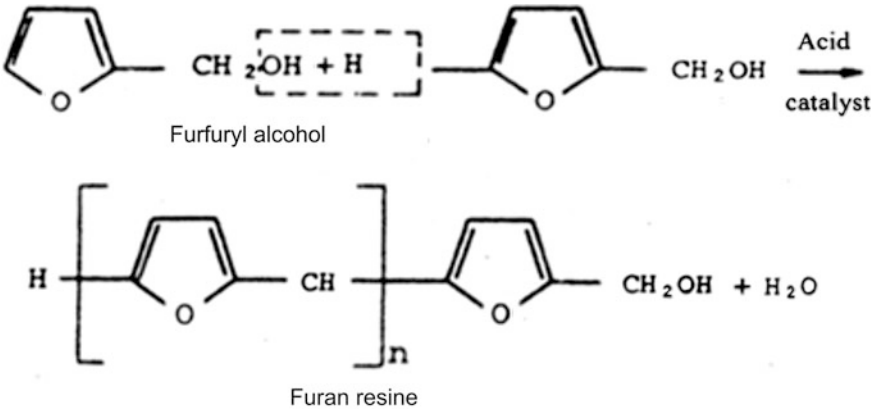

Fig. 2.1 The furan acid-catalyzed no-bake curing mechanism

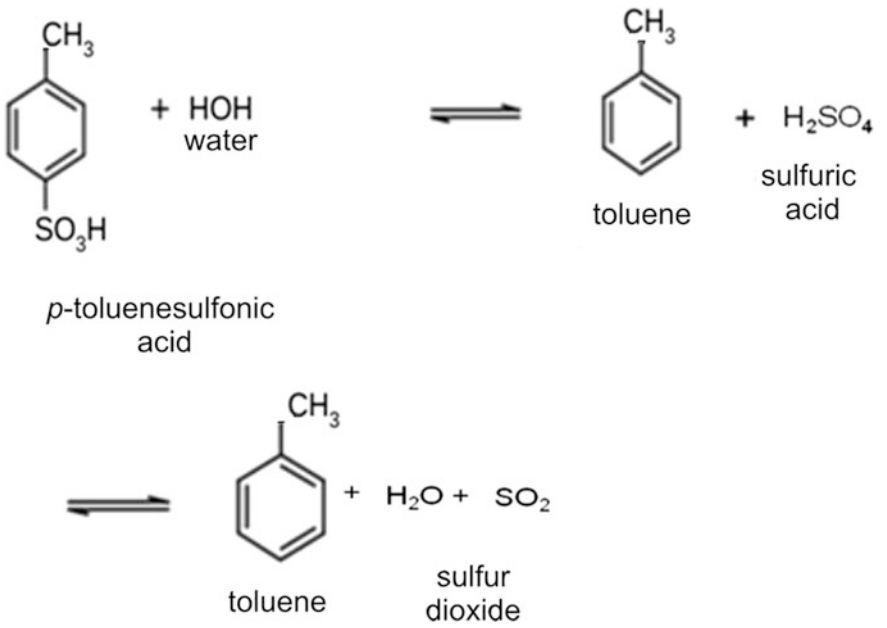

Fig. 2.2 Decomposition of *p*-toluenesulfonic acid under the influence of temperature

the amount of acid and a two-part system can be formulated with a well-controlled curing time.

The conventional sulfonic acid hardener for no-bake furan resin contains toluenesulfonic acid, which decompose under the thermal effect of the liquid metal during pouring, according to the following equation [13] (Fig. 2.2):

The resulting SO_2 adsorbs on the surface of the liquid metal, and decomposes to give a sulfur atom:

$$SO_{2(g)} = S + 2O$$

Sulfur atoms diffuse in the liquid metal causing the sulfidation of the surface layer of the casting. Sulfur may enter into a reaction with Mn, Fe, Mg to form sulfides of the S type (Fe, Mn, Mg) having low melting point. Therefore, much attention is paid to how to reduce the impact of SO_2 gas released from the sand mold with furan resin on the quality of the castings.

Furan binders can be modified with urea, formaldehyde, phenol, and a variety of other reactive or non-reactive additives. In this way different furan resins, which are based on furfuryl alcohol are obtained [10]:

- furan resin (FA);
- urea-formaldehyde–furfuryl alcohol (UF–FA);
- phenol-formaldehyde–furfuryl alcohol (PF–FA);

- urea-formaldehyde–phenol–furfuryl alcohol (UF–PF–FA);
- resorcinol–furfuryl alcohol (R–FA).

Nitrogen content in furan resin varies from 0 to 2 %, i.e., zero, low, medium, and high nitrogen furan-types. Water content can range from 0 to 30 %. The lower the nitrogen and water content, the higher is the grade of furan binder [14].

UF resins contain about 17–18 % mass N. Nitrogen may cause defects in the cast steel and high quality cast iron castings, so that it is reasonable to use a resin with a high FA content (80–95 % mass FA, 3.5–1 % mass N) although they are more expensive than resins with a lower FA content. This is particularly advantageous when using high-quality sands for which the resin additive is a <1.0 %), and hence the nitrogen content is low.

There are also UF–PF resins available with a low content of nitrogen, which are the most commonly used sands of lower quality, when it is necessary to add more of the resin (>1.2 %).

A silane (0.1–0.3 % mass) is nearly always added to enhance the resin-sand bond (to significantly increase strength and to improve its moisture and humidity resistance).

The function of the FNB acid catalyst is to neutralize the alkaline contaminants (materials having a pH value greater than 7) in the sand. Then it initiates and sustains the FNB's condensation-type curing and cross linking reaction. The acid catalysts are in order of increasing reactivity, 75 % phosphoric, 85 % phosphoric, toluene sulfonic, xylene sulfonic, and benzene sulfonic sometimes with an addition of sulfuric or phosphoric or lactic acid, usually used in a diluted form [10]. All of the acid catalysts are carried in water, and the sulfonic-types usually contain various percentages of alcohol as well. The use of phosphoric acid may necessitate a lower reclaim rate.

The amount of FNB binders used ranges between 0.9 and 1.2 % based on sand weight. Acid catalyst levels vary between 30 and 50 % based on the weight of the binder and depend on the temperature of the sand and the necessary curing rate. The speed of the curing reaction can be adjusted by changing the catalyst type or percentage, given that the sand type and temperature are constant (the optimum temperature of the sand is 20–30 ºC) [15–17].

The use of furan binders is, however, associated with a number of casting defects, the most serious being sulfur damage, which leads to a poor surface finish in some steel and destruction of near-surface graphite spheroids in ductile irons. The presence of urea-based resins in some types of furan binders may also lead to nitrogen damage [11].

The thermal decomposition products of the medium nitrogen furan binders are expected to include hydrogen, carbon monoxide, carbon dioxide and methane. The use of urea extenders may add nitrogen compounds to the effluent and the sulfur-bearing acids may introduce sulfur compounds, including sulfur dioxide and hydrogen sulfide to the effluent [18–22].

Since furfuryl alcohol was classified by the European Union as a compoud with a probable carcinogenic influence in terms of its effect on the body, the EU directive (Regulation EC No. 1272/2008) requires that the content of free (monomer) furfuryl alcohol in resin be less than 25 % mass.

To limit the emissions of sulfur compounds during the pouring of molds with molten metal, new types of catalysts were developed, where part of the sulfonic acid was replaced with inorganic acids. The sulfur content of these catalysts is 20–50 % of that in traditional sulfonic acid [23, 24].

Molding sands hardened with sulfonic acids may be subjected to a reclamation process but the sulfur content in the molding sand is increased, which favors the occurrence of defects in castings from iron alloys, particularly ductile iron. This can also be a problem due to the environmental emissions generated during pouring SO_2 gas.

Molding sands with furfuryl resins undergo mechanical reclamation well and it is often possible to reduce the addition of the resin when using reclaimed sand and matrix. The loss on the ignition of reclaimed sand should be less than 3 % mass. The content of sulfur and nitrogen in reclaimed sand should not exceed 0.15 % mass. The nitrogen content of 0.15 % mass or more in molding sand can cause defects in cast iron and steel castings. The sulfur content greater than 0.15 % in sand mold can cause degeneration of the nodular graphite into flake graphite in the surface layer of SGI castings.

The calculation of the amount of sulfur by weight of molding derived from the acid catalyst (*PTSA*) (*example*)

A binder component which introduces sulfur into the sand mold with furfuryl resins is the acid catalyst. This is generally a mixture of p-toluenesulfonic acid (PTSA) 65 % (MW 172.2, the sulfur content of 18.62 % mass) and sulfuric acid (H_2SO_4), concentrated at 1 % mass (MW 98.08, a sulfur content of 32.68 % mass). Let's do the calculations for the weight of 1 kg sand, which contains 0.5 % mass of the catalyst, i.e. 5 g of acid catalyst/1 kg of molding sand (1 % mass using resin in sand mold).

Example

Since the sulfuric acid in the acid catalyst is 1 % mass, so the content of inorganic sulfur in 5 g of catalyst:

$$S_{H_2SO_4} = 0.0163\,\text{g S}$$

The catalyst also contains 65 % mass of PTSA, then 5 g of catalyst contains organic sulfur in the amount of:

$$S_{PTSA} = 0.60\,\text{g S}$$

The total amount of sulfur contained in 5 g of catalyst:

$$0.0163\,\text{g} + 0.60\,\text{g} = 0.6163\,\text{g S}$$

Hence the sulfur contained in the catalyst equals 12.33 %, whereas the sulfur coming from PTSA—12.00 % (organic sulfur) and sulfur coming from H_2SO_4, only 0.33 % (inorganic sulfur). Which means that PTSA brings 97.3 % of sulfur to the sand mold and sulfuric acid only 2.7 %.

As we may see from the above calculations, the most effective way of reducing the quantity of sulfur introduced into the sand mold by the acid catalyst is to reduce the amount of sulfonic acids added or replace them with other compounds. Sulfur contained in sulfuric acid represents a small fraction of the total sulfur contained in the acid catalyst.

Figure 2.3 shows the dependence of the total amount of sulfur in the acid catalyst on the share of the PTSA in the acid catalyst, at a fixed concentration of sulfuric acid.

For example, at a fixed concentration of 8 % H_2SO_4, reduction of the PTS acid from 65 to 50 % will reduce the total amount of sulfur by 19 %. A similar effect could be achieved by reducing the share of sulfuric acid from 8 to 0.5 %.

Figure 2.4 shows the dependence of total sulfur in the acid catalyst on the share of the H_2SO_4 in the acid catalyst, at a fixed concentration of the PTSA.

Both graphs show that the effective and efficient reduction of the total amount of sulfur in the acid catalyst should primarily be achieved by reducing the share of the PTS acid. However, to obtain an adequately strong hardener it is necessary to replace a portion of the sulfonic acid with a strong sulfur-free acid. In contrast, efforts to reduce the amount of sulfur by reducing the amount of sulfuric acid in the acid catalyst are not very effective. Binders developed by different manufacturers for foundry for low-sulfur catalysts composed of a mixture of non-sulfur strong organic acids and aliphatic or aromatic toluenesulfonic acid, and H_2SO_4 are

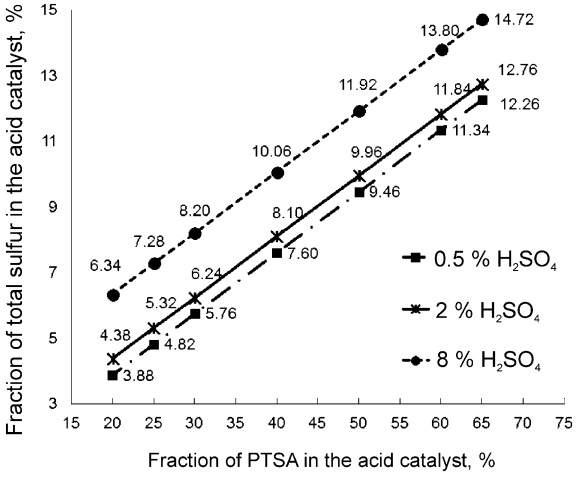

Fig. 2.3 Dependence of the total sulfur content on its share in the acid catalyst PTSA

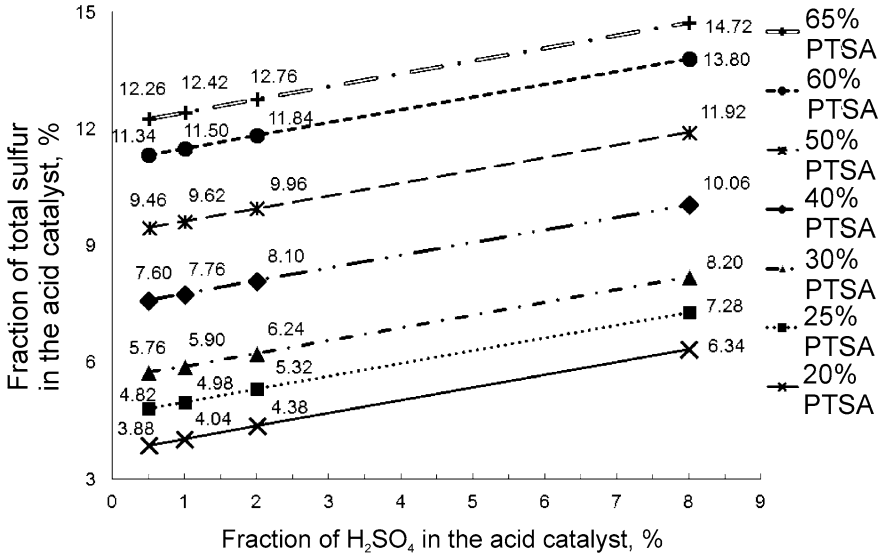

Fig. 2.4 The dependence of the amount of the proportion of the total sulfur acid H_2SO_4 catalyst

effective (possibility of reducing the sulfur content of the acid catalyst by about 50 %). A disadvantage of the acid catalyst is a higher price compared with a conventional acid catalyst based on the PTS acid.

New acid catalyst that contains only 0.25 % mass of free H_2SO_4 and two times less S than conventional catalysts has been developed.

2.5.2 Phenolic, Acid Catalyzed

Acid-cured phenolic no-bake resins as the components are relatively cheap, it is mainly used for the production of large parts. It is applicable for all alloy types. The hardening of these resins is more difficult and less regular compared to the furan resins. Sand mixes made with these resins have adequate flowability for the filling of mold patterns or core boxes. The resins are either phenol-formaldehyde (PF), or urea-formaldehyde/phenol-formaldehyde copolymers (UF/PF). For example, phenol-formaldehyde resins (resins "resole") are obtained by the reaction of phenol with excess formaldehyde in an alkaline environment (a formaldehyde/phenol ratio higher than one). They have a linear construction, and are soluble in organic solvents. Resole resins include methylene (–CH_2–) and hydroxymethylene groups (–CH_2OH–). One disadvantage of acid-cured phenolic no-bake resins is their relatively poor storage stability (Fig. 2.5).

The catalysts for the phenolic no-bake resins are strong sulfonic acids, such as p-toluene, xylene or benzene-sulfonic, sometimes with the addition of sulfuric acid,

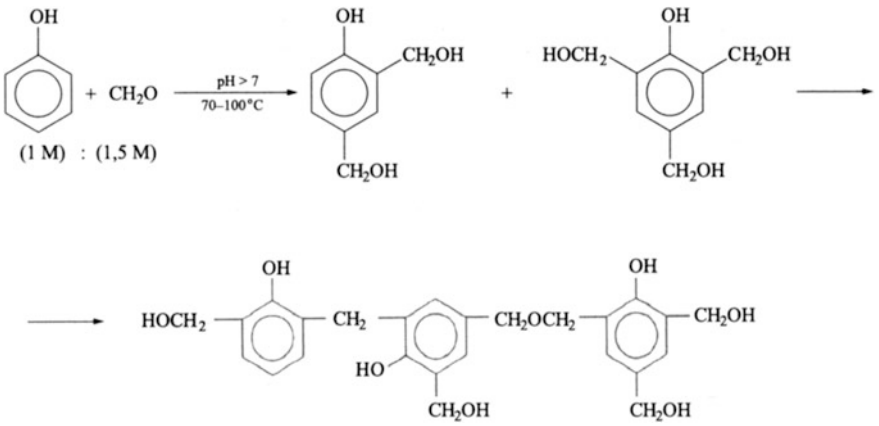

Fig. 2.5 Reaction scheme of PF resole resin formation

usually used in a diluted form. Phosphoric acids will not cure phenolic resins at the rate required for most no-bake foundry applications.

The resole resin may be polymerized with a strong acid (sulfonic acid):

$$\text{Phenolic resin(resole resin)} + \text{Acid catalyst} \rightarrow \text{Cured polymer} + \text{Water}$$

The catalyst initiates further condensation of the resin and advances the cross-linking reaction [25–27].

The condensation reactions produce water which results in a dilution effect on the acid catalyst that tends to slow the rate of cure. Due to this effect, it is necessary to use strong acid catalysts to ensure an acceptable rate of cure and good deep set properties.

Thermal decomposition products of phenolic resin include CO, CO_2, phenol, benzene, toluene and PAHs. Use of a sulfur-containing organic acid produces SO_2 and H_2S on the mold/metal interface [28–30].

2.5.3 Shell (Croning) Process

This process is the only one among all molding and core-making processes that can use pre-coated sand, directly available from suppliers and ready for use, although pre-coating the sand may also be performed at the foundry.

The sand is cured by heating it in a metallic pattern, producing a hardened surface layer. The cured sand forms a “shell”, which has given its name to the process. This process gives high dimensional accuracy and a good surface finish to

the castings, good shake out and de-coring properties and allows a nearly unlimited storage time for the pre-coated sand. Its use is restricted to the production of small or medium sized molds and cores in mass production.

The shell sand binder uses a novolac resin (phenol-formaldehyde) that requires formaldehyde to create the phenolic polymer that binds the sand. Novolac resins are obtained during the reaction of phenol with formaldehyde in acidic medium, using a slight insufficiency of formaldehyde (Fig. 2.6).

Since novolac resins contain only methylene groups (–CH_2–) and do not contain methylol groups (–CH_2OH–) such as resole resins, the same heating of these resins does not cause further cross-linking reactions and (they are thermoplastic). Only the addition of a formaldehyde-releasing compound causes end hardening.

This binder component is added to the sand in the form hexamethylenetetramine (as a hardener), that decomposes at 160 ºC into ammonia and formaldehyde when heated:

When pre-coated sand contacts the heated pattern, the hexamethylenetetramine decomposes and the formaldehyde cross-links the resin binder to form the characteristic strong bond. The presence of hexamethylenetetramine in sand mold does not cause bonding and the mixture needs to be heated to a predetermined temperature in order to harden it.

$$\text{Phenolic resin(novolac resin)} + \text{Hexamethylenetetramine} + \text{Heat} \rightarrow \text{Cured polymer} + \text{Water}$$

During the thermal decomposition of the binder CO, CO_2, and various hydrocarbons will be emitted, in addition to traditional gas, and additionally nitrogen

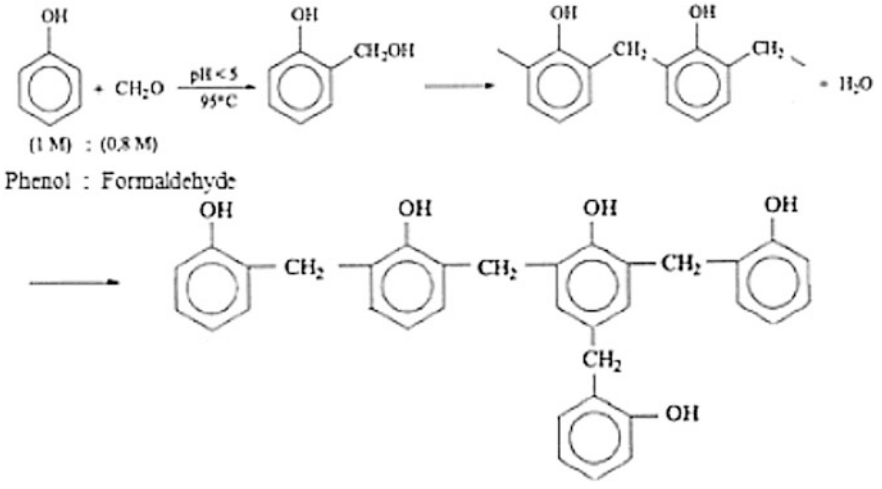

Fig. 2.6 Formation of a "novolac" phenol-formaldehyde resin

compounds in significant quantities. Also, when coated sands are heated, free formaldehyde may be released [31].

2.5.4 Furan Hot-Box

The hot box process is a development of a shell molding process, however it differs from it with three elements: it is only used for the preparation of cores, full cores are made (no shell) and the binding reaction is exothermic, which promotes the further hardening process after removing the heat source, namely, after removing the core of the core box.

The process can produce cores of a high dimensional accuracy and good mechanical strength. It provides a high dimensional accuracy, which can only be achieved by means of using high quality (metal) patterns, which can be very expensive. For this reason, the furan hot-box process is currently used in the manufacturing of small or medium sized cores in mass production.

Conventional hot box resins are classified simply as furan or phenolic types. The furan types contain furfuryl alcohol, the phenolic types are based on phenol, and the furan-modified phenolic has both. All conventional hot box binders contain urea and formaldehyde resin binder and a heat activated catalyst are pre-mixed with sand and the mixture is blown into a heated corebox, where it is cured. A wide range of resins: urea-formaldehyde, urea-formaldehyde–furfuryl alcohol, urea-formaldehyde-phenol are used. The catalysts are aqueous solutions of ammonium chloride or ammonium nitrate (acid salts), with urea additions to reduce the free formaldehyde. The typical amount of catalyst used varies from 10 to 25 % mass based on the resin weight. The addition ratio for the resin varies from 1.2 to 3.0 % mass based on the sand weight. The temperature used for the pattern ranges mostly from 230 to 290 ºC.

The furan hot box resin has a fast cure compared to that of the phenolic-type system and can therefore be ejected faster from the core box. Furan resin also provides a superior shake out and presents fewer disposal problems due to the lack of phenol. Typical resin content is 1.5–2.0 % mass. A simplified hot box reaction mechanism is:

$$\text{Liquid resin} + \text{Catalyst} + \text{Heat} = \text{Solid resin} + \text{water} + \text{heat}$$

Hot curing processes are characterized by major emission problems: when heated, the resins and catalysts emit noxious chemicals including ammonia and formaldehyde that can be the source of odor nuisance. Ammonia is decomposed into nitrogen and hydrogen; the said gases dissolve in the melt casting and often cause pinholes in the cast steel and ductile iron casts. Therefore, resins with a lower content of nitrogen, formaldehyde and water are used for the casting from these materials.

2.5.5 Warm-Box

This process is very similar to the hot-box process and uses the same production techniques. Only the type of resin differs, which allows for curing at a lower temperature. However, this kind of resin is significantly more expensive comparerd to those used in the hot-box process. The binder is furfuryl alcohol-based, with a typical composition containing around 70 % mass furfuryl alcohol or a low polymer of furfuryl alcohol. Accordingly, the tool temperature can be held at around 180 °C, which leads to major energy savings of about 15–25 % mass compared to the hot-box. The warm box resin is a minimum-water (<3 %), furfuryl alcohol-type resin (furfuryl alcohol content: ~70 %) that is formulated for a nitrogen content of less than 2.5 % mass. Since the resin/sand mix exhibits a high degree of rigid thermoset properties when fully cured, little or no post strip distortion or sagging occurs.

The catalysts are copper salts derived from aromatic sulfonic acids, in water or an alcohol solution. The catalyst amount used is 20–35 % mass, based on the resin weight. These catalysts are unusual in that they impart an excellent latent property (unreactive at room temperature, reacting only upon heating) to the binder system, but still form strong acids when heated. They promote a thorough curing action at temperatures of approximately 65 °C or higher.

A simplified warm box curing reaction mechanism is:

$$\text{Furan resin} + \text{Latent acid}(\text{H}+) = \text{Cured furan binder}$$

The binder components remain stable when mixed together in the proper ratios in sand until activated by heat, which decomposes the catalyst and releases the acid that causes the resin to polymerize. The pattern temperatures used range from 150 to 230 °C. The optimum temperature of 190 °C is about 55 °C below the operating temperature for hot box binders. Warm box resins are low in nitrogen.

References

1. Reisener H (1962) Some aspects of the formation and structures of a skin on iron castings and a method used to obviate its occurrence. Br Foundryman 55:362–369
2. Matijasevic S, Gomes-Gallardo J, Wallance J (1974) Ferritic surface layers on gray iron castings. AFS Trans 82:571–622
3. Narasimha G, Wallace J (1975) Factors influencing the ferritic layers on the surface of gray iron castings. AFS Trans 83:531–550
4. Boonmee S, Stefanescu DM (2012) The mechanism of formation of casting skin on cg iron and its effect on tensile properties. Foundry Trade J 186:225–228

5. Martin F, Karsay S (1979) Localized flake graphite structure as a result of a reaction between molten ductile iron and some components of the mold. AFS Trans 87:221–226
6. Xiaogan H, Jin X, Xuqi D, Yaoke W (1992) Nodular iron surface deterioration due to PTSA in resin. AFS Trans 100:9–15
7. Riposan I, Chisamera M, Stan S (2013) Control of surface graphite degeneration in ductile iron for windmill applications. Int J Metalcast 7(1):9–20
8. Tinebra JP, Wilson SJ (1993) No-bake chemical binder systems: their effect on microstructural and physical properties of ductile iron. AFS Trans 101:169–174
9. Riposan I, Chisamera M, Stan S, Skaland T (2006) Factors influencing the surfaces graphite degeneration in ductile iron castings in resin mold technology. In: Proceedings of the 8th international symposium on the science and processing of cast iron, Beijing, China
10. European Commission (eds) (2005) Integrated pollution prevention and control. Reference document on the best available techniques in the smitheries and foundries industry
11. Campbell J (2011) Complete casting handbook. Elsevier, Oxford
12. Baier J, Koppen M (1994) Manual of casting defects. incidence and avoidance of defects attributable to moulding sands. IKO-Erbsloh, Marl, pp 221–226
13. Jin XU (2005) An investigation of the abnormal structure at the surface layer of nodular iron castings produced by furan resin bonded and sulfonic acid cired sand mold. J Foundry 12:1245–1249
14. Bats CE, Scott WD (1977) Decomposition of resin binders and the relationship between the gases formed and the casting surface quality. Part 3. AFS Trans 85:209–226
15. Archibald JJ, Smith RL (1962) Resin binder processes in molding methods and materials. American Foundrymen's Society, New York
16. Walton C F, Opar T J (1981) Iron casting handbook. Iron Casting Society, New York
17. Carey P, Lott M (1995) Sand binder systems. Part V—Furan no bake. Foundry Manag Technol 123(7):26–31
18. Wilkes GF, Wright RL (1972) TSA—another catalyst for furan no-bake. Foundry 100(3):81–94
19. Nelson B (1973) An evaluation of toluenesulfonic acid as catalysts for furan no –bake foundry binders. AFS Trans 81:153–157
20. Holtzer M, Dańko R, Kubecki M, Żymankowska-Kumon S, Bobrowski A, Kmita A, Górny M (2014) Influence of the reclaim addition to the moulding sand with furan resin on the emission of toxic gases at high temperature. In: 71st world foundry congress: advanced sustainable foundry, Bilbao, 19–21 May 2014
21. Holtzer M, Bobrowski A, Dańko R, Kmita A, Żymankowska-Kumon S, Kubecki M, Górny M (2014) Emission of polycyclic aromatic hydrocarbons (PAHs) and benzene, toluene, ethylbenzene and xylene (BTEX) from the furan moulding sands with addition of the reclaim. Metalurgija= Metallurgy 53(4):451–454
22. Holtzer M, Żymankowska-Kumon S, Bobrowski A, Dańko R, Kmita A (2014) The influence of reclaim addition on the emission of PAHs and BTEX from moulding sands with furfuryl resin with the average amount of furfuryl alcohol. Arch Foundry Eng 14(1):37–42
23. Tan Rui, Liu Jlajun (2010) Study on modified furan resin foundry binder systems for large steel castings. In: Proceedings of 69th world foundry congress, Hangzhou, HA catalog, 16–20 October 2010
24. Hussein NIS, Ayof MN, Mohamed Sokri NI (2013) Mechanical properties and loss on ignition of phenolic and furan resin bonded sand casting. Int J Mining Metal Mech Eng (IJMMME) 1(3):223–227
25. Florjańczyk Z, Penczek S (eds) (2002) The polymer chemistry, vol 2. Publishing House of the Warsaw University of Technology, Warsaw (in Polish)
26. Lewandowski J L (1997) Materials for foundry molds. Akapit, Kraków (in Polish)
27. Ellinghaus W (1993) Kernherstellungsverfahren der neunziger jahre. Giesserei 80(5):142–146

28. Psimenos ACh, Eder G, Scheitz W (2009) Die schwefelreduktion beim nobake verfhren. Giesserei-Rundschau 56(H1/2):2–6
29. Psimenos ACh, Scheitz W, Eder G (2007) Neue emissionsarme no-bake Harz und –Harter. Giesserei 94(04):42–53
30. Brown JR (ed) (2000) FOSECO Ferrous Foundryman's Handbook. Butterworth Heinemann, Foseco International Ltd, Oxford
31. Holtzer M, Bobrowski A, Dańko R, Żymankowska-Kumon S, Kolczyk J (2013) Influence of a liquid metal temperature on a thermal decomposition of a phenolic resin. Arch Foundry Eng 13(2):35–38

Chapter 3
Methods of the Mold Sands Quality Assessment

Rafal Dańko

Abstract This chapter on methods for assessing the quality of the matrix and molding sand presents the most important properties of these materials, from the point of view of the feasibility of using these molding sands for producing sound castings. In the case of matrix testing (both fresh and reclaimed), attention was drawn to the size and shape of the grain, which have a decisive influence on the permeability of the molding sand, on the content and the activity of the binder for the matrix used for the preparation of green sand, loss on ignition and the chemical nature of the matrix evaluated on the basis of the parameters such as ADV and pH. The next section presents complementary research methods of molding sand properties with reclaimed sand. Modern systems require evaluation and a careful approach to the factors that determine molding sand suitability for both technological use as well as the impact on the surrounding environment. In this context, a full evaluation of the quality of the reclaimed matrix goes beyond the usual instrumental methods and requires the addition of advanced apparatus research methods. This allows one to put the evaluation of the reclaimed matrix into perspective, both in terms of its use for the preparation of molding sand, as a substitute for fresh sand, and also in terms of environmental protection. Such modern methods may include, inter alia, an assessment of gas excretion in molding sand, identification of the type of emitted gases, the content of BTEX gases that are particularly dangerous to humans, and the evaluation of the surface of the casting made in molding sand with reclaimed sand.

3.1 Investigations of the Molding Sands Fresh and Reclaimed Matrix

The main component is the molding sand matrix—mostly quartz and, in the case of the regeneration process, the reclaimed sand. Matrix molding materials should have the following properties:

© The Author(s) 2015

M. Holtzer et al., *Microstructure and Properties of Ductile Iron and Compacted Graphite Iron Castings*, SpringerBriefs in Materials,
DOI 10.1007/978-3-319-14583-9_3

- resistance to high temperatures,
- resistance to metal oxides at elevated temperatures,
- low thermal expansion,
- lack of polymorphic transformations,
- an appropriate particle size distribution.

All these requirements are met only by several types of sand, including: alumina, zirconium and chromite. However, due to the high price of these materials they are only applied where economically justified. More frequently, less expensive materials do not always satisfy the requirements mentioned above, for example quartz, which is characterized by significant thermal expansion or the occurrence of polymorphic transformations. However, quartz sand, due to its availability and low price is currently most commonly used molding and core sands.

It is assumed that the sand (to which the reclaim also belongs) should be the subject of the following tests allowing its quality to be assessed:

- grain composition,
- the content of the binder,
- pH,
- ADV (Acid Demand Value),
- chemical composition,
- sintering temperature,
- loss on ignition (LOI).

Sand grains, depending on the conditions under which sand was created may have a different size, homogeneity, and shape. The full characterization of the sand grains should be extended to include an assessment of the size, homogeneity and shape of particles, the more that these parameters affect the technological properties of the molding sand, and thus the quality of the castings [1, 2].

The size of the sand grains influences the technological properties of the molding sand and the course of events taking place on the surface of the mold cavity or the core upon contact of the surface with the liquid metal. The effect of the sand grains particle size is reflected primarily in the case of mold sands permeability (P_i), the property of which, when other parameters remain constant, increases exponentially with the increasing diameter of the sand grain particles. This relationship is given by the following formula:

$$P_i = c \cdot d_L^2 \tag{3.1}$$

where:

d_L the average grain size of the sand matrix, mm

c ratio—depending on the shape and uniformity of the sand grains

Excessive increase in the sand grains size with simultaneously high homogeneity, favors the phenomenon of penetration of the liquid metal into the pores of the molding sand, which increases the roughness of the casting surface, and in extreme

cases, can cause casting defects such as burn-on. The excessively low permeability of the molding sand may in turn be dangerous so it is not possible to discharge gases arising at the interface of the metal-mold casting.

The homogeneity of the sand grains affects not only the technological properties of the molding sand, but also the behavior of the mass under high temperatures. The effect of the grain sands homogeneity on the behavior of the molding sand under the influence of high temperatures is observed in the case of materials with high thermal expansion, especially quartz sand. Molding sands with sand grains of high uniformity obtain the structure (after densifying) that creates a low leveling effect of the possibility of expansion of the individual particles of the sand grains for thermal expansion of mold sand. Therefore, it is not always advantageous to use very homogeneous quartz sand grains, and sometimes even deliberately use less homogeneous grain sands, that is, one in which the main part of the grains consists of several fractions of particles of different sizes.

The shape of the sand grain particles is also important for the strength of the molding sand due to its significant impact on the specific surface area. This volume is also very important when it comes to the use of binding materials. The consumption will be smaller when the shape of the grains are closer to spherical shape. In carrying out the molds, the links between the matrix and the compaction of molding sands are also measured. The insufficient compacting is observed for the molding sand containing the grains of an angular shape. It can also lead to deterioration of molding sand susceptibility, which can cracks in castings made with alloys with a higher shrinkage.

The value of pH and Acid Demand Value (ADV) are very important especially in the assessment of the quality of the reclaimed sand grains as it affects its applicability in various technologies. Reclaimed matrix should be used in the technology similar to the spent sand origin technology.

The term adhesive means all materials present in the sand, clay and sand molds with a size equal to or less than 0.02 mm. The principle of assessment binder content in the matrix consists of sand washed away from the surface of the particles and then its separation using Stokes formula for the speed of movement of the particles in the liquid:

$$v = \frac{F_s}{6\pi R\eta} \tag{3.2}$$

where:

v speed of movement of the particle, m/s
F the force applied to the particles, N
R radius of the particle, m
H dynamic viscosity of the liquid, N s/m^2
F_s Stokes force, N

$$F = \frac{4}{3} \cdot \pi R^3 (\gamma_1 - \gamma_2) \tag{3.3}$$

where:
γ_1 specific gravity of the material particles, N/m^3
γ_2 specific gravity of the liquid, N/m^3

Using both designs are:

$$v = \frac{d_L^2 (\gamma_1 - \gamma_2)}{18\eta} \tag{3.4}$$

Evaluation of the content of the binder in the sand grains is particularly important in terms of its use for the preparation of chemically-bonded sand, in which case the binder content in the matrix should be close to 0.

The chemical analysis of sands are carried out to determine whether given in the standards its composition requirements are met. The chemical analysis and determination of the components of mineral sands of silica sand grains includes:

- silicon dioxide,
- iron oxide (III),
- dialuminium trioxide,
- titanium dioxide,
- calcium oxide,
- magnesium oxide,
- carbonates,
- clay substances,
- feldspar.

The entire designation carried out above is made during the evaluation of the deposit and periodically during operation. Current analyses in foundries include the following components: SiO_2, Fe_2O_3, carbonates.

The high temperature of the molten metal requires the use of molding materials of suitable strength to the temperature, meaning, a high fire resistance. Generally the requirements for fire resistance sands and thus molding increases with the increasing temperature of the molten alloy. A small fire resistance value may cause the formation of surface defects such as burn on. It should be noted that the results of the determination of the sintering temperature, do not give a full assessment of the molding material for resistance to the high temperature of the molten alloy. It is connected on the one hand to the operation of additional factors (e.g. the interaction of the metal oxide and the molding material), and on the other with the methods of research, which does not adequately reproduce the conditions existing in the mold.

3.2 Investigations of the Molding Sand Properties, Including Molding Sand with Reclaim

Assessment methods of molding sands, including the molding sands with the reclaim as well as criteria for evaluation of reclaim quality are presented in Table 3.1. The molding sands, due to their nature, are divided into two main groups: the classic molding sands with bentonite and chemically bonded sand, which in turn can be divided into molding sand with an organic binder and an inorganic binder.

The specificity of molding sands with resins, resulting from an organic binder and the nature of its chemical composition, which may affect the quality of castings made from these types of molding sand requires the use of more sophisticated methods of assessing recovered silica sand grains in addition to the standard tests.

The negative impact on the casting surface high-value loss on ignition reclaimed grain sands, as evidenced by its excessive gas evolution ability, is known and described in the literature [2–5], as well as accumulation in the reclaimed sand grains an excessive amount of sulfur and nitrogen, which is the reason for the changes in the microstructure casting surface layer [6–9].

Listed below investigations of molding sands with organic binders with reclaimed matrices belong to the group of important, however still treated as marginal, examinations. These investigations concern assessments of:

- gas evolution rate of molding sands with the matrix after the recycling process,
- carcinogenic aromatic hydrocarbons from the BTEX group (benzene, toluene, ethylbenzene, xylene) content in gases generated during thermal decomposition of molding sands with organic resins,
- determination of sulfur and nitrogen content in molding sands,
- castings surface quality, including surface defects and porosity.

The AGH—University of Science and Technology conducted research on these issues, using molding sand with furfuryl resin, hardener with p-toluenesulfonic acid

Table 3.1 Proposed criteria for the evaluation of molding sands and reclaims from the spent green sands and chemically bonded sands with organic and inorganic binders [3]

Tested parameter	Green sand	Chemically bonded sand	
		With organic binder	With inorganic binder
Sieve analysis	+	+	+
Loss on ignition	+	+	+
The content of clay	+	–	–
Activity of clay	+	–	–
Bending strength	–	+	+
Compressive strength	+	–	–
Compatibility	+	–	–
Friability	+	+	+

(PTSA). Different matrix were used in research: fresh silica sand and reclaims with various purification degrees, characterized by the loss on ignition value.

The molding sand prepared for testing, marked with symbols: sand 1–sand 4, had the following composition:

- sand grains (fresh silica sand or reclaim)—98.5 % mass,
- furfuryl resin—1.0 % mass,
- hardener (p-toluenesulfonic acid)—0.5 % mass.

Granulometric characteristics and loss on ignition of sand grains variants are shown in Table 3.2. The granular analysis of the grain sand was performed by using Analisett22 NanoTec laser apparatus according to the procedure outlined in [2].

It can be noticed, that the loss of ignition of the molding sand with the high-silica matrix after six circulation cycles (sand 4) is nearly three times larger (1.9) than of the molding sand prepared on the fresh sand matrix. Despite the reclamation process, preceding the sand preparation, the matrix itself shows a significant increase of the LOI as the number of circulation cycles increases. This indicates that a spent binder, not removed during the reclamation treatment, is accumulating on grains. The observed effect constituted the justification of undertaking investigations of the molding sands gas evolution rate. The prepared molding sands, to a certain degree, represent other—applied in foundry practice—molding sands with organic binders, in which the reclaimed matrix constitutes either a total or a partial substitute of the fresh silica foundry sand.

Table 3.2 Characteristics of the sand grains size and the loss on ignition of tested sand grains and molding sands (sand 1–sand 4)

Molding sand	Molding sand characteristics		Characteristics indication of the sand grains used in preparation of molding sands (sand 1–sand 4)			
			Grains size analysis (Analisette 22 NanoTec)			Loss on ignition of sand grains
	Type of sand grains	Loss on ignition LOI (%)	d_a (mm)	d_g (mm)	S_t (cm^2/g)	LOI (%)
Sand 1	Fresh silica sand	1.47	0.287	0.235	1173	0.02
Sand 2	Reclaimed sand 2 cycle	2.89	0.304	0.241	1713	1.44
Sand 3	Reclaimed sand 4 cycles	3.86	0.305	0.243	1777	2.41
Sand 4	Reclaimed sand 6 cycles	4.26	0.312	0.252	1812	2.81

d_a the average arithmetic grain size of the sand matrix, mm
d_g the average geometric grain size of the sand matrix, mm
S_t grain specific surface, cm^2/g

3.3 Studies of the Gas Emission from the Molding Sands

Intensive thermal destruction of organic components during casting and large amounts of greenhouse gases emission, posing a threat both to the quality of the casting, as well as for the work safety conditions in the foundry. Endangering factors are:

- the possibility of the migration of gases to the casting and the deterioration of the quality of its surface,
- harmful conditions at pouring stations resulting from the chemical composition of the gases, mainly the presence of polycyclic aromatic hydrocarbons or BTEX compounds of the group.

Own research on greenhouse gases were carried out according to the original method developed at the Faculty of Foundry Engineering of the AGH-University of Science and Technology.

Investigations of the amount and kinetics of gases generated in the process of liquid metal pouring were performed for molding sands variants (sand 1–sand 3), which characteristics can be found in Table 3.2. The obtained emissivity pathways as a time function are shown in Fig. 3.1.

It can be noticed that the most intensive gas evolution occurs directly after pouring the mold with liquid metal. The evolution kinetics presented in Fig. 3.2 allows to state that—under the investigated conditions—the most intensive evolution occurs in the first 90 s after metal pouring. Two peaks of the highest evolution kinetics can be exposed. The first peak is seen directly after pouring shaped elements with liquid metal and the second one approximately 80 s later.

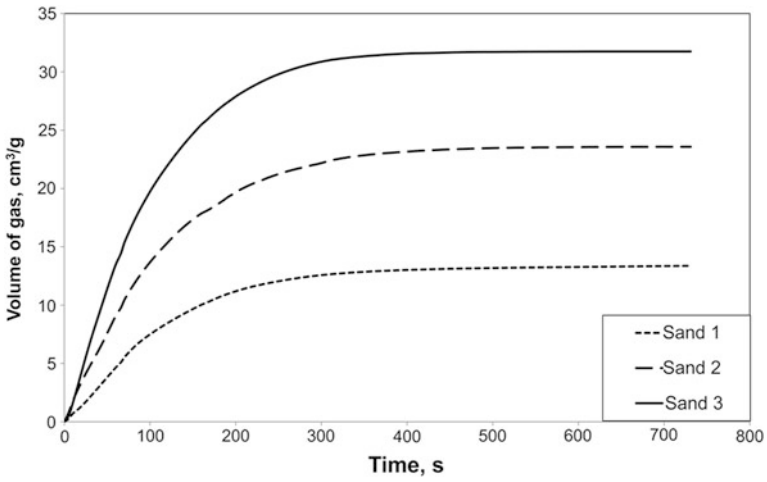

Fig. 3.1 The volume of gas emitted by the test weight of molding in the process of casting molten metal. The pouring temperature is 1350 °C

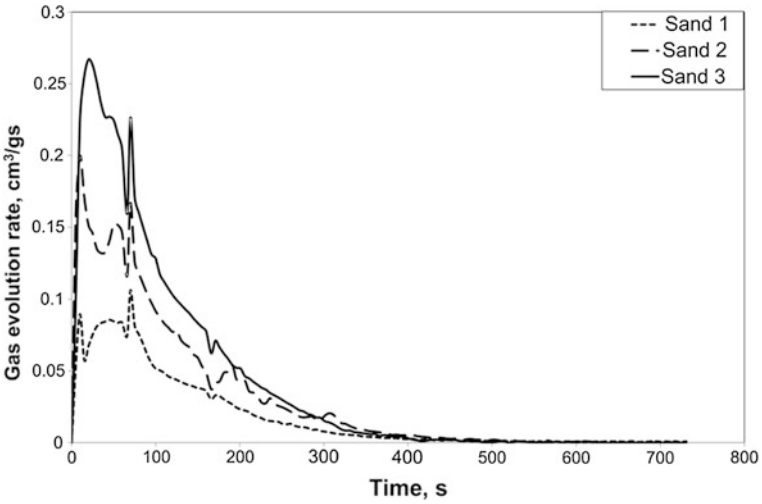

Fig. 3.2 The kinetics of test gases emitted by weight of molding in the process of casting molten metal. The pouring temperature is 1350 °C

The analysis of pathways indicates also that both volume and kinetics of evolving gases depend essentially on LOI of the tested molding sand. The presentation of gas volumes generated by molding sands versus LOI is shown in Fig. 3.3. An application of a molding sand of a higher LOI causes a directly

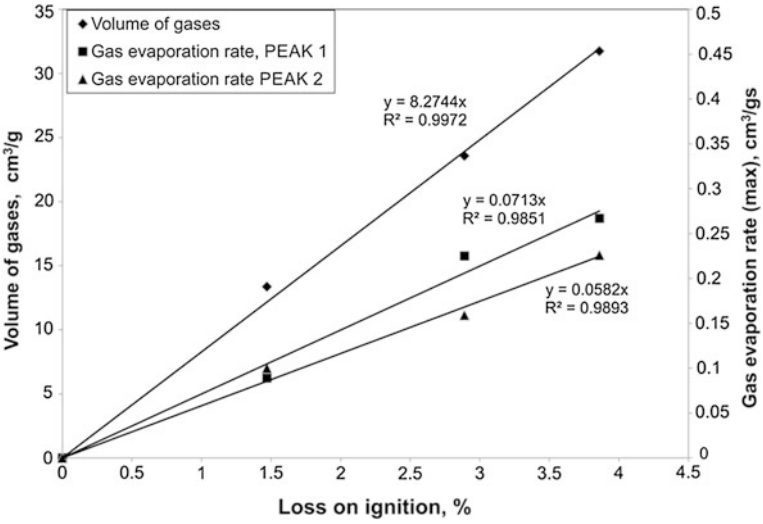

Fig. 3.3 The volume and the kinetics of gases generated as a result of flooding fittings made of molding sand studied as a function of the loss on ignition of molding sand

proportional increase of the gas evolution. A similar conclusion can be drawn from the analysis of the maximum values in the curves of the kinetics of the gases emission from the tested samples, also presented in this figure.

3.4 The BTEX Content in the Exhaust Gases Emitted from the Mold

The gases emitted from the mold after pouring the liquid metal normally consist of compounds that are particularly dangerous, which are aromatic hydrocarbons: benzene, toluene, ethylbenzene and xylene, known as BTEX. At present, the developed standards for emissions from this group are still acceptable for the foundry industry, however attempts are being made to reduce them in the new developed binders.

The study was carried out to determine the content of BTEX compounds emitted from molding sands with furfuryl resins hardened by PTSA. The research was sand 1–sand 3 (Table 3.2), the results of which are shown in Fig. 3.4.

Based on these results it can be concluded that the amount of gases emitted from the BTEX group is greater in the case of molding sands exhibiting a greater LOI. The nature of the change is similar to that found in global greenhouse gases, which allows for the approximate estimation of BTEX emissions based on the knowledge of the loss of ignition of the molding sands. For practical purposes it would be useful to include data on the gas excretion ability and gas BTEX group emission in the catalogs of binders.

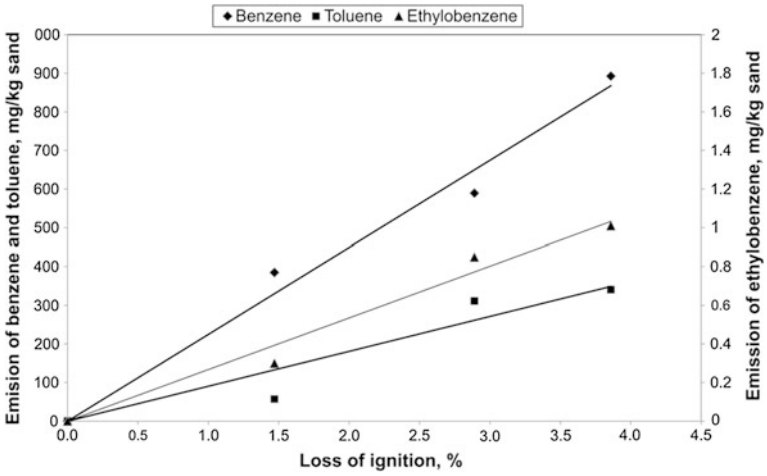

Fig. 3.4 The results of measurement of gas BTEX in the tested molding sands 1–3 with furfuryl resin hardened by p-toluenesulfonic acid

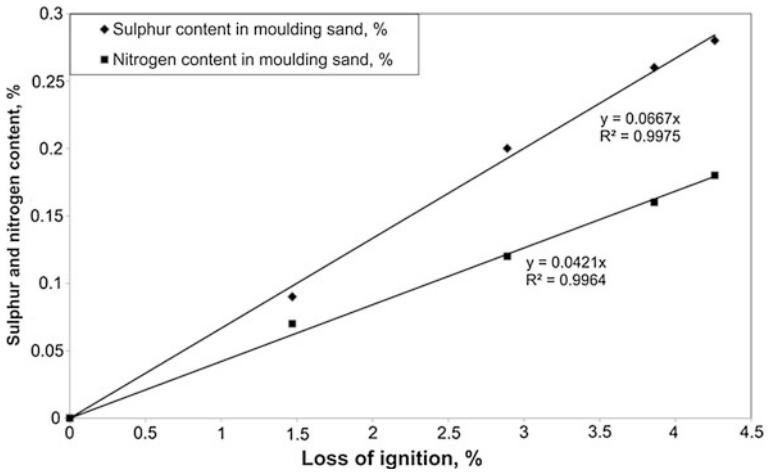

Fig. 3.5 Results of measurements of sulfur and nitrogen in the investigated molding sands with the furfuryl resin hardened by p-toluenesulfonic acid

3.5 Examination of Sulfur and Nitrogen in Molding Sands

Within the study on the quality of the regenerated sand grains, the examination of sulfur and nitrogen content was conducted in 4 molding sands listed in Table 3.2.

The obtained results presented graphically in Fig. 3.5 confirm the effect of accumulating the sulfur and nitrogen content in molding sands which underwent multiple reclamation treatments. The increase of sulfur and nitrogen content in molding sands analysed versus their LOI is nearly linear. Thus, a determination of the limiting thresholds and allowable content of elements being dangerous for the coatings surface microstructure—justifies the more detailed investigations [6–11].

3.6 Experimental Casting Surface Quality

3.6.1 Visual Assessment

Molding sands 1–4 were used to produce the wedge forms according to the ASTM A 536-84 standard. The thermal load of the molding sand, expressed as the mass of the cast to the molding sand: m_{cast}:m_{sand} = 1:1.6 by weight of the casting equal to 1.7 kg. The average apparent density of the thickened molding sand was about 1,600 kg/m^3.

After pouring the molds with liquid spheroidal cast iron of the PN-EN-GJS-500-7 grade, at a pouring temperature of 1400 °C, cooling and casting knocking out, their surfaces quality was analysed. Macroscopic photos of the wedge casting surface cast in molds of self-hardening molding sands with organic resin of various ignition losses are presented in Fig. 3.6.

It can be noticed that the best (visually assessed) surface quality has the casting made in the mold made of the molding sand 1, prepared on the matrix of the pure high-silica sand. The successive castings have worsening surfaces and are developing blowholes as LOI (characterising indirectly the gas evolution rate) of the applied moding sands increase (see Fig. 3.1).

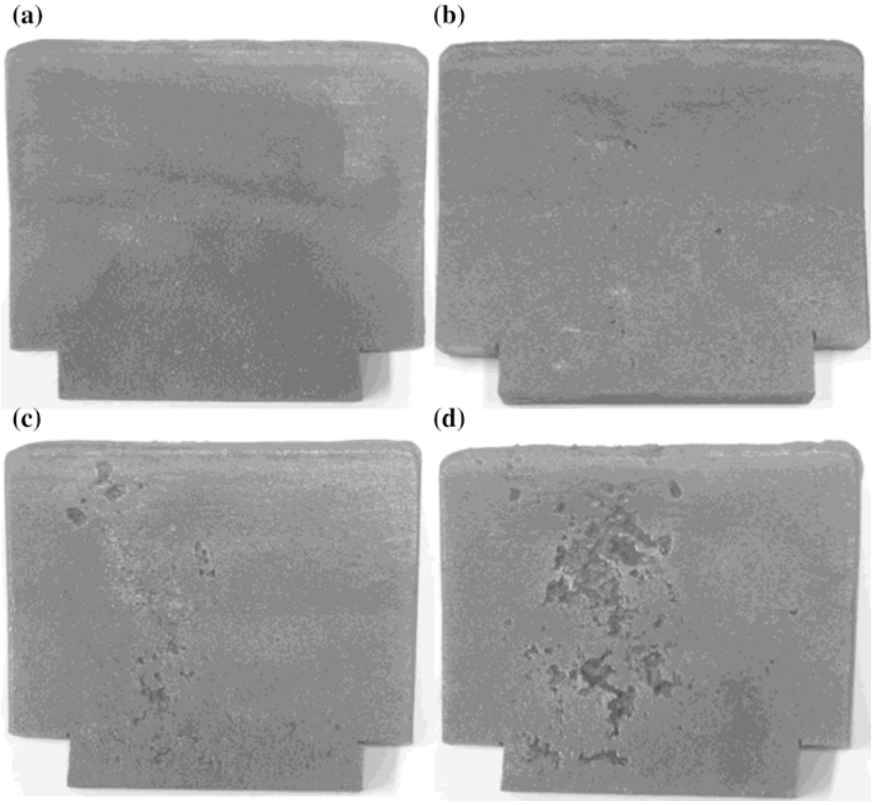

Fig. 3.6 Area of wedge casts ASTM A 536–84 cast from ductile iron in molds with the molding sands of various loss on ignition: **a** sand 1; LOI = 1.47 %, **b** sand 2; LOI = 2.89 %, **c** sand 3; LOI = 3.86 %, **d** sand 4; LOI = 4.26 %

3.6.2 Rating Casting Surface Geometrical Parameters

The study of geometrical parameters of the surface of castings made using a TalyScan 150 camera, Taylor Hobson using TalyMap Expert software v.2.0.19. The measuring length was 6 mm. Measurement accuracy—10 microns.

The study included the height parameters identified in the research process symbols: S_q, S_t, S_h, and S_a defined as follows:

- S_q the rms value of the deviation from the surface of the averaged test surface,
- S_t distance between the elevations and depressions on the surface of the line,
- S_z arithmetic mean of absolute heights of five highest elevations and five deepest cavities of the fracture surface
- S_a arithmetic mean of the absolute height of the five highest peaks and the five lowest valleys of the fracture surfaces

The taken measurements enabled a three-dimensional image representation of the examined surface (3D) sample cut from the cast wedge cast from ductile iron in the chemically-bound molding sand with a different LOI, as shown in Fig. 3.7a–d.

The cumulative list of the determined height parameters for castings made in molds prepared from the investigated molding sands presented in Fig. 3.8, allows to state that the geometrical parameters of the casting surfaces are significantly worsening as sands of an increasing ignition loss are applied. This unfavourable effect can be explained, among others, by changes of the matrix geometrical parameters, which result from the analysis of the average diameters values of high-silica sand grains and reclaims (see Table 3.2). In the case of the matrix reclaimed in the recycling process the grains diameter increases together with its ignition loss, which is related to the accumulation of the spent binder layer on high-silica grains.

Another reason of such worsening of the surface quality is a higher gas evolution rate of the molding sand. This causes local influencing of the casting surface by the binder thermal decomposition products.

The use of reclaimed matrix in the molding sand preparation process, as a substitute for fresh sand requires the development of assessment methods in terms of the harmful effects stemming from the sand grains to the quality of the castings. The posted findings justify the desirability of periodic checks on the grain sands after recycling for the accumulation of the substances that may pose a potential threat to the quality of the casting.

The presented techniques of assessing molding sands on matrices, which underwent recycling processes in multicyclic pathways, introduce new elements into

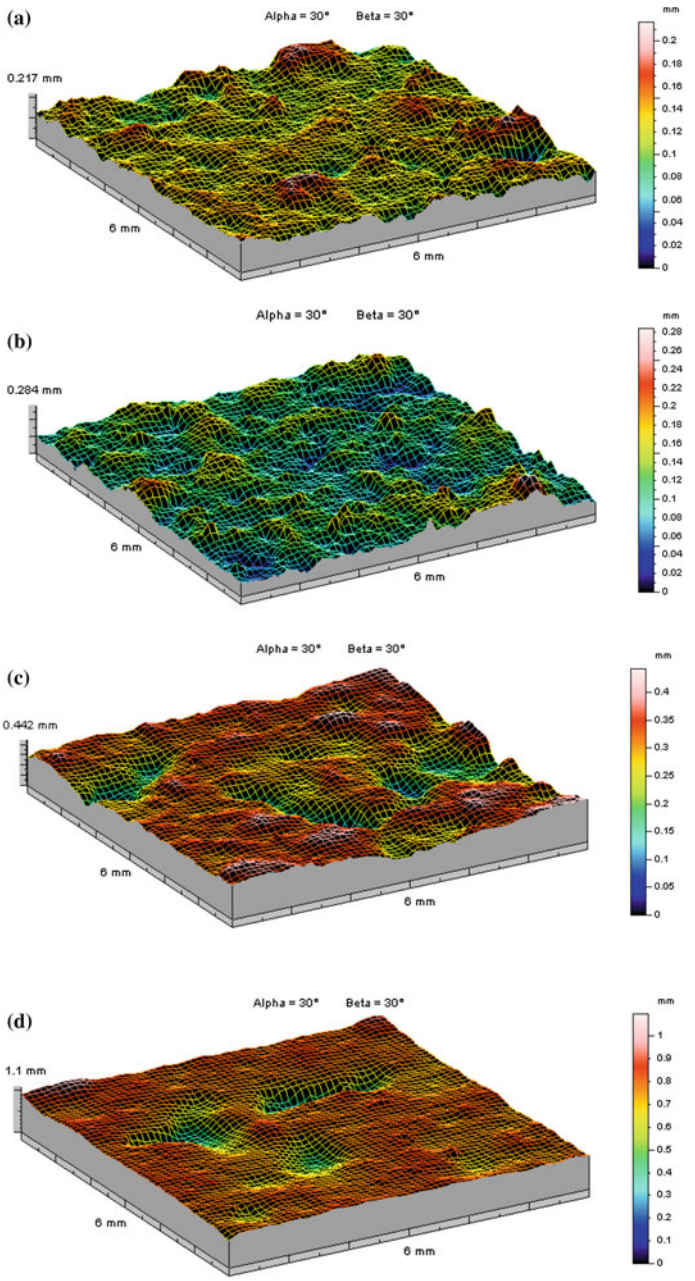

Fig. 3.7 Three-dimensional images (3D) of the surface of the samples of the casting cast in the mold from molding sand **a** sand 1, **b** sand 2, **c** sand 3, **d** sand 4

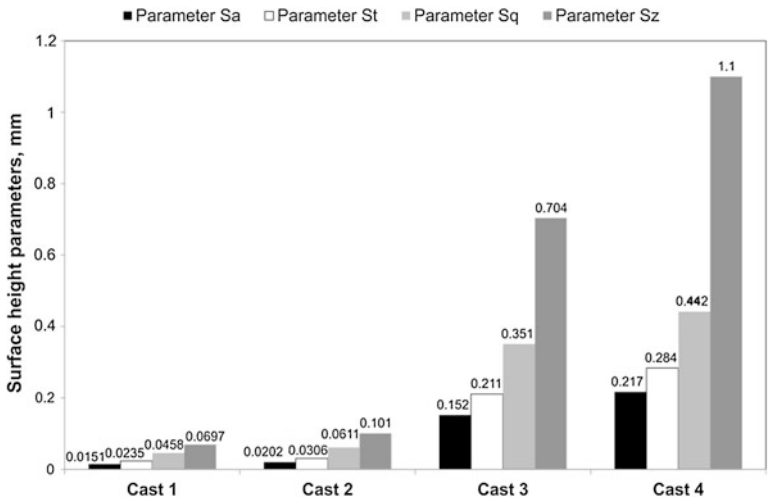

Fig. 3.8 Summary of the geometrical parameters of the height S_a, S_q, S_t, S_h obtained for the cast wedge made according to ASTM A 536–84, made in the molds of the tested types of molding sand

the matrix qualification as a substitute of high-silica sands. Broadening of conventional methods of the matrix quality assessment is especially useful, when obtaining the molding sands of optimal—from the point of view of utilising the reclaim and the casting quality—technological parameters at simultaneous fulfilment conditions related to the environment protection, is aimed.

References

1. Lewandowski JL (1997) Materials for foundry molds. Akapit, Kraków (in Polish)
2. Dańko R, Holtzer M (2010) Moulding sands grain size investigations by means of the laser method of measurement. Arch Metall Mater Sci 55(3):787–794
3. Dańko J, Dańko R, Łucarz M (2007) Processes and devices for reclamation of used moulding sands. Monography. Akapit, Krakow (in Polish)
4. Dańko J, Holtzer M, Dańko R (2010) Problems of scientific and development research concerning the reclamation of used foundry sands. Arch Foundry Eng 10(4):29–34
5. Dańko R (2013) Assessment method of overheating degree of a spent moulding sand with organic binder, after the casting process. Arch Foundry Eng 13(2):11–16
6. Riposan I, Chisamera M, Stan S, Skaland T (2006) Factors influencing the surface graphite degeneration in ductile iron castings in resin mold technology. In: Proceedings of the 8th international symposium on the science and processing of cast iron, Beijing, China
7. Torrance JW, Stefanescu DM (2004) Investigation on the effect of surface roughness on the static mechanical properties of thin-wall ductile iron castings. AFS Trans 112:757–772
8. Boonmee S, Stefanescu DM (2013) Effect of casting skin on the fatigue properties of CG iron, Int J Metalcast, 15–26

9. Boonmee S, Stefanescu DM (2012) The mechanism of formation of casting skin and its effect on tensile properties. Foundry Trade J Int 186:225–228
10. Stefanescu DM, Wills S, Massone J (2009) Quantification of casting skin in ductile and compacted graphite irons and its effect on tensile properties. AFS Trans 09–12:587–606
11. Dańko R, Holtzer M, Górny M, Żymankowska-Kumon S (2014) Effect of the quality of furan moulding sand on the skin layer of ductile iron castings. ISIJ Int 4(6):1288–1293

Chapter 4
Reclamation of Used Molding Sands

Rafał Dańko

Abstract In this chapter, the main attention is focused on the theoretical and practical aspects of the reclamation of the molding and core sands. The definition and methods of reclamation characteristics for the initial and proper processes associated with the basic operations of the matrix from spent molding sands are shown. Within the theoretical description of the mechanical reclamation process the occurrence of these so-called elementary operations were highlighted, that result in the removal of waste of binding materials from the surface of the matrix (sand grains), and which include friction, abrasion and crushing. The next section discusses the most common, practical solutions for reclaimers used in methods for the dry reclamation—the vibrating reclaimer used for reclaiming the molding sands matrix, which has a good susceptibility to reclamation of spent furan sands, the pneumatic reclaimer, which is used to reclaim the molding sands matrix that are harder to reclaim, and the thermal regenerator, used in the case of the reclamation of molding sands with organic binders, where the effect of the removal of the binding material from the grains is up to 100 %. It also presents methods for combined pneumatic-thermal-pneumatic reclamation, used mostly for the reclamation of various sands from different technologies. The so-called unconventional methods of reclamation are mentioned at the end, where mechanical-cryogenic reclamation performed at about −80 °C is discussed.

Reclamation of used molding and core sands is defined as a treatment of spent molding and core sands allowing to recover at least one component of properties similar to the properties of the fresh component and to reuse it for casting molds and core production. In traditional technologies of casting molds and core production on the basis of high-silica sands with binding agent addition, the reclamation consists mainly of a sand recovery and very seldom of a sand and bentonite recovery [1–4].

The matrix circuit in a foundry where the molding sand with chemical binders applied is shown in Fig. 4.1 [5].

© The Author(s) 2015

M. Holtzer et al., *Microstructure and Properties of Ductile Iron and Compacted Graphite Iron Castings*, SpringerBriefs in Materials,
DOI 10.1007/978-3-319-14583-9_4

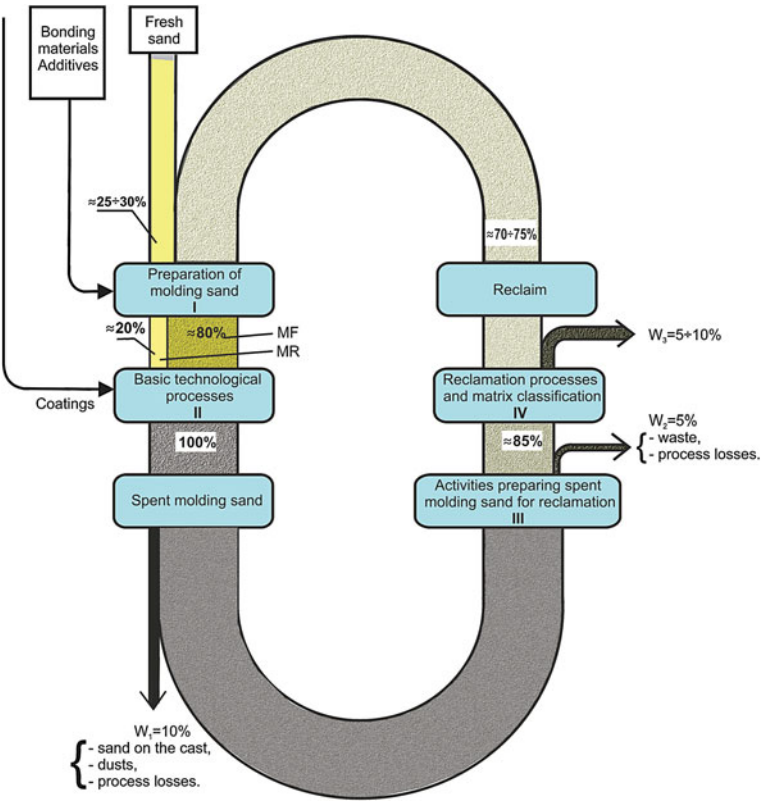

Fig. 4.1 Diagram of the recycling process molding matrix with resins: *I* preparation of molding sand and core sands, matrix; *II* the basic process steps: creation of molds and cores, pouring, solidification and cooling of castings, shaking out castings and molding sand, *III* crushing and preparing the molding sand consumed in the matrix reclamation process, *IV* the matrix reclamation process, dust extraction and separation of technologically useful grains [5]

Preparation of the spent molding sand to the reclamation process covers its crushing to lumpiness accepted by the equipment used for the reclamation and careful separation of the metallic and non-metallic impurities. In a number of systems, the mechanical reclamation process is carried out in two stages, the first of which is to lump the used molding sand to the same size as the diameter of the largest grains of the matrix (so-called preliminary regeneration) [1, 6], while the second step involves the proper reclamation, in which the release of spent sand grains from enveloped waste binding material occurs [1, 7, 8].

The introduction of the reclamation process in foundry is justified by the following factors [1]:

1. improvement of materials management in the foundry by reducing the consumption of fresh sands, reducing the cost of their purchase and the elimination of drying,

2. the reduction of excessive exploitation of sands suitable for foundry, very important due to the depletion of these resources,
3. landscape devastation limitation by increasing the pit occupied by sand mines and improvement of the environment,
4. limitation of landfill sites occupied by the spent molding sands and the penetration of toxic substances into the environment from landfills as a result of washout by rain.

The well-known, used in foundry classification of molding sands, taking into account their degree of wear was introduced in [1]. According to this criterion the following molding sands can be distinguished:

1. output sands—prepared from the same fresh molding materials, wherein the fresh material also includes reclaimed sand, or reclaimed matrix sand,
2. used sands—used at least once to produce the mold in which the cast was made,
3. refreshed sands—the used molding sand to which a suitable quantity of fresh molding material was added, whereby fresh materials include reclaimed sand, bentonite, lustrous carbon carrier, and water.
4. spent sands—not suitable for further use, the matrix of which can be reclaimed in the reclaiming process.

After shaking out the casting from the mold, spent molding and core sand appear as a byproduct of production. Possible ways of dealing with this material are shown schematically in Fig. 4.2.

An important issue in determining the optimal methods for predicting reclamation for a particular casting plant is the identification of the used molding sand circulation system. Typically, it is the determination of the type and quantity of the molding sand and core technology used in the plant.

In terms of suitability for reclamation process, molding sand is divided (according to the proposal of the European Union reference document [3]) for mono sand technology, where only one type of molding sand is used and a mixture of several types of molding sand in various technologies (mixed sands technology). Distinguished operations have also been introduced to prepare molding sand for

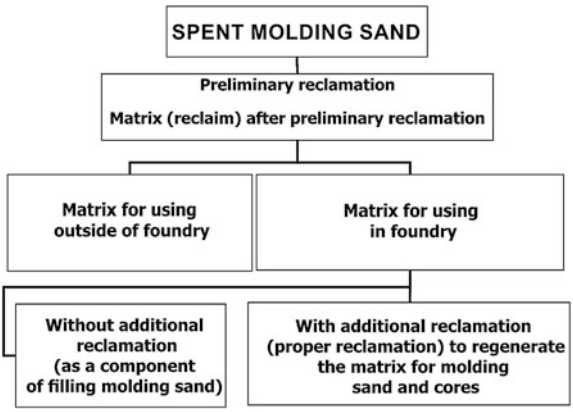

Fig. 4.2 The methods used for spent molding sand management [1]

reclamation, which is defined as the primary reclamation and reclaiming treatment, giving the final reclaimed sand that was described as a proper (secondary) reclamation.

The widespread implementation of molding sands reclamation covers almost all of the known and used molding sand foundry technology, which can predict the molding sand of high, medium and low susceptibility for reclamation. Some types of molding sands, despite their technological advantages and relatively low price, are eliminated because their matrix reclamation does not provide reclamation of a quality comparable to the quality of the fresh sand.

Spent molding sand, regardless of the method of reclamation from the matrix, is processed in the respective systems implemented reclaiming devices, usually to the following sequence of steps:

1. the preliminary reclamation consisting of: preliminary separation of mechanical, mainly metallic, contaminations, breaking lumps, sieving of spent sands and separating grain size ranges for the proper reclamation, repeating separation of metal contaminations,
2. proper reclamation, implemented in a dry or wet environment, the task of which is to free the spent grain surface of the used residual bonding material,
3. remove unwanted products from the matrix by its dedusting regeneration or rinsing,
4. the separation of the matrix of a certain size and uniform grains (grain size classification).

Reclaimability is characterized by a set of characteristics of the spent molding sand, determining its susceptibility to release matrix grains form the covering of the binding material, at a certain reclaiming treatment method.

Reclaimability is determined by the strength of the interaction between the waste, the usually partially burnt binder and the surface of the matrix grain. Molding sand characteristics that determine the value of these forces include:

1. matrix and its characteristics (size distribution, the surface of the grain shape, morphology and porosity of the surface of the grains),
2. type, number and physiochemical properties of the binder used (density, viscosity, wettability),
3. chemical properties of the matrix and binder (pH, reactivity, the ADV),
4. type of technology from which spent molding sand was reclaimed,
5. degree of thermal degradation of the used molding sand (binding material).

Figure 4.3 shows a schematic intake of the reclamation methods, the basic criterion for the classification of the environment in which the reclamation process is carried out. In this regard, there are two basic methods—wet and dry.

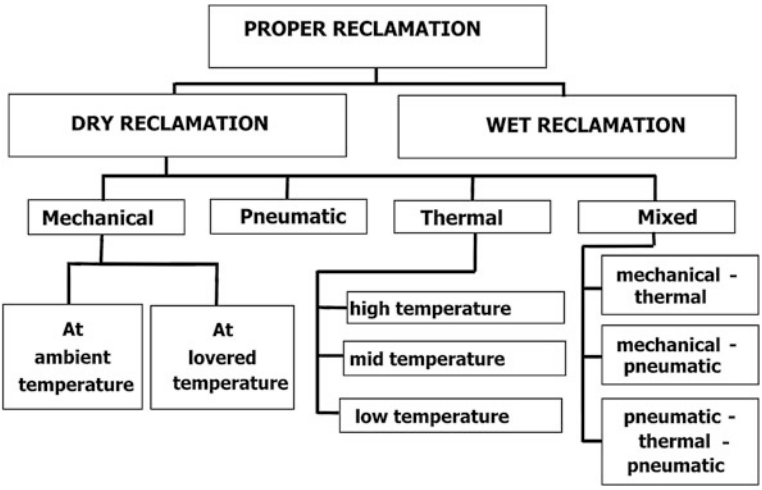

Fig. 4.3 Schematic approach of proper reclamation methods [1]

4.1 Reclamation of the Matrix of Molding Sand in an Aqueous Environment (Wet Reclamation)

Reclamation in an aqueous medium [9–11]—the so-called wet method is the most effective method of reclaiming the matrix from the spent molding sand with the binder water-soluble binders, which include the spent green sand and spent molding sands with water glass. Wet method is not suitable for the recovery of sand from the molding sand of with organic binders which do not show wettability and solubility in water (i.e. hydrophobic).

Reclamation systems in an aqueous environment are often connected to the high pressure aqueous shake out of castings and cores.

Perspective elements to be taken into account in the analysis of the complete recycling of the used molding sand with bentonite by mean of wet reclamation is potential for the recovery of bentonite and lustrous carbon carrier from the sludge and its reusing into the molding sand production.

Berndt's [12] studies, cited also in the work of Leidel [4, 13] indicate that in aqueous suspension in which the proportion of water was about 88 % of the weight; an exemplary structure of the composition of the remaining 12 % of the solid phase was as follows: 33 % of mass was quartz sand, 40 %—binder components (including the active clay 33 and 7 % quartz powder) 27 % carbonaceous components, which contain about 25 % of the coke dust.

Activities carried out in the wet regeneration include: separation of metal parts, grinding, screening, proper reclamation, classification according to the size of the matrix grains, dewatering of the recovered matrix, drying and cooling of the recovered the matrix and its storage.

The development of other, less expensive and more versatile methods of recycling and environmental considerations and the protection of natural resources of water caused the wet methods of recovery to have a narrow scope of implementation. They are replaced by varieties of mechanical reclamation that are less efficient but cheaper and considered to be less detrimental to the environment.

The factors that limit the use of wet methods of recovery are the following features:

1. restricting the use for spent green sand and spent sands with water-soluble binders, unsuitable for practical molding sand reclamation with resins insoluble in water,
2. considerable expense ratio of water in older solutions of 10–15 m^3 per 1 Mg of reclaimed sand. Disposal of water in later embodiments is 6–8 m^3/h,
3. need for water purification and post-reclaiming treatment,
4. need to create water and sand pulp, and then only recover the matrix from the pulp,
5. drying and cooling of the reclaimed sand,
6. large surface area required for the production of machinery and equipment, water clarifiers and sludge,
7. high operating costs.

4.2 Dry Methods of Reclamation

Dry methods include the following methods for the proper reclamation carried out at the following temperatures:

1. ambient: mechanical, pneumatic,
2. high: thermal, mixed, two or three step (thermo-mechanical, pneumatic-thermal-pneumatic, or others),
3. lowered: mechanical and cryogenic.

4.2.1 Mechanical and Pneumatic Reclamation

The regeneration process of dry mechanical means has now found its widest application in foundry, due to the high potential of this process:

- matrix recovery of almost every used sand, assuming a limited degree of purification of the residue binding material on the matrix,
- the application to the regeneration of relatively simple devices, often with a different primary purpose thereof (e.g. mixers),
- smaller, compared with other methods, costs of implementing the reclamation process.

Fig. 4.4 Pictorial diagram of liberating sand grains from coatings of spent binding material—as a result of the elementary rubbing operation [1]

The dry method of reclamation by mechanical means is used mainly for the reclamation of molding sand with self-hardening synthetic resins and molding sand with an inorganic bond.

It seems, that the variety of reclamation influences utilized in actual systems should be considered as a set of elementary operations, which have certain common features, regardless of the type of the reclamation process. Elementary operations occurring during the mechanical reclamation, realized at the ambient temperature are illustrated in Figs. 4.4, 4.5 and 4.6. They can be characterized as follows:

Rubbing (Fig. 4.4)—elementary operation of the reclamation process, based on the gradual thinning of a binding material coating being removed by a mutual frictional influence. Rubbing occurs in a cluster of loose sand grains being in a relative motion and directly contacting with each other.

Abrasion (Fig. 4.5)—elementary operation of the reclamation process, based on the gradual thinning of a binding material layer being removed from the grain surface by the mechanical influence of the constructional elements of machines.

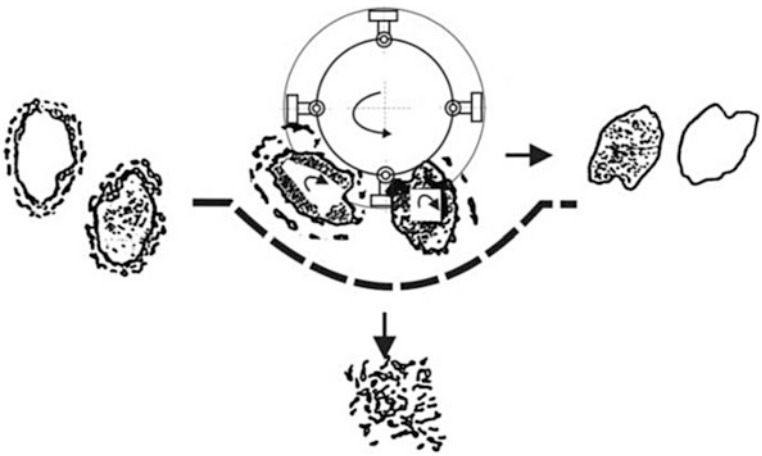

Fig. 4.5 Pictorial diagram of liberating sand grains from coatings of spent binding material as a result of the elementary abrasion operation [1]

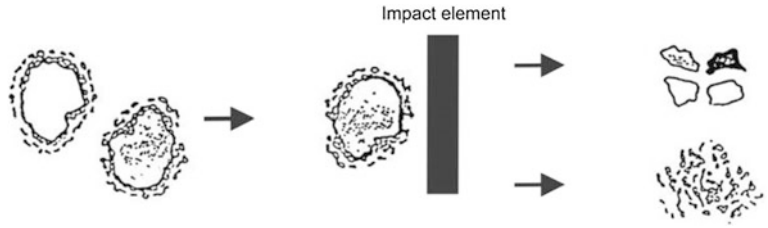

Fig. 4.6 Pictorial diagram of liberating sand grains from coatings of spent binding material as a result of the elementary crushing operation [1]

The abrasion of coatings occurs in larger clusters or on individual sand grains being in a relative motion versus movable or stationary constructional elements of machines with which they are in contact. By analogy to the rubbing elementary operation, the abrasion operation is pictorially presented in Fig. 4.5.

Crushing (Fig. 4.6)—elementary operation of the reclamation process, based on pitched change of binding material coatings thickness on sand grains and on the diminution of its particles. Crushing is caused by the pressure of external forces either dynamic or static, causing an increase of contact loads transmitted onto the coatings by the sand grains. The cracking of the coatings and breaking bridges joining individual grains is the result of such influence. Crushing occurs in moments of violent changes of grain momentum caused e.g. by their impact on appropriately shaped elements of the device or on impact plates, vertically or horizontally oriented, in the loose medium being in motion.

Figure 4.7 shows a diagram of the reclaimer built on the basis of the mechanical Gamma-Mill type vibrating crusher, intended to reclaim the matrix of the molding sand with the chemically hardened binders. The gamma-mill type of reclaimer can be used as a standalone device for crushing and reclamation of used molding sand,

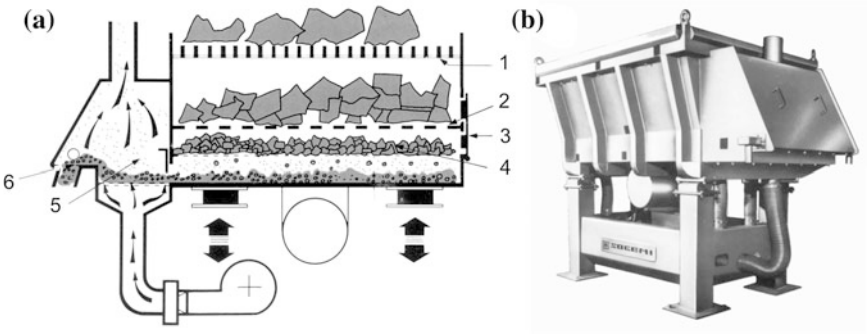

Fig. 4.7 Schematic Gamma-Mill type reclaimer and—the device: **a** *1* grate for shaking out and preliminary crushing of used molding sand, *2* intermediate grate for grinding molding sand, *3* a window to remove metal contaminants, *4* compartment sieve for final grinding and sieving, *5* classificatory pneumatic fluid bed, *6* sieve chute reclaimer, **b** view [1]

Fig. 4.8 View of REGMAS 1.5 reclaimer at the testing site at Faculty of Foundry Engineering AGH University of Science and Technology, Poland

or as part of a more extensive reclamation system in which the packages of molding sand shake out are subject to a separate grate. In the first case—not crushed molding sand is loaded on a grate (1) in an amount corresponding to the permissible load of the grate. Then they are pre-crushed under the influence of vibration of the apparatus by crushing and abrasion of the rib surface, and finally by reducing the size of the successive pours crushing-grinding elements (2) and (4). Residues of metallic impurities and non-metallic materials are removed periodically through a window arranged in a side wall of the reclaimer (3).

Another option is the REGMAS vibrating reclaimer, proposed in a series of 1.5, 3, 4 and 5 Mg/h, which is a modern solution for autonomous reclamation station for small and medium-sized foundries. The reclaimer allows for the implementation of the preliminary and proper reclamation of spent sands.

The REGMAS vibratory reclaimer [14, 15], integrated functionally with a pneumatic cascade classifier, is intended for the mechanical reclamation of dry, virtually any used molding sand. It can be installed in reclamation slots of small and medium-sized foundries. The view of the reclaimer with cascade classifier without the outer housing is shown in Fig. 4.8. On the basis of detailed studies carried out to implement the all steps of the reclamation, after prior separation of the used molding sand impurities (mainly metal), in the REGMAS reclaimer the following structural elements were used:

- grate crushing system and three sieves of decreasing mesh,
- sieve to separate the grain of reclaimed sand class 1.25–1.5 mm
- vibratory drive system and-abrasive-crushing chamber buffer of different labor,

- vibrating transport system inside the unit,
- pneumatic dedusting and classification of matrix to obtain a certain size and uniformity of grain size,
- automatic or semiautomatic control system.

For the molding sand difficult to reclaim- the possibility to increase the intensity of reclamation by 3° of change in the vibration frequency and 3° of change in the value of the driving force was used.

Spent molding sand, after separation of metallic impurities, is supplied to the filling machine. Preliminary reclamation is carried on the grid and disintegrating unit 3 sieves, of which the lowermost sieve has the shape of a cone with the vertical clearances between the palisade elements (slots) measuring 1.25 mm. Loose metal shearing (balls) are placed at the bottom of the reclaimer, in its buffer part, which carry out the proper reclamation together with the vibration impact. Molding sand sieved through a conical sieve is fed through a vibrating spiral encircling the column through the screw feeder device to the pneumatic classifier grate fed from the bottom of the speed-controlled fan or air blower. The reclaimer is driven to vibrate with two rotodynamic engines of controlled and adjustable vibration speed and with a set driving force value. Speed overdrive is done automatically according to the programmed course of the reclaiming treatment cycle and adjusted to the reclaimability of the used molding sand.

Spent molding sand having a high degree of matrix oolitization are reclaimed by a pneumatic reclamation, typically hard to reclaim, in which the release of enveloped waste matrix binder requires material crushing operation dominance. These are: highly worn green sands (high degree of oolitization), molding sand with water glass hardened with CO_2, molding sand with cement, molding sand bonded with phosphate, and rarely molding sands with synthetic resins.

Figure 4.9. shows a schematic view of a SIMPSON Pro-Claim type pneumatic regenerator consisting of two parts connected in the reclaiming series.

In the pneumatic reclaimers, the intensive machining process of worn molding sand provided by gravity through the hopper (1) is the result of elementary rubbing and abrasion of the coating binder material during transport in the pipe accelerator (2) and the dynamic performance of the air-mixture stream of sand on the impulse disc (3). A very sharp change in direction of the traffic flow and its momentum as a result of a stroke of the shield has the effect of crushing the shells binding material used, and the further movement of the molding sands layered disc shaped surface treatment promotes matrix grains due to continuing its operations in the accelerating shaft for rubbing and wearing coating. The number of cycles of the regeneration treatment, which is subjected to spent molding sand is governed both by the number of individual units of the reclaimer (2–6), and within a given component by setting the steering wheel plate (9), through which you can vary the circulation of the reclaimed material within a given unit of the reclaimer, causing an increase or decrease depending on the weight of the used reclaimability. Opening the hatch to release the dust flow collector unit (4) allows for the classification of the product on a vibrating sieve (5), the removal of waste from screening (6), dust extraction to the

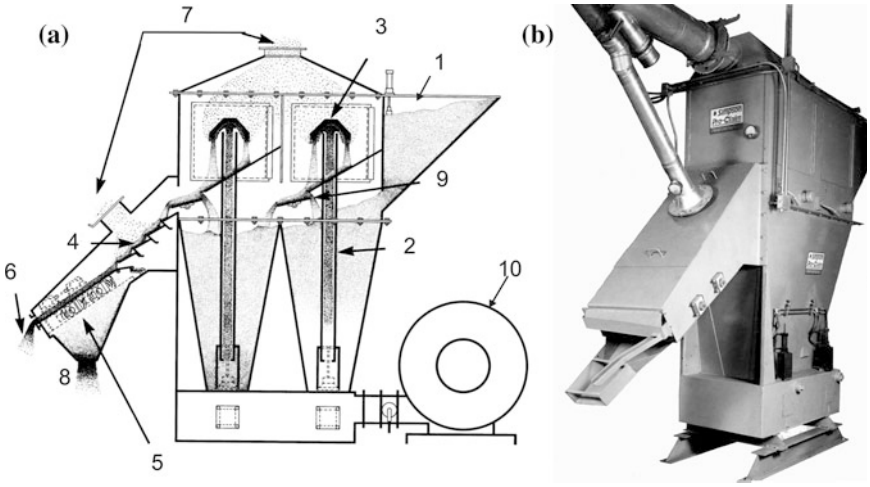

Fig. 4.9 **a** Diagram of a SIMPSON Pro-claim type double cell reclaimer: *1* charge of molding sand, *2* accelerator, *3* impact shield, *4* dedusting part, *5* vibrating screen (classifier) sieve, *6* waste of sieving, *7* dusty air exhaust, *8* reclaimed sand, *9* steering plate (flap), *10* centrifugal fan, **b** view of reclaimer [1]

dust extraction system (7) and receiving dedusted reclaimed sand (8) of a certain class of grain. Pneumatic reclaimers are well suited for the reclamation treatment of molding sands with strong bonding adhesive requiring a dominance crushing operation of the binder coating the used material, for example, the molding sand with water glass hardened by esters. In this case, it is recommended that pre-treating of the worn molding sand takes place in the drying process at a temperature of about 150 °C.

It should be noted that in most cases, the methods used for mechanical and pneumatic reclaiming do not meet the full recycling of the spent molding sand, being confined primarily to the recovery of the quartz matrix, which with an efficiency of about 75–80 % is allowed for the development of significant quantities of materials containing valuable components separated by weight cyclones and air extraction systems.

4.2.2 Thermal Reclamation

The dry thermal reclamation method is intended to the reclamation of used molding sands with organic binders, but also serves to deactivate the components of spent green sand in the reclamation systems in which the selection is not conducted, and also to neutralize post reclaiming dust and molding sand not subjected to reclamation and going to a landfill and which sets the specified requirements relating to toxicity when depositing.

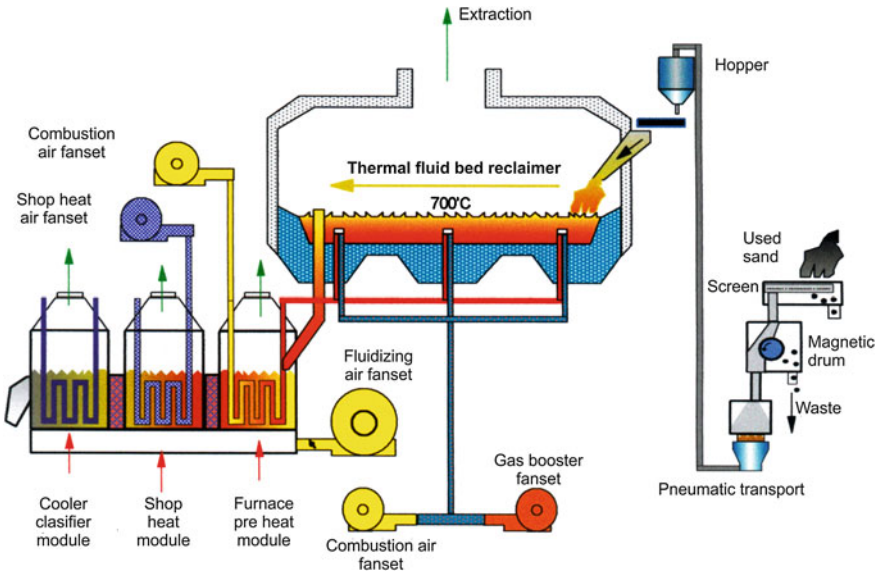

Fig. 4.10 Schematic of RICHARDS ENGINEERING PXG type thermal regenerator [1]

The high temperature thermal reclamation of green sands results in the complete inactivation of the binder, and thus significantly increases the reclaimability of such a used sand [16–18].

The advantages of thermal methods are the very thorough removal of the binder, making full use of the reclaimed sand to perform fresh moldings and cores.

While the disadvantages are: high costs of construction and operation, as well as, in some cases, the need to neutralize the waste gases.

The degree of matrix purification subjected to a thermal reclamation treatment and a typical adjuvant is high—a condition comparable with a fresh sand matrix. The reclaimability ratio of the molding sand in cold-box technology subjected to thermal reclamation reaches a value close to 80 % with the recovery time of 5 min. At the same time, the reclamation index value for the molding sand in the hot-box process is about 65 %.

Figure 4.10 shows a RICHARDS ENGINEERING PXG "Phoenix" type thermal reclaimer diagram. Regenerators of this type are offered in terms of productivity from 0.75 to 6.0 μg/h, a performance gain in the next unit of 0.25 μg/h. PXC "Compact" type thermal regenerators with a capacity of 0.25–0.5 μg/h were developed for the purposes of smaller foundries.

The spent molding sand of the buffer tank is fed by pneumatic transport to the upper tray equipped with a vibrating feeder, which provides molding sand to the working chamber thermal regenerator from the side. The fluidized bed is produced in the cavity, located symmetrically in the central part of the fluidization chamber, at a certain distance from the walls and the shell of the chamber, thereby protecting them from direct exposure to high temperature. The introduced molding sand is

gradually consumed and "dissolved" in the bed heated to a temperature of 700 °C, so that a rapid combustion fusion bonds the coatings on the surface of the resin grains. As a result, the circulation of the bed, the spent reclaimed sands particles move towards the discharge, which is an overflow pipe, arranged at a certain height above the bottom. This ensures a defined bed height, even in the absence of a power ground. The average residence time of the matrix in the fluidized bed is 15 min, which is sufficient to heat the spent molding sand to the temperature, allowing for the resin to burn, but not yet high enough to lead to the decomposition of the resin pairs. To avoid atmospheric emissions of vapors of organic compounds not completely distributed, the temperature in the space separating the regenerator is raised to a value of 800–900 °C. The combustion gas is introduced directly into the fluidized bed in a stream of air supplied by a high-pressure centrifugal fan. Proper selection of the amount of supplied gas and air helps keep the fluidized bed temperature within the specified range.

After regeneration, the matrix is to be cooled in the initial heat exchanger. The final cooling of the reclaim takes place in a fluid bed cooler equipped with a water heat exchanger and a dust extraction system.

4.2.3 Mixed (Combined) Two or Three Stages Reclamation

With a comprehensive settlement of the problem of reclamation of used mixed sands, it seems preferable to use at least two-stage system, which is a combination of intensive extraction at the beginning of the spent molding sand before the appropriate mechanical or thermal reclamation and final matrix dedusting removing reclamation products (dust from abrasion of material binding matrix grains, ashes).

A classic example of a combination of heat and pneumatic method is illustrated in Fig. 4.11—the three stage regeneration FATA system. The three stage FATA system called Fataluminium used for reclamation of used green sands—containing cores with resin binders, is a combination of two stages of pneumatic reclamation carried out at the beginning and end of the process, and thermal reclamation. The first stage pneumatic regeneration is designed to start the partial coating of the bonding material from the surface of particles and dedusting material. The second stage of reclamation is carried out in the Hot-Rec reclaimer, wherein the organic components of the binder burn in a fluidized bed heated to a temperature of 700–900 °C, where the hygroscopic moisture removal and total deactivation of the bentonite take place. Pneumatic reclamation, carried out in the third step consists of grinding and removing combustion products of an organic binder and inactive binder from the surface of the matrix grains.

Electricity consumption is 76 kWh per 1 Mg of the reclaimed sand, and the consumption of gas is equal to approximately 8 Nm^3/Mg reclaimed sand (920.000 kJ/Mg). Two-stage heat recovery enables the heating of the air supplied to the combustion chamber to the temperature of about 600 °C, which is the source of significant fuel savings.

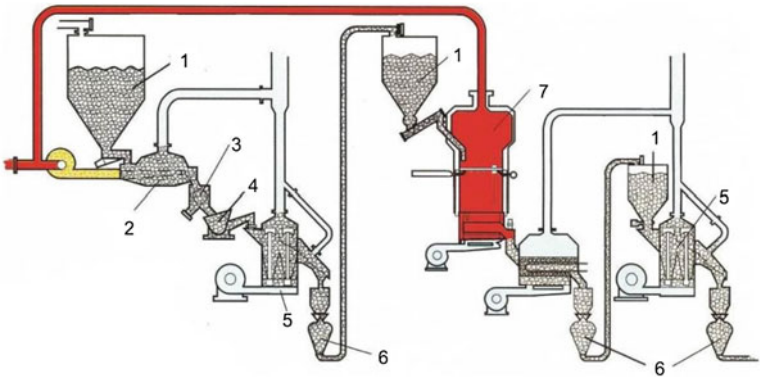

Fig. 4.11 Schematic installation by FATALUMINUM for three-stage reclamation: *1* worn molding sand tank, *2* dryer, *3* magnetic separator, *4* vibration crusher, *5* pneumatic reclamation (initial and final), *6* pneumatic transport feeder, *7* Hot-Rec fluidizing reclaimer [1]

4.2.4 Cryogenic Reclamation

In Tordoff's [19] and other publications' [20, 21] successful attempts to use the new physical phenomena to intensify the process of reclamation of worn conventional molding sand (green sand) and the molding sand bond with chemical methods were shown.

The reclamation process consists of subjecting the spent molding sand to a very low temperature (about −80 °C), which leads to changes in the mechanical properties of the binder coating material. The spent adhesive becomes hard and brittle, and the subsequent mechanical impact after the freezing process of the grains is more effective to clean the matrix of the spent molding sand.

The diagram of an industrial plant built in the United States for reclamation in the cryogenic temperature range of the matrix in classical molding sand and green sand are shown in Fig. 4.12.

The factor generating the low temperature is liquid nitrogen having a boiling point of −195.8 °C. The use of nitrogen does not cause a direct threat due to the fact that it is not very chemically active.

The installation includes a long rotating drum in which the heat exchange between the nitrogen and ground is realized. After cooling the spent sand, using the dispenser drum (rotary), is fed to the crusher, implementing the first stage of the reclamation treatment. The fragmented sand is then fed to the rotary sieve, wherein the first stage of the reclamation is performed. The reclaimed sand is received from the sieve at a temperature of about −80 °C, thus prior its entry into the sand circulation system, heating the matrix to the temperature of about 20 °C is required.

In the AGH—University of Science and Technology, cryogenic reclamation studies were carried out at an experimental station for the mechanical and

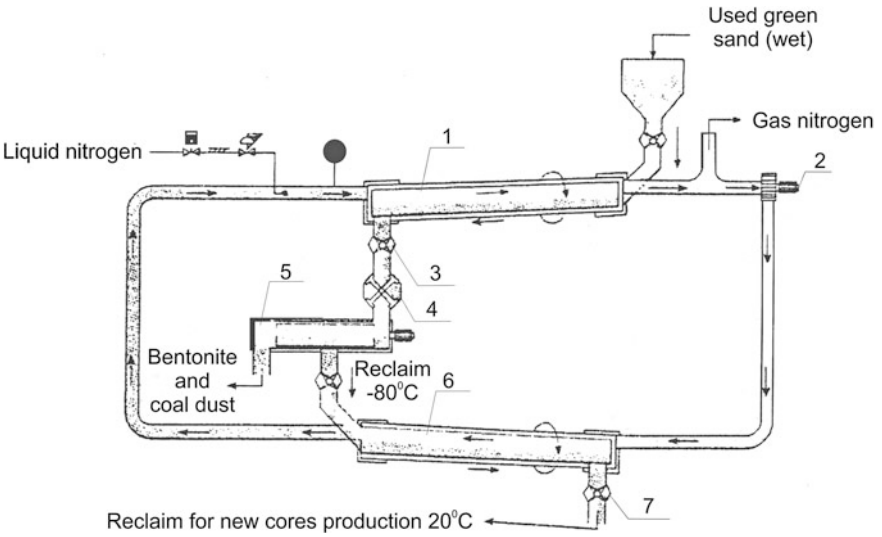

Fig. 4.12 The installation diagram for the process of reclamation in the cryogenic range of temperature: *1*, *6* rotary tunnel, *2* blower, *3* rotary feeder, *4* crushing hammer, *5* rotary sieve [1, 19]

cryogenic-mechanical reclamation. The aim of the experiment was to compare the effects of mechanical recovery and cryogenic-mechanical spent sands from different technologies.

As a result of the experiments, it was found that, the reclamation process at a temperature of −80 °C causes a significant increase in their reclaimability for all the tested waste molding sand (green sand, molding sand with water glass, molding sand with furan resin). The greatest increase was observed for the reclaimability of molding sand with water glass, then bentonite and a synthetic resin [20].

Figure 4.13 shows images of the surface morphology of the reclaimed green sand carried out using a scanning microscope.

Comparison of the initial state and the two varieties of reclamation processing based on the appearance of the surface of reclaimed sand indicates the existence of significant difference in the release of the grain surface from the binding material used. After mechanical reclamation, the grain surface is smoothed out at a given time, however, as shown by studies of binder content in the reclaimed sand—the stage of removing layers of binding material used in this case was very small. Much better results of removing of used binding material from the matrix is observed after mechanical-cryogenic reclamation (Fig. 4.13c). On this basis one may believe that the increased effect of cryogenic-mechanical reclamation is triggered in this case by the increased brittleness of the coating of the bonding material under treatment in extremely low temperatures.

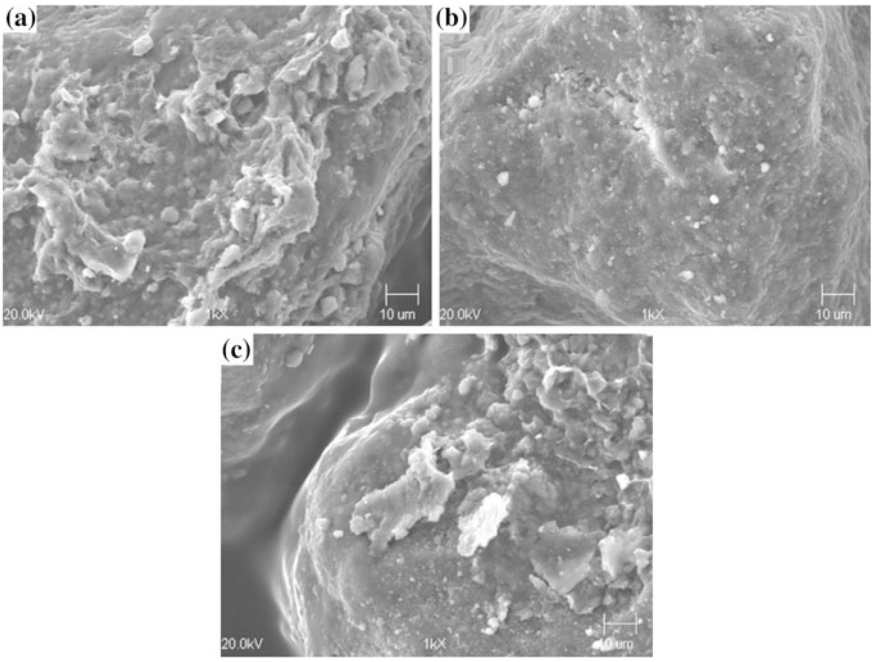

Fig. 4.13 The surface morphology of the grains: **a** spent *green* sand, **b** reclaimed molding sand after mechanical reclamation and pneumatic classification; reclamation time of 5 min, **c** molding sand after cryogenic-mechanical reclamation and pneumatic classification; reclamation time of 5 min

References

1. Dańko J, Dańko R, Łucarz M (2007) Processes and devices for reclamation of used moulding sands. Monography. Akapit, Krakow (in Polish)
2. http://www.epa.gov/sectors/sectorinfo/sectorprofiles/metalcasting/reuse.pdf. Accessed 24 Jan 2015
3. http://eippcb.jrc.ec.europa.eu/reference/BREF/sf_bref_0505.pdf. Accessed 24 Jan 2015
4. Leidel DS (1994) The influence of sand and binders on reclaimability. Foundry Trade J 168 (3497):384–387
5. Dańko R (2012) Strength model of self-setting moulding sands with synthetic resins in an aspect of the integrated matrix recycling process. Archives of Foundry Engineering, Gliwice (in Polish)
6. Dańko R (2006) Theoretical and technological basis of selection of optimal methods of dry recycling of waste foundry sands. Ph. D. Thesis, AGH-UST, Faculty of Foundry Engineering, AGH, Kraków (in Polish)
7. Polzin H, Nitsch U, Tilch W, Flemming (1997) Regenerierung anorganisch gebundener Altsande mit einer mechanisch arbeitender Pilotanlage. Gieserei-Praxis 23/24:500–507
8. Boenisch D (1991) Reclamation of spent sands containing bentonite. Guidelines for an economical leading to minimized waste. Giesserei 77(19):602–609

9. DalleRieve L (2002) Wet reclamation central plant. Experience in Italy. In: International conference "Foundry waste possibilities in the future" conference organized by EU thematic network foundry waste
10. Fiore S (2010) Wet regeneration treatment for the reclamation of waste foundry sands: a case study. Foundry Trade J 252–255
11. Zitian F, Fuchu L, Wei L, Guona L (2014) A new low-cost method for reclaiming mixed foundry waste sand based on wet-thermal composite reclamation. China Foundry M 11 (5):402–407
12. Berndt H (1980) New aspects in processing technology and quality assurance of clay bonded molding sands. Giesserei 67(21)
13. Leidel DS (1985) Reclamation of sodium silicate bonded sands. AFS Trans 93:429
14. The device for vibratory reclamation of used up foundry sands. Patent Application Publication US2014/0027549 A1. Accessed 30 Jan 2014
15. http://www.regenerator-poig.pl. Accesses 15 Jan 2015
16. Łucarz M (2015) Setting temperature for thermal reclamation of used moulding sands on the basis of thermal analysis. Metalurgija = Metallurgy 54(2):319–322
17. Łucarz M (2015) Thermal reclamation of the used moulding sands. Metalurgija = Metallurgy 54(1):109–112
18. Łucarz M (2013) The influence of the configuration of operating parameters of a machine for thermal reclamation on the efficiency of reclamation process. Arch Metal Mater Sci 58 (3):923–926
19. Tordoff WL, Miller J, Trembly J (1999) New development in sand reclamation. CIATF Tech Forum 377–386
20. Dańko R (2010) Experiences gathered during reclamation of used water glass and bentonite sands in extra low and ambient temperature. Int J Cast Metals Res 23(2):92–96
21. Wang JN, Fan ZT (2010) Freezing–mechanical reclamation of used sodium silicate sands. Int J Cast Met Res 23(5):257–263

Chapter 5
The Mold/Casting Interface Phenomena

Mariusz Holtzer

Abstract Many of surface defects in casting are caused by interaction of the metal with the molding sand. These phenomena occurring on the mold/cast interface can be divided into three groups: metal penetration (mechanical, chemical, vapor state, water explosion penetration and eutectic exudation penetration); transition of elements from the molding sand into casting and from the casting into the mold and gas generation by thermal decomposition of the binder and/or coating. Transition of the casting elements such as P, N, H, C, S, Si from the molding sand to the surface layer of the casting and elements such as Mn, C from casting to the molding sand is also possible. Frequently, this can cause changes in the chemical composition of the surface layer of the casting, which may consequently lead to changes in the casting microstructure and properties. Gases emitted from the molding sand, core or protective coating during pouring liquid metal are often due to the cause of the so-called gas porosity. The rate of the evolution of gases from the mold and cores, and their volume depends strongly on the binder used. Air present in the mold cavity may also be the cause of porosity.

The mold/metal interface can be divided into the following main groups of phenomena taking place there:

- metal penetration,
- transition of elements from the molding sand to casting and from casting to molding,
- gas generation by thermal decomposition of the binder and/or protective coating.

5.1 Metal Penetration

The common castings surface defect is caused by metal penetration into the molding sand. Metal penetration is a casting surface condition resulting from either physical, mechanical and/or thermo-chemical reactions or a combination of these at the

© The Author(s) 2015

M. Holtzer et al., *Microstructure and Properties of Ductile Iron and Compacted Graphite Iron Castings*, SpringerBriefs in Materials,
DOI 10.1007/978-3-319-14583-9_5

mold/metal interface. Metal penetration is defined as a surface condition in casting in which metal or metal oxides have filled the voids between sand grains without displacing them from mold/metal interface. This defect is responsible for major economic losses to the foundry industry [1–4]. Draper and Gaindhar [3] classified penetration defects on the basis of appearance, in order of severity, as follows:

- Rough surface: the molten metal has penetrated the mold surface up to the midpoint of the first layer of sand grains, and does not chemically react with sand; occasionally, the sand grains adhere to the casting surface but can be removed easily.
- Burn-in: The molten metal has penetrated the mold surface up to the midpoint of the first layer of sand grains and has chemically reacted with the sand, producing crystalline fayalite (Fe_2SiO_4); the surface of the casting can be easily cleaned by sand blasting.
- Burn-on: Similar to burn-in, but resulting in the formation of vitreous fayalite that cannot be cleaned easily.
- Metal penetration: The molten metal has penetrated beyond the first layer of the sand grains; the resultant mass of metal and sand grains strongly adheres to the casting surface requiring removal by chipping or grinding. Penetration is quite similar to the burn-on defect, in that the presence of partially liquid metal at the mold/metal interface and local overheating of the mold are necessary conditions for the defect to occur. However, penetration is different from burn-on in that the metal penetrates deeper from into to mold. The depth of the penetration defect is limited by the temperature of the mold away from the casting surface.

However, this work will use penetration defects terminology based on the mechanism by which the penetration proceeds.

Five basic mechanisms are believed to be responsible for penetration (a) liquid state penetration occurs in 75 % of the cases, in which the effect is merely the mechanical balance between the driving pressure and the capillary effects, (b) in 20 % of cases penetration is driven by chemical reactions and (c) vapor state penetration, water explosion penetration and eutectic exudation penetration may control 5 % of the penetration problems [4–7].

Metal penetration is more prevalent in casting ‘hot-spots’, in thick sections and in ‘transition zones’ from thin to thick metal.

5.1.1 Mechanical Penetration

This process includes the transportation of liquid in the pores between the grains of molding sand. It is the physical nature and can be represented by the pressure balance on the mold/metal interface [8, 9] (Fig. 5.1).

The liquid metal is forced into the interstices of sand grains by metallostatic, dynamic and expansion pressure. On the opposite side of the interface, that liquid metal is impeded from entering the sand aggregate by the capillarity, gas and

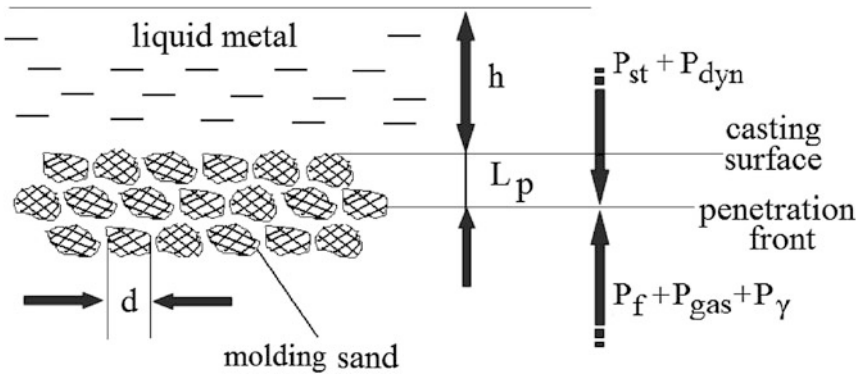

Fig. 5.1 Pressure balance during metal penetration into the molding aggregate

friction pressure. The governing equation that describes the pressure balance at the mold/metal interface can be written as:

$$P_{met} + P_{dyn} + P_{exp} = P_y + P_{gas} + P_f \tag{5.1}$$

where:

P_{met} metallostatic pressure;
P_{dyn} dynamic pressure (goes to zero as soon as the mold is filed);
P_{exp} expansion pressure (When the cast iron solidifies, part of the liquid solution of carbon atoms in the iron transform into an austenite-graphite eutectic. The specific volume of the eutectic is larger than that of the liquid, because of the graphite. Due to expansion during solidification, the pressure can push out the liquid metal into the interstices of the sand grain); (only for cast iron);
P_γ capillarity pressure;
P_{gas} gas pressure (pressure resulting from the expansion of gases evolved during mold filling);
P_f friction pressure (from the friction between the liquid metal and the sand grains; as the permeability of the molding sand increases, the frictional resistance to penetration decreases).

The terms on the left-hand side are all pressures, exercised on the metal. The terms on the right-hand side describe the ease or difficulty with which the metal moves through the sand. When the left hand side of this equation is larger than the right hand side, liquid metal can penetrate into the interstices of the sand mold, resulting in penetration defects.

Capillary pressure has the largest influence on the right-hand side (the main force opposing penetration), i.e. penetration condition [3, 5, 8, 10]:

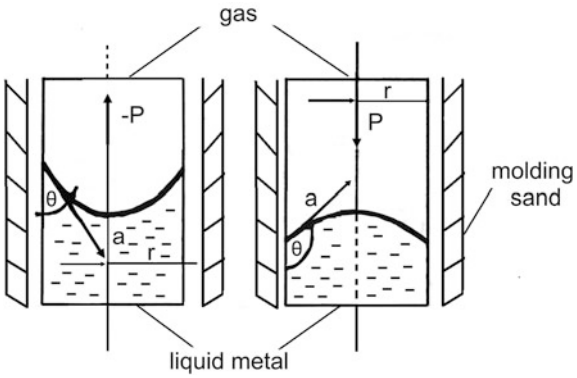

Fig. 5.2 The interaction of the forces at the penetration of the liquid metal in the molding sand: *r* radius of the pores between the grains of the matrix, m; *θ* iron/sand contact angle, degrees; *p* capillary pressure, Pa; and *a* static

$$P_{pen} = -2 \cdot \sigma \cdot \cos\left(\frac{\theta}{d_p}\right) \tag{5.2}$$

where:

P_{pen} capillary pressure, preventing the penetration of the liquid metal in the mold material, Pa;

σ the surface tension of the liquid metal (liquid-vapor surface energy; N/m);

θ contact angle between the molten metal and the material used for mold (iron/sand contact angle degrees);

d_p the average pore opening between sand grains; m.

When the angle $\theta > 90°$, the pressure P_{pen} is positive and then it prevents the penetration of the capillary pressure, and when the angle $\theta < 90°$, the pressure P_{pen} is negative (underpressure is created) and the conditions for the penetration of liquid metal in the molding sand will be created (Fig. 5.2). The actual contact angle θ is a function of the alloy composition and the pouring temperature. You can calculate the minimum amount of the metal column h at the density ρ at which the metallostatic pressure will be in equilibrium with the forces of the liquid metal surface tension. Metallostatic pressure is determined with the equation:

$$P_{met} = h \cdot \rho \cdot g \tag{5.3}$$

where:

g acceleration is due gravity, m/s^2;

Comparing the Eqs. (5.2) and (5.3) we can calculate the value of h, which is a measure of metallostatic pressure (the critical height) [11].

$$h = \frac{2 \cdot \sigma \cdot \cos\theta}{r \cdot \rho \cdot g} \tag{5.4}$$

If the contact angle is $\theta < 90°$ the liquid metal wets the mold material, which favors the penetration of the metal in the capillary tube (the size of h in the Eq. (5.4) assumes a positive value). Wherein, while the angle θ is above a certain value, the penetration phenomenon will not occur. This value is referred to as the so-called critical contact angle θ_{cr}. If $\theta > \theta_{cr}$ no penetration is expected; if $\theta < \theta_{cr}$ penetration can be expected. The critical θ_{cr} contact angle can be calculated from the Eq. (5.5):

$$\theta_{cr} = \cos^{-1}\left[\frac{d_p}{4\sigma}\left(\rho g h + pV^2\right)\right] \tag{5.5}$$

where:

ρ density of liquid alloy, kg/m^3;
g acceleration is due gravity, m/s^2;
h metallostatic head height (the height of the metal in the mold above the area where penetration is occurring), m;
V velocity with which the metal hits the mold, m/s;
d_p equivalent diameter of the capillary spaces between the sand grains, m;
σ liquid-vapor surface energy of the alloy, N/m.

Stefanescu [1] introduced the so-called Penetration index, which is expressed by the formula (5.6):

$$P = \frac{\theta}{\theta_{cr}} \tag{5.6}$$

Metallostatic penetration operates from the moment the metal enters the casting cavity until a solid skin has formed (Fig. 5.3).

In the case of metals and alloys with low specific gravity the risk of penetration is low, because the height of the column of metal would have to be very high.

Metal penetration decreases with decreasing pore size between the grains of the matrix. There is a close relationship between the penetration depth and the permeability of the mold, the matrix grain size and sintering temperature of the mold. The coal dust contained in the green sand during heating tends to swell, thereby reducing the pores between particles in a form in which mechanical penetration is difficult.

Protective coatings are applied in order to avoid or reduce the phenomena of mechanical penetration. The impact of various elements such as the size of the contact angle when developing a protective coating for the mould should also be taken into account. The smaller particle size of the matrix of the coating makes it difficult for the liquid metal to penetrate into the pores of the mold. The coating

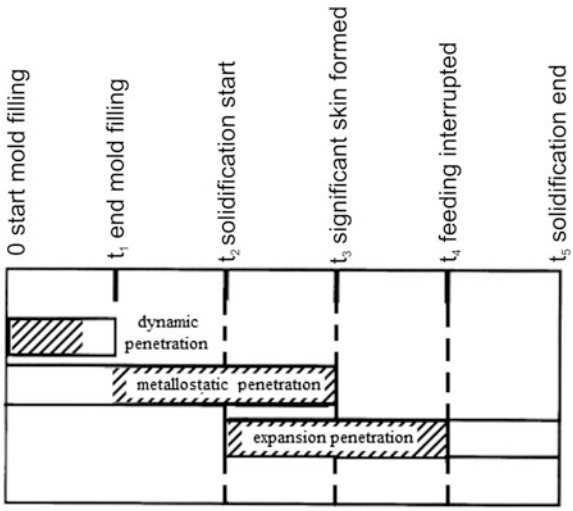

Fig. 5.3 Three types of mechanical penetration as a function of time [5]

composition should be chosen so as to increase the contact angle between the liquid metal and the coating (mold material).

Lustrous carbon carriers are one of the additives used in the green sand for iron castings. As a result, the temperature influences contained coal, which is pyrolyzed and deposited from the gas phase on the hot surface of the liquid metal in the 650–1000 °C temperature range. The resulting lustrous carbon film prevents the mold material from being wetted by the liquid metal (and hence the phenomenon of mechanical penetration is reduced) and improves the end face of the casting.

The molten metal penetration depth into the molding sand is also affected by the presence of elements reducing metal viscosity. For example, the addition of 0.9 % P to the steel causes a significant increase in the fluidity, which leads to a deep penetration of the metal in the mold even at relatively low temperatures. In the opposite direction does Ti work, which decreases the fluidity of steel, so that the penetration phenomenon occurs only at high temperatures. The dissolved oxygen content in the molten metal, which reduces the contact angle θ and thereby facilitates penetration, is an important factor. In general, the phenomenon of molten metal penetration (given the type of molding matrix) is compounded when:

- temperature of the molten metal poured into the mold is high,
- metallostatic pressure is high,
- molding sand matrix is coarse,
- apparent density of the mold is small.

The particle size of the molding sand matrix and the metallostatic pressure are those factors that can be controlled in order to reduce the extent of penetration.

Summary: The mechanical penetration can occur in all iron alloys castings. The factors that play the largest role here are: the metallostatic pressure, the rate of metal introduction into the mold, the matrix grain size and the degree of compaction of the mold. Protective coatings may be used to limit or to eliminate the phenomenon of mechanical penetration; the reduction of the impact speed of the metal to a mold or choosing a type of matrix that is less wettable by FeO may also be implemented.

5.1.2 Chemical Reaction Penetration

Chemical penetration occurs when there is a reaction between the metal and the molding sand (core) layer, or between the metal and the atmosphere at the interface mold/metal. A new phase that can react or dissolve the molding sand matrix is created as a result of this reaction. This process is more complex than mechanical penetration [4, 12–18]. Precise control of the thermodynamic conditions prevailing in the mold is difficult and impractical. Such parameters as temperature, composition of the atmosphere, the diffusion of ions, reaction kinetics and the materials activity are functions of the distance from the surface of the casting. Furthermore, the conditions in the mold change during the pouring and solidification of the molten metal. Reactions occurring between the molding sand and the liquid alloy depend significantly on the nature of the atmosphere in the mold. The concentration of oxygen at the mold/metal is rather high before the mold is poured, both in the form of oxygen present in the air and the oxygen in the steam. The interfacial oxygen concentration is quite high before casting, both in the form of molecular oxygen from air and the oxygen contained in water vapor. When molten steel is poured into a mold, the heat from the steel first expands the air between the sand grains [19, 20]. Then, if the mold is a green sand mold, the heat converts the moisture in the sand at the interface into steam, producing a dry sand zone. This dry sand zone expands as the casting solidifies and the heat is transferred into the sand. The steam than flushes the air from the interface and from the mold area, which is at a temperature above the boiling point of water. The oxygen contained in water vapor may react with the carbon dissolved in the steel or iron, or other components dissolved in the alloy. The reaction of water vapor with carbon dissolved in the steel, or iron or other components of the alloy is also possible. The reaction of the oxidation of carbon is thermodynamically favored and will proceed in first order (before the iron oxidation) (5.7).

$$[C] + O_{2(g)} = CO_{2(g)} \tag{5.7}$$

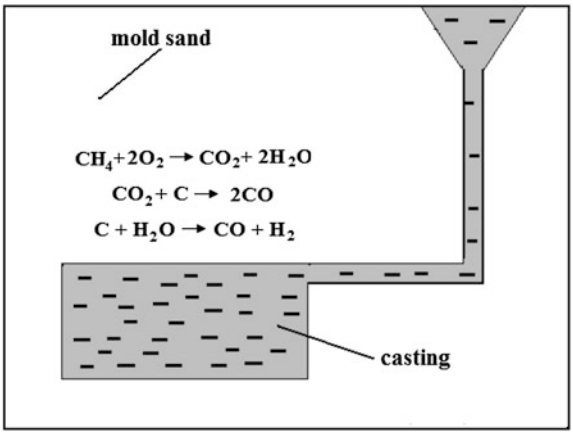

Fig. 5.4 Formation of a reducing atmosphere in mold green sand through the reaction of the hydrocarbons with oxygen

$$\Delta G = -394{,}100 - 0.84 \cdot T \frac{J}{mol} \quad \Delta G_{1673} = -395{,}505 \frac{J}{mol}$$

In the case of green sand, the following reactions occur (Fig. 5.4):

- Steam reacts with the carbon contained in the mold $C_{(s)}$ (5.8) and the carbon dissolved in the liquid steel [C] (5.9):

$$H_2O_{(g)} + C_{(s)} = H_{2(g)} + CO_{(g)} \tag{5.8}$$

$$\Delta G_{C(s)} = -357{,}700 - 32.85 \cdot T \frac{J}{mol} \quad \Delta G_{1673} = -412{,}658 \frac{J}{mol}$$

$$H_2O_{(g)} + [C] = H_{2(g)} + CO_{(g)} \tag{5.9}$$

$$\Delta G_{[C]} = -380{,}300 + 9.41 \cdot T \frac{J}{mol} \quad \Delta G_{1673} = -379{,}614 \frac{J}{mol}$$

- when there is an excess of steam, relative to the amount of carbon it reacts with CO to produce significant amounts of CO_2 (5.10):

$$H_2O_{(g)} + CO_{(g)} = H_{2(g)} + CO_{2(g)} \tag{5.10}$$

$$\Delta G = -528{,}400 + 141.66 \cdot T \frac{J}{mol} \quad \Delta G_{1673} = -291{,}403 \frac{J}{mol}$$

- while the interfacial atmosphere remains oxidized due to the large concentration of H_2O and CO_2, elements with a high chemical affinity for oxygen present in the alloy such as Fe can be oxidized (5.11 and 5.12):

$$H_2O_{(g)} + Fe_{(l)} = FeO_{(l)} + H_{2(g)} \tag{5.11}$$

$$\Delta G = -478{,}000 + 100.11 \cdot T \frac{J}{mol} \quad \Delta G_{1673} = -310{,}516 \frac{J}{mol}$$

$$CO_{2(g)} + Fe_{(l)} = FeO_{(l)} + CO_{(g)} \tag{5.12}$$

$$\Delta G = 50{,}400 - 38.5 \cdot T \frac{J}{mol} \quad \Delta G_{1673} = -14{,}011 \frac{J}{mol}$$

However, at first, the oxidation reaction of the remaining amount of carbon will proceed (5.13 and 5.14):

$$CO_{2(g)} + C_{(s)} = 2CO_{(g)} \tag{5.13}$$

$$\Delta G_{(S)} = 85{,}350 - 87.23 \cdot T \frac{J}{mol\ CO} \quad \Delta G_{1673} = -60{,}586 \frac{J}{mol\ CO}$$

$$CO_{2(g)} + [C] = 2CO_{(g)} \tag{5.14}$$

$$\Delta G = 74{,}050 - 62.1 \cdot T \frac{J}{mol\ CO} \quad \Delta G_{1673} = -36{,}536 \frac{J}{mol\ CO}$$

The progress of the reaction (5.13) and (5.14), the oxidation potential of the gas is expressed by the ratio CO_2/CO which is declining [4, 21, 22].

To assess the magnitude of the oxidative potential of the atmosphere in the form an equilibrium phase diagram was developed by Darken [23, 24] for the Fe–Si–O–C (Fig. 5.5).

This diagram differs from the regular ones—on the coordinate axis the CO_2/CO ratio is indicated instead of the temperature. The quotient above shows the ability of the oxidizing gas atmosphere; the atmosphere is more oxidizing at a higher CO_2 content. The temperature and the melting point is given on the abscissa where iron saturated with oxygen is selected (approx. 1525 °C). If the atmosphere is the condition P_{CO2}/P_{CO} = 2/98, the oxidation of iron will not occur. With a ratio of P_{CO2}/P_{CO} = 10/90 liquid iron can only be oxidized at 1566 °C (point B). In contrast, when the composition of the atmosphere reaches P_{CO2}/P_{CO} = 50/50, the iron oxidation occurs even at 1200 °C (point A).

The molding sand with resins which do not contain water, except the moisture present in the air burning substances containing carbon in oxygen atmosphere take place. In contrast, when dealing with the masses of water glass, which is less water

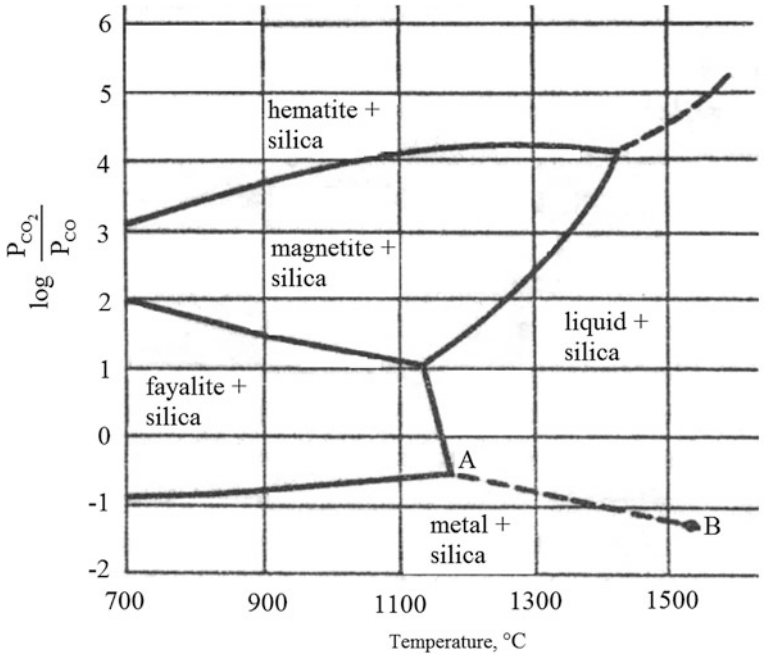

Fig. 5.5 Phase diagram of the Fe–Si–O–C [23, 24]

than in the green sand and no carbon-containing substances, the reaction between atmospheric oxygen and carbon dissolved in the metal bath.

$$[C] + \frac{1}{2}O_{2(g)} = CO_{(g)} \tag{5.15}$$

FeO resulting from the reaction (5.11) and (5.12) has a smaller contact angle (21°) than the Fe (154.5°) relative to the silica (SiO_2). This change in the value of the angle θ can be a cause of penetration, depending on the values of other variables, FeO wets the sand and is drawn up between the sand grains. FeO also can react with and dissolve the silica sand creating fayalite (Fe_2SiO_4)[1] (5.16), compound, T_m = 1593 K:

$$2FeO_{(l)} + SiO_{2(s)} = Fe_2SiO_{4(s)} \tag{5.16}$$

[1]Iron in solid or liquid state does not react directly with the oxide material of the mold. Iron must be present in ionic form (salt or oxide) [25].

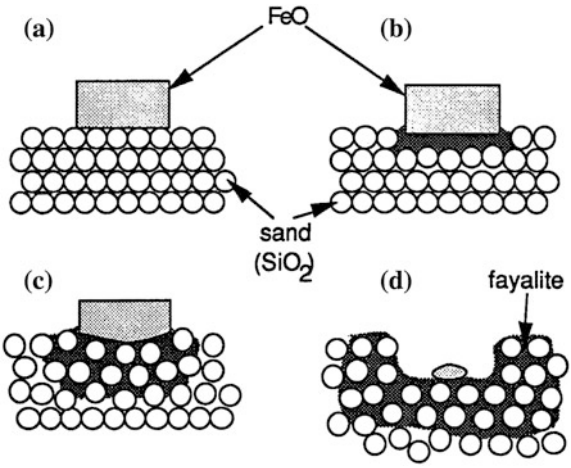

Fig. 5.6 Penetration of an FeO sample in a silica sand substrate: **a** initial stage; **b** FeO begins to react with silica, producing fayalite; **c** FeO begins to sink; **d** hole resulting from the fayalite reaction [26]

$$\Delta G^{o} = -34{,}520 + 37.2 \cdot T \ \frac{kJ}{mol} \quad (1493-1642\ K)$$

$$\log K = -\frac{1.782}{T} + 1.96$$

In practice, the presence of FeO and Fe_2SiO_4 in molding sand or at the border mold/metal demonstrates the chemical nature of penetration. The high temperature process ensures that the chemical reactions are at the thermodynamic equilibrium.

Oxides of other metals present in the alloy may also form [26, 27]. This is particularly disadvantageous in the case of alloys containing high levels of manganese, which is readily oxidized (Mn affinity for oxygen is greater than Fe), and the resulting oxides form together with silica low melting silicates, which strongly adhere to the mold. These silicates: $MnSiO_3$ (meta-silicate manganese) and Mn_2SiO_4 (ortho-silicate manganese) (Fig. 5.6).

They form on cooling the liquid, according to the reaction (5.16) on the casting surface the solid phase is composed of fayalite and the glassy phase. Fayalite crystallizes from a temperature of 1220 °C. The composition of fayalite is usually given as Fe_2SiO_4, but as can be seen in the phase diagram for the FeO–SiO_2 system, as it occurs at all FeO concentrations (Fig. 5.7). Two eutectics are shown: between iron oxide and fayalite, and fayalite and silica. From the high content of SiO_2 on the phase diagram tridymite is accompanying fayalite, from the high concentrations of FeO there is wustite. FeO (1369 °C) and Fe_2SiO_4 (about 1227 °C), which have a lower melting point than iron (1539 °C) or silica (about 1727 °C), which means that the formation of fayalite, and thus the penetration phenomenon may occur even after the solidification of the casting [28] (Fig. 5.8).

Barlow et al. [19] gave the equation, which depending on the concentration of carbon can predict to which the critical concentration of carbon in the steel will follow more oxidation of iron, and thus the likelihood of the chemical penetration:

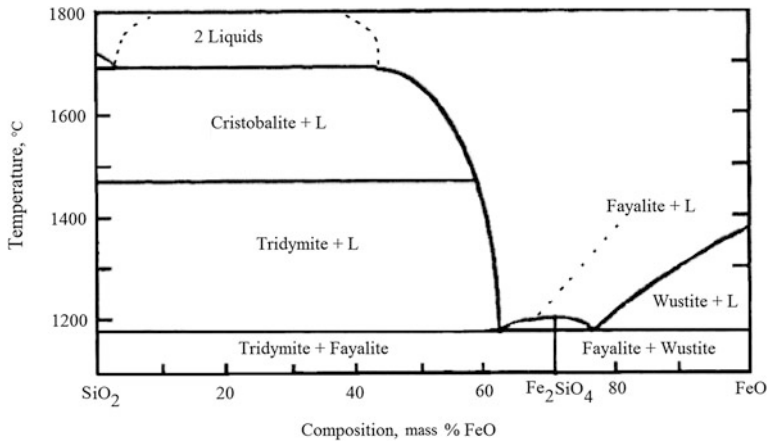

Fig. 5.7 The FeO–SiO_2 phase diagram [15]

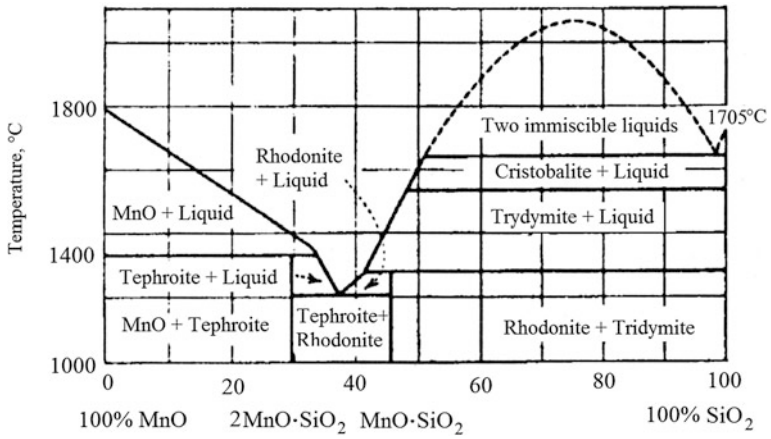

Fig. 5.8 The MnO–SiO_2 phase diagram [28]

$$C_{cr} = \frac{P_{CO2}^3}{P_{CO}^3} \cdot (0.1) \cdot \exp(0.002 \cdot T) \tag{5.17}$$

C_{cr} where it is critical carbon concentration, P_{CO2}—partial pressure of CO_2, P_{CO}—partial pressure of CO, T—temperature.

The CO_2/CO ratio calculated from this equation is approximately 0.2 for the mean concentrations of carbon in the steel and the temperature used in the casting of steel. The oxidation of iron will follow at values $C_{cr} < 0.2$.

Since an essential step in the process is to create a chemical penetration of metal oxides (mainly FeO), so to limit this phenomenon you need to create reducing or inert atmosphere on the mold/metal interface. In the case of cast iron, due to the high carbon content in the alloy, a reducing atmosphere is produced in the first moments after pouring the metal into the mold. Oxygen diffuses into the mold where it reacts with the dissolved carbon to generate CO at the interface metal/mold. In this way a reducing atmosphere is created at the interface. Therefore, it is important to the CO/CO_2 ratio on the border of the mold/metal. With an increase CO_2 levels the tendency to oxidize the metal will increase. When performing cast in green sand and lustrous carbon carriers, carbon additionally reacts with oxidizing gases and produces an even more reductive atmosphere. **Research has shown that there is no chemical penetration in the case of cast iron**.

However, in steel, you may find that the carbon content is insufficient to protect the casting surface from oxidation. Higher concentrations of carbon in the mold are not used, because carbon could diffuse into the steel causing its carburization [20, 29].

A combination of two phenomena can occur between the metal going into contact with the molding sand: the penetration of molten steel in the initial stage and then the formation of iron oxide and fayalite after the solidification of the steel. Hence, penetration can occur further after the steel solidifies. In the case of large castings, the formation of fayalite and iron oxide can appear for a long period after solidification. Fortunately penetration products, which takes place after the solidification are easy to remove. By contrast, the penetration of the products that arise when the casting surface layer was in a liquid state can be very difficult to remove. This would suggest that the fayalite does not adhere to the casting with physical force.

In the case of some castings the presence of fayalite layer facilitates the knocking out. This may be a result of different oxidation products being formed.

Protective coatings can eliminate chemical penetration if they are properly selected and properly applied. Certain materials also have a tendency to expand during heating. This increases their ability to reduce the gas diffusion interface. The smaller particle size of the shell makes it difficult for the steel to penetrate into the pores of the mold. Therefore, even if oxidizing gases are present in the mold, they cannot oxidize steel, because they cannot get to the steel and penetration is prevented.

On the mold/metal border, after pouring molten metal, layer gas consisting primarily of H_2, CO and CO_2 (depending on the type of binder) is an impediment to the diffusion of water into the interface, while the carbon can diffuse at a rate almost the same as in the beginning. This implies that the ability to oxidize the atmosphere drops rapidly [4, 21].

When the formation of the solid metal at the mold/metal interface start in, the ability of carbon to diffuse into the interface significantly decreases. This may cause a slight increase in the oxidative properties of the atmosphere.

Based on the three developed models of coupled chemical penetration (thermodynamic model for the evaluation of the critical carbon content, the model for

carbon diffusion to the interface and the model for oxygen (water vapor) flux to the interface) Stefanescu [1] introduced a quantity called "chemical penetration rate" (chemical penetration index), defined as follows:

$$PI_{chem} = \frac{C_{act}}{C_{cr}} \tag{5.18}$$

where:

C_{act} actual carbon content (carbon content in the steel at the interface; it is a function of time and temperature);

C_{cr} the critical carbon content (the minimum carbon content at the interface required to prevent the oxidation of the iron; it is a function of temperature).

If the $PI_{chem} > 1$ chemical penetration is not likely to occur, since a sufficient amount of carbon diffuses in the depth of steel casting to the border of phases, which is to protect the iron from oxidation. In contrast, when the $PI_{chem} < 1$ chemical penetration is likely because the concentration of atoms at the interface is less than the required contents of the critical need to protect the iron from oxidation.

Figure 5.9 shows the various areas, which are formed on the surface of an iron alloy in the case of chemical penetration phenomenon diagrammatically.

Summary: Chemical penetration can take place only in steel castings. The more oxidizing atmosphere is in the mold cavity, the more likely the occurrence of this phenomenon. Steels with a higher carbon content are less likely to generate chemical penetration than low carbon steels. This is due to the presence of a sufficient amount of carbon that protects the metal from oxidation. The use of carbon containing additives for green sand or molding sand with resins limits the occurrence of the chemical penetration.

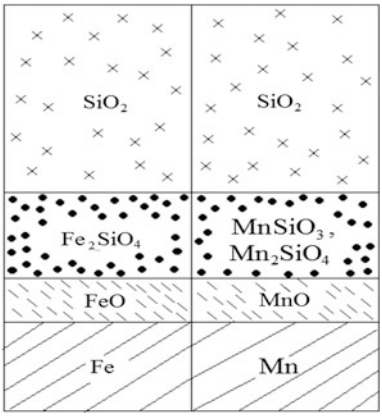

Fig. 5.9 Phases formed on the surface of the steel casting as a result of the chemical penetration

5.1.3 Vapor State Penetration

The mechanism of chemical penetration and penetration in the liquid state does not satisfactorily explain all the phenomena that take place on the mold/metal border. In particular, these mechanisms do not explain either the forms of penetration in areas where the temperature of the metal solidus was never reached, or changes in the chemical composition of the surface layer of the metal in the casting. The concept of penetration in the vapor was developed in order to clarify these phenomena [4, 11, 30].

This phenomenon can be described as a process consisting of a step to form metal vapor diffusion of these vapors to the intergranular space of the mold, and then condensation of the vapors on the grains of sand.

Due to the too short time for the metal vapor to be able to diffuse into the surface layer form and condense there in a sufficient quantity, this mechanism is unlikely in the case of small castings. The basic prerequisite for this type of penetration is that the atmosphere in the cavity of the mold is reducing.

However, as a result of this mechanism large quantities of metal cannot be transported, however it plays an important role in certain cases as a metallic material covers the matrix grains as a thin film that improves the wettability of the metal-matrix. This favors the launch of two other mechanisms of penetration (mechanical and chemical) [4]. Metal film deposition on the matrix grains also changes the characteristics of the heat transfer in porous materials, mainly because the radiation has the largest share in the exchange of the heat in the mold. As a result, the point reaches a higher temperature in the mold and therefore the transport of the liquid alloy may occur to a greater depth. Although penetration of the liquid is interrupted when the metal solidifies, the vapor transport continues.

Examples of penetration participate in the vapor penetration phenomenon in the total system can be high manganese cast steel (Hadfield)—quartz sand matrix in which the Mn diffuses in the vapor state into the molding (the vapor pressure of manganese at a temperature of 1523 °C is relatively high and is P_{Mn} = 3210 Pa, and for comparison, the vapor pressure of iron P_{Fe} = 3.18 Pa) [11, 31].

It can generally be assumed that the mechanism of penetration into the vapor state is highly likely in the case of massive castings, for which the clotting time is relatively long, which makes it possible to produce high-pressure metal vapor. This mechanism is particularly privileged when the poured alloy contains volatile elements.

5.1.4 Water Explosion Penetration

Water explosion penetration is a process where molten metal collides with the mold wall with a certain critical force. This causes an explosive evaporation of the water present at the sand grain/metal interface. The increased pressure in the vicinity of

the interface, caused by this explosion mechanically forced the liquid metal into the pores of a mold aggregate. As a result, the oxidation of metal and chemical reactions takes place, which causes the sintering of the molding sand and casting. Water explosion penetration can happen with all cast metals made in a green sand molding. The water explosion penetrations become more prominent in high-pressure green sand molding and when high density molds are produced [32].

Brummer et al. demonstrated that the correlation between mold compaction and explosion penetration is not a simple one [33].

5.1.5 Expansion Penetration (Eutectic Exudation Penetration)

This type of penetration is specific for cast iron. When cast iron solidifies with an austenite-graphite, eutectic structure has been demonstrated to expand significantly. Expanding metal exerts pressure on the walls of the mold. If the mold is rigid, and if the metal cannot be pushed back in the riser or the gates because they have solidified, the pressure results in metal penetration, called expansion penetration (or exudation penetration). Expansion penetration appears to occur mostly in gray cast iron and rarely in ductile iron. The penetration tendency increases with the carbon equivalent (CE), reaching a maximum at a eutectic composition, and decreases with increasing phosphorus content (disappears completely at a concentration of about 0.2 % P) [7, 34].

The phenomenon of penetration expansion involves multiple complex mechanisms based not only on the volume change due to precipitation of the solidifying phases and the thermally induced deformation of the mold surface but also on the deformation of the columnar austenite zone. Expansion penetration appears both before and after the columnar to equiaxial transition. The penetration phenomenon after the columnar to equiaxial transition results from the deformation of the columnar austenite network, which swells outward and pushes the sand grains of the mold back. The penetrated liquid containing segregated elements from the periphery of the eutectic cells is pressed through the damaged columnar network to the mold surface. The penetration phenomenon before the columnar to equiaxial transition occurs as the eutectic phase surplus between the columnar austenite networks is squeezed to the mold surface while the interconnected columnar austenite network simultaneously diverges away from the convex mold surface. These two mechanisms of expansion penetration have been observed separately but also transitions between them have been observed. The mechanisms of penetration revealed emphasize the roll of inoculation of both the primary austenite and eutectic cells and their influence on the volume change and deformation of the solidifying phases.

Expansion penetration results from the pressure exerted by the expansion of graphite during eutectic solidification.

5.2 Move of the Elements from Molding Sand to Casting and from Casting to Molding Sand

The processes taking place at the mold/metal interface can also lead to changes in the concentration of certain elements in the surface layer of the casting, and even deeper (to a few millimeters) [11, 35–40]. The metalographic examination of a number of fractures indicates that the source of certain casting surface problems may be the accumulation of undesirable elements at the casting surface. This accumulation may result from the elements present in a particular chemically bonded sand system. The transition of elements is possible for both ways (e.g. Mn, C) from cast to molding sand, and vice versa, from molding sand to casting (e.g., P, N, H, C, S, Si). The consequence of these effects can be the reduced mechanical properties of the casting, and thus its utility value, in particular fatigue, wear and corrosion resistance. The AFS Cured Sand committees have developed a table which outlines the various elements present in chemically bonded systems.

Table 5.1 shows the effects of elements passing from the molding sand on the quality of castings, depending on the used binder and the possible ways to prevent this phenomenon.

Possible elemental effect:

1. tears, cracks,
2. loss of mechanical properties,
3. pronounced tears, cracks and loss of mechanical properties,
4. slight loss of mechanical properties,
5. surface enrichment of sulfur in steel, nonferrous metals,
6. graphite reversion in ductile iron,
7. surface enrichment of P in steel,
8. surface enrichment of P in nonferrous metals and possible embrittlement.

Table 5.1 Effect of elements passing from molding sand into the top layer cast on its properties [40]

Binder	Possible elemental effect				Solution
	C	N	S	P	
Furan resin sulfonic acid cured	1, 2	2	5, 6		a, b, c, d, e, g, i
Furan resin phosphoric acid cured	1, 2	2		7, 8	a, b, c, d, e, h, i
Phenolic resin sulfonic acid cured	1, 2		5, 6		a, b, c, d, g, i
Phenolic-urethane resin	3	4			a, b, c, d, f
Alkyd oil urethane resin	3	4			a, b, c, d, f
Shell	1, 2	2			a, b, c, d, f
Phenolic (furan) novolac resin hexamethylenetetramine hardened	1, 2	2			a, b, c, d, e
Furan resin SO_2 cured	1, 2	2	5, 6		a, b, c, d, e, g, i

Solution:

a. reduce loss on ignitron through good reclamation practice and/or new sand addition,
b. reduce binder/catalyst levels;
c. apple wash/coating;
d. use appropriate sand additives;
e. use yellow ochre sand additives;
f. reduce or eliminate N_2 level in resin;
g. reduce N_2 level by controlling isocyanate portion;
h. check S level in base metal;
i. check P level in base metal;
j. change catalyst.

5.2.1 Carbon Pick-up and Loss

Carbon capture from molding sand and core is particularly important in the case of steel castings, corrosion resistant, which require a carbon content ≤0.03 %. The use of organic binders mass significantly enhances the effect of this type. The thickness of the carburized layer reached 1–2 mm. Even small amounts of absorbed carbon may reduce the corrosion resistance of the casting and lead to corrosion cracking. However, in the carbon steel casting in the as-cast carbon content increasing to approximately 0.2 % may cause an increase in the tensile strength of about 496–643 MPa, and an elongation reduction from about 21–13 %. In the case of the cast iron, the increase of the carbon may also cause a change in the surface layer microstructure of the casting. Where the structure of ferrite or mixture of ferrite and pearlite normally be expected, with a higher concentration of carbon the amount of pearlite will increase and a certain amount of cementite may even occur.

Carbon captured from the molding sand can be dissolved in the liquid steel after pouring it into the mold. Another source of carbon in the form can be a molding itself (e.g. graphite) or graphite coating protection. Graphite in the protective coating may be in direct contact with the liquid steel during the filling of the mold cavity and can be dissolved in the liquid metal. In this case, it may be assumed that the carbon capture is more limited to the surface. Increasing the carbon content in the casting of cast iron with spheroidal graphite can also change the microstructure of the casting [41]. The mechanism of carbon absorption from the organic binder comprises the reaction of CO, which is generated as the main gas in the pyrolysis of the binder. The atmosphere within the mold, i.e., in the spaces between the grains, is enriched with CO. The gas pressure in the heating as the molding sand increases to a value higher than the atmospheric pressure, while the pressure locally at the border mold/metal may reach a relatively high value. The top layer of the casting can absorb carbon from the carbon-rich atmosphere. This occurs even through the protective coating layer because these coatings are permeable but less than the molding sand itself. Carbon

can be absorbed from gases present in the form of the steel in both solid and liquid, wherein the solid state diffusion is much slower. After knocking out the casting, the casting surface conditions change drastically. Rapid cooling of the casting takes place, which is further exposed to the air with the low concentration of CO. The process of carbon capture is stopped and depending on the temperature of the casting may be reversed, that is, the carbon contained in the surface layer of the casting can react with the oxygen in the air, causing decarburization.

Decarburizing the surface layer
Surface decarburization of steels is often noted with acid–catalyzed furan resin binders [42]. In the investment casting of steel, the decarburization of the surface layer is particularly affected because atmospheric oxygen persists in the mold as a consequence of the inert nature of the mold, and its permeability to the surrounding environment. Doremus and Loper [36] have measured the thickness of the decarburized layer on a low-carbon steel investment casting and find that it increases mainly with mold temperature and casting modulus.

In iron castings the decarburization of the surface gives a layer free from graphite. This adversely affects machinability, giving pronounced tool wear, especially in large castings such as the bases of machine tools. The decarburization mainly seems to be the result of oxidation of the carbon by water vapor since dry molds reduce the problem. An addition of 5–6 % coal dust to the mold further reduces it.

5.2.2 Sulfur Pick-up

Sulfur-containing organic acids (toluenesulfonic acid, benzenesulfonic acid, or xylenesulfonate) used as catalysts in the molding sand with furan or phenolic resins, under the influence of temperature of the molten alloy are degraded, releasing include SO_2 which is adsorbed on the surface of the liquid metal, where it is decomposed with the release of atomic sulfur. Sulfur going into metal reacts with Mn Fe, Mg to form the corresponding sulfides with a low melting point. Additionally, the presence of sulfur in the iron causes degradation of vermicular and nodulus graphite due to the binding of magnesium. Sulfur plays an important role in the penetration of molten metal into the mold and generating related to that casting defects. Sulfur as a surface-active element present in the mold material increases the fluidity of molten metal at the mold/cast border, which facilitates the penetration of the liquid metal into the pores between the grains of the matrix [43].

5.2.3 Nitrogen Pick-up

Nitrogen is considered one of the elements facilitating the formation of flake graphite. The main sources of nitrogen are organic resins and catalysts used for

molding sand and cores. Also, additives such as coal dust are nitrogen-containing impurities. Nitrogen is released from a binder immediately, if it is present in free form, or formed by the decomposition of ammonia. Ammonia is released during the pyrolysis of important components of many binders, such as urea, amines (including hexamine used in shell molds) and ammonium salts included in binders used in hot-box or Croning technologies [44]. The pyrolysis of ammonia releases nitrogen and hydrogen according with the formula:

$$NH_3 = N \text{ (in statu nascendi)} + 3H \text{ (in statu nascendi)}$$

The evolving ammonia can be absorbed by the green sand and will be re-evolved after pouring molten metal into the mold.

Nitrogen adsorption by iron castings may cause a change in the matrix into more pearlite and carbides, whereas the effect of nitrogen on the morphology of graphite is limited. Nitrogen content greater than 60 ppm can result in the formation of flake graphite.

5.2.4 Phosphorus Pick-up

Phosphoric acid used as a binder to the molding sand hardened with furan resin leads to the contamination of the iron castings surface with phosphorus [42, 45, 46].

Phosphoric acid is generally used interchangeably with sulfonic acids, where the quantity of sulfur dioxide or hydrogen sulfide generated during the pouring of the molten metal into the mold is too high. The exact mechanism for this phenomenon is not fully understood but may involve the formation of free phosphate by the reaction between phosphate, carbon and silica. Studies have shown that the local increase in the concentration of phosphorus in the surface layer of the casting results in the deterioration of the mechanical properties, especially in thick-walled castings, in which the phosphorus uptake will occur to a greater extent. More pronounced effects of this type were observed in castings made with the participation of the molding sand hardened with reclaimed sand containing phosphoric acid. The high content of phosphorus can also be the cause of the occurrence of pitting on the surface of castings. Thick casting are particularly prone to this type of drawbacks, especially when the PO_4^{3-} ion content exceeds 0.75 % mass. Molding sand with the binder hardened with phosphoric acid should contain a maximum of 60 % of the reclaimed sand. In gray iron the presence of the hard phosphide phase in the surface causes machining difficulties associated with rapid tool wear.

5.2.5 Transfer of Elements from Casting to Molding Sand

Holtzer [11, 31], who studied the interaction process of high-manganese cast steel (11.4 % Mn, 1.1 % C, 0.8 % Si, 0.038 % P, 0.004 % S, 0.39 % Cr, 0.55 % Ni) with molding sand with the silica sand and chromite sand matrix showed that in both systems diffusion of Mn into the molding sand occurred. In the case of green sand with a silica sand matrix, both in the application of an inert and oxidizing atmospheres, in molding sand the phase with a high Mn content occurred of up to 30–35 %, with Si and O, to form a manganese metasilicate phase ($MnSiO_3$). The depth of penetration of the molding sand with Mn was up to several millimeters and strongly increased with the increasing contact time of the liquid metal with the molding sand. The application of a protective coating on the mold did not stop the Mn penetration process, however, it greatly limited its scope. There was a significant decrease in the content of Mn in the metal sample (from 11.4 % in the starting sample to 7.00 % in the sample after melting and keeping in the furnace for 1 min). At the same time the Si concentration in the metal sample grew to about 2 % (in the starting sample, the Si content was 0.8 %). This was caused by the following reaction: $2Mn + SiO_2$ (from sand matrix) = $2MnO + Si$. Due to the prolonged contact time of the molding sand with the molten metal, a silicate phase appeared in the molding sand comprising, not only Mn but also Fe. The depth of Mn penetration into the molding sand with the chromite sand matrix was considerably lower than that of silica sand, as a result of lower permeability of the first molding sand. In addition a α-Fe phase appeared in the molding sand with chromite sand matrix, resulting from the reduction of the FeO oxide by Mn. However, the Cr metal content increased greatly, exceeding 2.5 % in some places. It has been shown that we are dealing with Mn vapor penetration as one of the fundamental processes, especially in the case of massive castings in the interaction between the liquid high-manganese cast steel and molding sand.

5.3 Gases Generated by Thermal Decomposition of the Binder

According to Gibbs [47] the main problem is that "More gas is generated by the core and mold than can get out, so you need to either increase their drainage (venting) or reduce the amount of gas." The practical question is, "can the gas go through the molding sand at the current permeability of molds? If not, it will penetrate into the metal forming oxides and bubbles."

Winardi et al. [48] includes four factors that ultimately affect the capture of gases through casting, wherein three of them are significant and can be measured:

- the amount of gas produced by binders and matrix,
- the volume, permeability, and the length of the vent in the mold,
- the density of molding sand.

The fourth factor, which is the viscosity of the gas, has a relatively small effect compared to the rest of the formation of gas defects.

Through the precise control of the first three factors and taking into account that the time they interact on each other (the resultant is the speed of gases emitted) can reduce the risk of gas defects.

The core washing can often generate significant quantities of gases and if this is done at the wrong time, these gases will be captured by casting. This is often mistakenly attributed mainly to binders, and in many instances, the amount of gas released from the protective matrix is greater.

It is possible to use different strategies when castings which have defects associated with the excessive emission of gases from the core are produced.

- Minimize the amount of binder and coating—only use as much of these materials to obtain adequate strength and resistance to penetration as necessary.
- Minimize the temperature of the liquid metal—the higher the temperature of the metal, the more gas is formed in contact with the binder and the coating, and the gases dissolve faster in the metal. Observe the pouring temperature not to create defects associated with the filling of the mold (casting misrun).
- Loosen molding sand—compacted molding sand is impervious to gas.
- Change the geometry of the cores production—molding sand density changes along the core box, when cores are made in a wind automatic machine. The highest density is in the core of the molding sand injection, and the smallest in the seats farthest away from that place in the core box. It has been found that it is possible to increase the venting of the core by blowing molding sand from the opposite side than the core mark.
- Time is important—gas defects form when the pressure of the generated gases is higher than the pressure of the advance of the front of the liquid metal. If the gas pressure prevails, then the gases will move the liquid metal forming defects. In contrast, the gas cannot pass through the front of solidified metal. Experience has shown that the gas is released from the core in the primary and secondary waves. If the establishment of the skin can be accelerated, e.g. by external cooling, the cast will solidify before the gases leave the core.
- Changing the wall thickness of the casting—if it is impossible to vent cores adequately, the gas in some cases may effectively pass through the metal layer. Reducing the thickness of the walls of some of the casting, we can make the gas find its way through the front of the metal and it comes out of the mold through the riser.

Water protective coatings generate more gas than alcohol protective coatings. Therefore, the use of water-based coatings can increase the amount of gas defects. However, the use of appropriate drying process castings with water coatings may be produced without defects.

5.3.1 Gas Porosity

Gases emitted from a molding sand, core or protective coating during pouring liquid cast iron are often the cause of the so-called gas porosity. The cause of this porosity can also be the presence of gas in the mold cavity, as well as gas absorption by the molten metal during the pouring of the mold cavity (where the metal flow is turbulent).

Gas porosity, manifesting itself in the form of bubbles, is a result of the physical or mechanical limitation to evolution of gases produced by the decomposition of molding sand or core in the mold cavity, when molding sand permeability is too low or there is a lack of vents in the mold [49]. The cause of defects in gas porosity can be classified into 2 groups [50]:

1. as a result of chemical reactions, which produce gases,
2. mechanical capturing of gases.

Ad. 1 The result of these reactions are large gas bubbles (pinholes) having a diameter of several centimeters. The most common example of these types of defects are CO bubbles generated by the reaction of carbon dissolved in the iron or cast steel with FeO contained in the mold cavity [50–54].

Ad. 2 Large bubbles are also the effect of the mechanical trapping of gases (blowholes) but the process is a physical one. These gases originate from the decomposition of the binder in the molding and core sands, protective coating or from the atmosphere of the mold cavity (e.g. nitrogen, hydrogen, oxygen).

5.3.2 Gas Emission from Cores and Molds

The theory developed by Winardi [55] implies that gas bubbles (blowholes) that go into the metal are formed when the local pressure of the gas at the mold/metal interface exceeds the metallostatic pressure. Almost all binder systems produce significant amounts of gases during casting. At casting temperatures, organic compounds are unstable and rapidly decompose into CO, CO_2 and (usually volatile) hydrocarbon mixtures. Since oxygen and/or nitrogen are essential components of polymeric resins, a mixture of N, H, NO_x, NH_3 and H_2O gases are frequently present at the mold/metal interface. Additional sources of nitrogen include sand additives and polymerization catalysts (urea, hexamethylenetetramine, triethylamine, ammonium chloride, seacoal). Even inorganic binders such as water glass and bentonites depend on water or organic additions (i.e. ester) to form chemical compounds. Water reacts readily with molten iron to produce hydrogen gas and is probably the largest contributor of hydrogen (5.19):

$$2Fe_{(l)} + 3H_2O_{(g)} = Fe_2O_3 + 3H_{2(g)} \tag{5.19}$$

The gas pressure with which they form the gas bubbles (blowholes) in the liquid metal can be determined based on the following Eq. (5.20) [56]:

$$P_{met} = P_C + \left(\frac{2\sigma}{r}\right) \tag{5.20}$$

where:

P_{met} metallostatic pressure, Pa;
P_C pressure of gases within the core and the mold, Pa;
σ the surface tension of the liquid metal, N/m);
r the radius of the gas bubble, m.

When the local gas pressure in the mold or core exceed the local metallostatic head of the liquid, a bubble will be blown into the liquid metal, which then freezes. Depending on the freezing rate and rate of gas generation a bubble will actually form in the liquid metal and then be trapped underneath the surface. These bubbles form while the metal at the mold/metal interface is still liquid and therefore early in the solidification event. The surface tension of ferrous metals varies with the alloy content. These gases are constantly diffusing from the interface mold/metal at a rate determined by the permeability of the sand. The permeability changes as the binder pyrolizes and will change drastically as tensile stresses mechanically form cracks in the bonded sand.

If the metallostatic pressure increases faster than the gas pressure (Fig. 5.10) (red line a′), the release of gases into the mold cavity is inhibited and gases are routed through the core characters. However, if the pouring speed is less than the mold

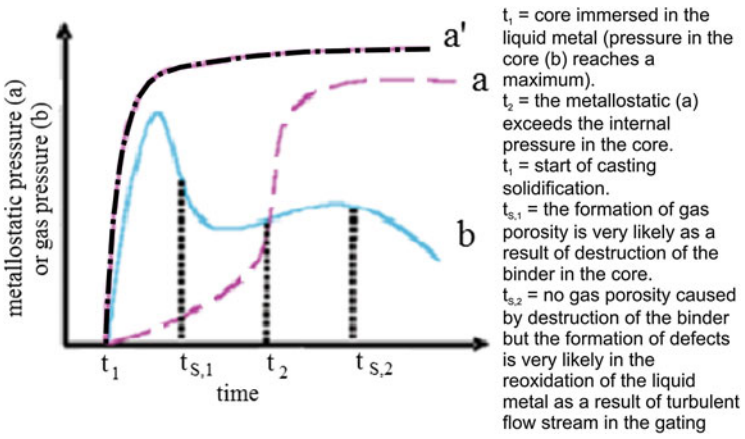

Fig. 5.10 Diagram illustrating the formation of gas porosity [48, 55]

cavity (red line a), the gas pressure is for a period of time greater than the metallostatic pressure, during which time gas bubbles leak through the metal causing defects. Increasing the speed of casting molds with the liquid metal (e.g. changing the gating system) or raising the temperature of pouring in some cases can eliminate these defects.

The resulting blowholes may be formed right at the surface of the cast or a short distance away, in the depths of the casting. The process of bubble formation is inhibited when the pressure exceeds the metallostatic pressure of the gases originating from the core or when on the surface of the core builds up. Due to the quality of the castings, the composition of the gases emitted by the molds and cores is very important. In the case of reducing gases, lower adhesion of molding sand to the casting is expected so you get a better quality of the casting surface. The presence of gases such as hydrogen, nitrogen and oxygen may be harmful, if the content exceeds the solubility limit of the solidifying metal [57].

Metallostatic head pressure can be readily determined by knowing the speed of casting, the size of the gating system, the viscosity of the molten metal and the temperature. The pressure inside the core or mold may be determined based on the rate of gas evolution, the viscosity, permeability and dimensions of the mold, and deployment or the core marks or the vents.

There are a number of factors that affect the local gas pressure reduction at the mold/metal interface, and therefore reduce the tendency of the blowholes formation. These include various chemical reactions which take place between the gases created during the decomposition of the binder, and the metal (5.21 and 5.22). This reduces the amount of these gases.

$$Fe_{(l)} + CO_{(g)} = FeO_{(l)} + [C] \tag{5.21}$$

$$Fe_{(l)} + \frac{1}{2}O_{2(g)} = FeO_{(l)} \tag{5.22}$$

In addition to these reactions, liquid metal absorbs H and N. The rate of absorption is pressure dependent, and this tends that reduce the total pressure at any one point on the casting surface.

The rate of gases evolution from the mold and cores, and their volume depends strongly on the binder used. If binders release large quantities of gas during the initial period when the casting surface is not yet solidified, they could be responsible for blowholes.

Green sands

The green sands generate a larger volume of gases at a higher rate than other molding sands due to the high moisture content of combustible components (Fig. 5.11). The release rate and the volume of gases depend on the bentonite content, water and lustrous carbon carriers, where the water content is the dominant factor. Green sand has low permeability, which connected to the high density and high speed of gas evolution promote the formation of defects in the form of gas bubbles. Lustrous carbon carriers are designed to facilitate the separation of the

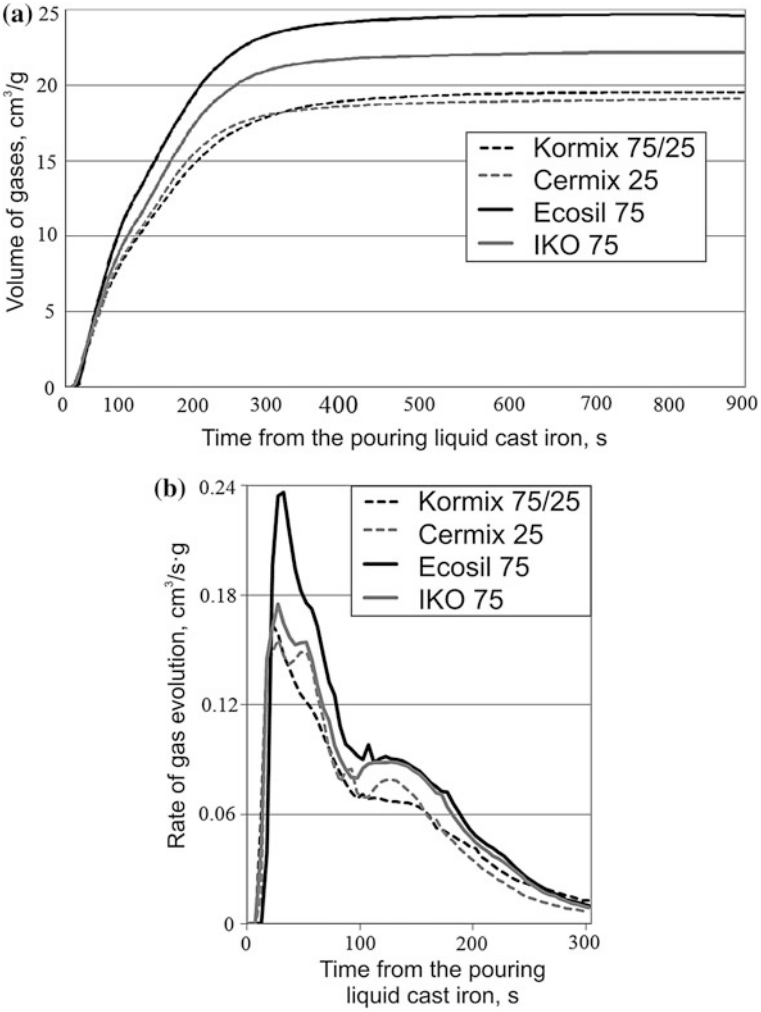

Fig. 5.11 The volume of gas **a** generated during casting molds made of green sand and coal dust, and the rate of their evolution **b** for different sorts of bentonite (a mold pouring with liquid cast iron at the temperature of 1350 °C)

casting from the molding sand during knocking out. For this purpose, it is firstly necessary to reduce the oxygen content in the mold cavity and produce a reducing atmosphere by generating carbon monoxide and/or hydrogen. This reducing atmosphere effectively prevents the oxidation of the surface of the liquid cast iron. The oxide layer, in contrast to the liquid cast iron, could wet quartz grains very well, leading to an increase in the sintering of silica sand.

Another important role of the lustrous carbon carriers is to create a very thin layer of carbon, the so-called "lustrous carbon", which can effectively prevent the

sintering of silica sand on the casting surface. Apart from the sintering of silica sand, the penetration of the green sand through the casting metal is also effectively inhibited by lustrous carbon formers [22].

5.3.3 Molding Sands with Organic Binders

The use of molding sand with organic binders in many cases leads to the appearance of gas porosity defects. This is due to the presence of organic substances included in the binder and hardener. The presence of nitrogen and hydrogen is particularly dangerous to the formation of gas porosity. Each of these elements, together with humidity, may enter into various reactions, in which conditions for the formation of gas porosity are created. Resins containing more than 5–6 % N are associated with gas defects, especially in ductile iron castings. You can specify the following reactions (5.23–5.27) occurring in this case, on the metal-mold border:

$$\text{binder} \rightarrow \text{H (in statu nascendi)} \rightarrow \text{H}_{2(g)} \tag{5.23}$$

$$\text{binder} \rightarrow \text{N (in statu nascendi)} \rightarrow \text{N}_{2(g)} \tag{5.24}$$

$$\text{Fe}_{(l)} + \text{H}_2\text{O vapour (binder)} \rightarrow \text{FeO}_{(l)} + 2\text{H (in statu nascendi)} \tag{5.25}$$

$$3\text{H}_2(\text{binder}) + \text{N}_2(\text{binder}) > 2\text{NH}_3(g) \rightarrow 6\text{H (in statu nascendi)} + 2\text{N (in statu nascendi)} \tag{5.26}$$

$$\text{FeO}_{(l)} + \text{C (binder)} \rightarrow \text{CO}_{(g)} + \text{Fe} \tag{5.27}$$

As a result of the organic binder thermal decomposition N and H are released in the statu nascendi or atomic form, which then dissolve in the liquid metal, from which gas bubbles are emitted during solidification, provided the content exceeds the solubility limit of the solid state. As a result, porosity defects will form in both —surface and subsurface. Another important source of hydrogen, which can cause gas porosity is the atmosphere in the mold cavity, in particular, the moisture content [58]. The composition and the chemical nature of the atmosphere at the metal-mold border of the casting during solidification depends upon the type of binder and pouring casting alloy.

Bates and Burch [59] reported on the volume and rate of the evolution of gases from cores made using different technologies that are in contact with the aluminum alloys, cast iron and cast steel. The pressure prevailing in the core can be calculated on the basis of this data. The use of the molding sand matrix containing reclaimed sand significantly increases the amount of flux gases, thus increasing the risk of gas porosity.

The effect of the residual binder on the reclaimed sand, which is reflected by an increased LOI on the rebonded sand, is to increase both the maximum rate of evolution and total volume of gas produced [60].

On the curves for the rate of gas emission from the molding sand with resin three peaks can be identified in the first 100–120 s after pouring the core with liquid cast iron [61]. According to Yamamoto et al. [62] Peak I attributed to the expansion of air plus the evaporation of free moisture and other volatiles in the core when the core was first covered with liquid metal; Peak II identified as the release of combined water (water of crystallization) in the binder and/or aggregate; and Peak III attributed to the general breakdown of the organics in the binder.

The pressure at the mold/metal or core/metal interface rises because the air being replaced in the mold must be evacuated and removed, the air in the mold or core heats up, and the binder or other mold materials boil, decompose and heat up. The mold or core materials prevent the immediate release of the gas pressure. The resistance of the mold or core depends on the distance to the vent or free surface. The resistance to gas flow through sand molds and cores is measured as permeability.

5.3.4 Mold Coatings

A protective coating is applied to reduce the reaction between the metal and the mold or core. They are prepared on the basis of alcohol or water. Alcohol coatings, however, do not require drying, and thus consume less energy but off emit VOC into the environment while burning. For this reason, a greater emphasis is placed on the use of water-based coatings, looking for low-cost and efficient methods of drying (e.g. microwave technique).

The benefits resulting from the application of protective coatings can be summarized as follows:

- reduction of castings purification costs since a better surface end is obtained,
- knock-out properties are improved,
- machining time of casting is reduced.

However, the use of protective coatings on cores to prevent core blows is usually improper [63]. Although the coating reduces the permeability of the surface, assisting to keep in the expanding gases, the additional volatiles from the coat, which appear never to be completely removed by drying, are usually present to excess (penetrate, break through the protective coating) to overwhelm the coating barrier. For example, the cores bonded with epoxy-acrylic resin with an aqueous protective coating generated 50 % more gases, which yield at a higher speed than the cores without a coating. Protective coating cores showed a greater tendency towards the formation of gas porosity.

In addition, there are many other reasons to avoid the use of protective coatings:

- the cost of materials used in the coating, particularly such as zirconium,
- possible deterioration of dimensional accuracy of the casting, since it is difficult to control the thickness of the coating,
- additional energy consumption for drying and expenditures on equipment for drying,
- the time required for drying limits productivity,
- cores are never dried out by the end of the application of a protective coating, which is why there is a danger of creating blow defects, if the core cannot be vented to the atmosphere.

In the case of sand cores and molds—important properties of the core sand or molding sand themselves, to which a protective coating is applied, especially the molding sand composition and its strength. Different expansion of the molding sand, core and the coating is important. This difference should be as small as possible and should not exceed 0.1 %.

The use of appropriate protective coatings on the mold is one of the possible solutions to prevent degradation of the graphite surface layer in the cast. The protective coating minimizes mold-metal interaction by being a protective layer and providing a desulfurizing effect.

The coatings can be classified in three categories [64]:

1. Inactive coating—these are coatings that are completely inert with respect to the melt.
2. Active coatings—coatings that alter the local chemistry of the melt. These coatings may have some inoculation effect.
3. Reactive coatings—coatings that have chemical reactions with the melt, such as deoxidation or desulfurization.

The application of a mold coating strongly influences the graphite deterioration in the surface layer of castings. It either promotes graphite degeneration to less compact morphologies, when using S-bearing coatings, or conversely, limites the surface layer thickness using desulfurization type coatings. If the coatings employed desulfurization materials, such as MgO, or mixture (CaO + MgO + Talc) or Mg-bearing FeSi, they acted to remove any S-released compounds from the mold sand (such as furan resin and phenolic urethane bonded sands) and they protect the graphite shape, improving graphite nodularity, at the metal- mold surface. MgO and Cao will behave as inactive coatings when there is no sulfur in the binder. The best results, for both lowering the surface layer thickness and increasing the graphite nodularity in the casting center were obtained when coatings incorporated active Mg, either as a fine size FeSiCaMgRE alloy or as a mechanical mixture of Mg in a fine size FeSi75 alloy [65]. Oxide type coating (MgO or MgO + CaO + Talc) acted mainly to neutralize sulfur migration from the mold in a desulfurizing reaction, whereas the Mg–Fe–Si coatings performed a complementary role beyond desulfurization with supplementary magnesium regenerating the nodularising potential prior to solidification.

References

1. Stefanescu DM (2008) The effect of mold/metal interface phenomena on the surface quality of casting. In: 10th Asian Foundry Congress (AFC10), Nagoya, Japan, pp 21–24, May 2008
2. Broks BE, Beckermann C, Richards VL (2007) Prediction of burn-on and mold penetration in steel casting using simulation. Int J Cast Met Res 20(4):177–190
3. Draper AL, Gaindhar JL (1975) The role of mold atmospheres in the penetration of steel in sand molds. AFS Trans 83:593–616
4. Svoboda JM, Geiger GH (1969) Mechanisms of metal penetration in foundry molds. AFS Trans 77:281–288
5. Stefanescu DM et al (1996) Cast iron penetration in sand molds. Part I: Physics of penetration defects and penetration model. AFS Trans 104:1233–1248
6. DiSylevestro G (1989) Experiences in defect diagnosis: metal penetration. AFS Trans 97:89–07
7. Dugic I (2006) The mechanisms of metal expansion penetration during solidification of grey cast iron. Dissertation no 1007, Department of Mechanical Engineering Linköping University, Jönköping
8. Stefanescu DM et al (1993) Metal penetration in sand molds: a fundamental approach to solving the problem. AFS Trans 101:789–796
9. Hayes KD et al (1998) Mechanical penetration of liquid steel in sand molds. AFS Trans 106:769–776
10. Frawley JJ et al (1974) Simulating mold-metal reactions in a small laboratory test. AFS Trans 82:561–570
11. Holtzer M (1992) A study of mechanism and degree of interaction between Hadfield liquid cast steel and molding sand. Scientific Bulletins of University of Mining and Technology, Metallurgy and Foundry Practice. Bulletin 142, Cracow 1992 (in Polish)
12. Giese SR et al (1996) Cast iron penetration in sand molds, Part II: Experimental evolution of some of the main parameters responsible for penetration. AFS Trans 104:96–207
13. Naro RL, Pelfrey RL (1983) Gas evolution of synthetic core binders: relationship to casting blowhole defects. AFS Trans 91:365–376
14. Asanti P (1968) Interface reaction of chromite, olvine, and quartz sands with molten steel. AFS Cast Met Res J 4:9–15
15. Pattabhi R et al (1996) Cast iron penetration in sand molds, Part III: Measurement of mold—metal interface gas composition. AFS Trans 104:1259–1268
16. Gertsman SL, Murton AE (1950) An investigation of metal penetration of steel sand cores. AFS Trans 58:595–603
17. Delannoy P et al (1990) A critical literature review of theories for the formation of casting metal penetration defects. AFS research report no 2
18. Svoboda JM (1994) Mechanisms of metal penetration in foundry molds. AFS Trans 102:461–473
19. Barlow JO et al (1997) Chemical penetration in sand molds in steel castings. AFS Trans 105:325–331
20. Lane AM et al (2001) Penetration of liquid steel in sand molds, Part II: Chemical reactions at the mold/metal interface during casting of steel. AFS Trans 109:1327–1345
21. Owusu YA, Draper AB (1978) Metamorphic zones in green sand molds poured with steel. AFS Trans 86:589–598
22. Engelhardt T (2010) New concepts to reduce the emission from green sand. Fonderie Aout – Septembre 7:24–36
23. Colligen GA et al (1958) The effect of temperature and atmosphere on iron–silica interface reaction. AFS Trans 66:452–458
24. Darken LS (1948) Melting points of iron oxides on silica; phase equilibria in the system Fe-Si-O as a function of gas composition and temperature. ACS J 70(6):2046–2053
25. Kubaschewski O, Hopkins B (1992) Oxidation of metals and alloys. Butterworths, London
26. Stefanescu DM (1991) An investigation on the role of sand-metal contact angle in the formation of casting penetration defects. AFS Trans 99:761–789

27. Chakraborty M et al (1986) Mold-metal reactions in casting high manganese steel in sodium silicate bonded sand molds. The British Foundryman 229–235
28. Colligan GA, Van Vlack LH, Flinn RA (1961) Factors affecting metal/mold reactions. AFS Trans 69:52–58
29. Wagner CG (1979) Observations on the penetration of steel into high density clay bonded molds with controlled atmospheres. AFS Trans 87:573
30. Lane AM et al (2001) Penetration of liquid steel in sand molds, Part II: Chemical reaction at the mold/metal interface during casting of steel. AFS Trans 109:1324–1345
31. Holtzer M (1990) Interfacial reaction between high manganese cast steel and silica sand or chromite sand. The Foundryman 135–141
32. Levelink HG, Van den Berg H (1984) Castings defects caused by water explosion. AFS Trans 71:421–432
33. Brümmer G, Dopp R, Levelink HG (1994) Determination of the sensitivity of molding materials to explosion penetration by application of a novel permanent test mold. Giesserei 81 (13):438–442 (in German)
34. Levelink HG, Julien FPMA (1973) Penetration and shrinkage by interaction of solidifying cast iron and casting mold—Part 2. AFS Cast Met Res J 9(2):105–109
35. Asanti P (1966) Burn on in steel castings. Mod Cast 49(4):71–73
36. Doremus GE, Loper C (1970) A study of decarburization accompanying the casting of steel in ceramic molds. AFS Trans 78:338–342
37. McGrath C, Fischer RB (1973) Surface carburization of stainless steel casting alloys. AFS Trans 82:603–620
38. Mekeel C, Fischer RB (1971) Surface carburization in corrosion resistant steel castings produced in molds bonded with organic binders. Trans AFS 79:600–614
39. Detrez P, Mascre C (1969) Quality of steel castings in relation to nitriding, carburizing or decarburizing effect of molds. AFS Cast Met Res J 5(4):165–172
40. Tani K et al (1987) Interfacial reaction between cast steel and olivine sand or silica sand. Trans Iron Steel Inst Jpn 27(3):197–204
41. Holtzer M (2013) Metallurgical and foundry processes of iron alloys: physicochemical fundamentals. PWN (in Polish)
42. Naro RL, Wallace JF (1992) Effect of mold-steel interface reactions on casting surface. AFS Trans 100:797–820
43. Svidro JT (2010) The effect of sulfur content in chemical bonded sand molds on the mechanism of penetration. Int Foundry Res/Giessereiforschung 62(4):32–41
44. Riposan I et al (2013) Control of surface graphite degeneration in ductile iron for windmill applications. Int J Met Cast 9–21
45. Holtzer M, Zych J, Retel K (1996) Effects of the interaction between mold and a liquid cast iron that the surface quality of castings. Przegląd Odlewnictwa 46(6):129–134 (in Polish)
46. Fallon MJ (1995) Experience in the manufacture of ductile irons. The Foundryman 88 (9):308–318
47. Gibbs S (2008) Illuminating core gas. Mod Cast 98(10):34–37
48. Winardi L et al (2007) Gas pressures in sand cores. AFS Trans 115:303–315
49. Naro RL, Pelfrey RL (1983) Gas evolution of synthetic core binder relationship to casting blowhole defects. AFS Trans 91:365–376
50. Monroe RW (2005) Porosity in castings. AFS Trans 113:519–546
51. Ryntz EF Jr et al (1983) The formation of blowholes in nodular iron castings. AFS Trans 91:139–144
52. Stefanescu DM (2005) Computer simulation of shrinkage related defects in metal castings—a review. Int J Cast Met Res 18(3):129–143
53. Orlenius et al (2007) Influence of melting process on hydrogen and nitrogen content in gray iron. AFS Trans 115:617–623
54. Elmquist I et al (2007) Influence of melting process on oxygen content in gray iron. AFS Trans 115:625–635

55. Winardi L, Griffin RD (2008) Effects of coating drying methods on loi, gas evolution and core permeability. AFS Trans 116:381–398
56. Hernandez B et al (1979) Mechanisms of pinholes formation in gray iron. AFS Trans 87:335–348
57. Hughes ICH (1988) Ductile iron casting. ASM metals handbook, 9th edn, vol 15, pp 647–666. Metals Park
58. Carter SF, Evans WJ et al (1979) Factors influencing the formation of pinholes in gray and ductile iron. AFS Trans 87:245–268
59. Bates CE, Burch R (2007) Core and mold gas evolution: porosity in casting. Foundry Manag Technol 135(5):17–18
60. Holtzer M et al (2014) Emission of policyclic aromatic hydrocarbons (PAHs) and benzene, toluene, ethylbenzene and xylene (BTEX) from furan molding sands with addition of the reclaim. Metallurgija 53(4):451–454
61. Holtzer M et al (2014) Influence of the reclaim addition to the molding sand with furan resin on emission of toxic gases at high temperature. In: Proceedings of 71st World Foundry Congress, Bilbao, 19–21 May 2014
62. Yamamoto Y et al (1980) Gas pressure in shell mold cores made of olivine sand during casting. AFS Int Cast Met J 5(2):60–65
63. Campbell J (2011) Complete casting. Handbook, 1st edn. Elsevier Ltd., Oxford
64. Boonmee S, Stefanescu DM (2013) Casting skin management in compacted graphite iron. Part I. Effect of mold coating and section thickness. AFS Trans 121:435–448
65. Chrismera M et al (2014) Iron casting skin management in no-bake mold-effects of magnesium residual level and mold coating. In: 71th World Foundry Congress, Bilbao, 19–21 May 2014
66. Glasser FP (1958) The system MnO-SiO_2. Am J Sci 256:398–412
67. (1984) Elemental effects of chemically bonded sand on casting surface. Mod Cast 21–25
68. Bates CE, Monroe RW (1981) Mold binder decomposition and its relation to gas defects in castings. AFS Trans 89:671–686
69. Scott WD, Goodman PA, Monroe RW (1978) Gas generation at the mold-metal interface. AFS Trans 86:599–610
70. Monroe RW (1984) The use of iron oxides in nobake bonded sand molds. Steel Found Res J 5:9–15

Chapter 6
General Characteristic of the Ductile and Compacted Graphite Cast Iron

Marcin Górny

Abstract This section provides basic information about the spheroidal graphite cast iron (SGI) and compacted graphite cast iron (CGI) which belong to the group of high-quality cast iron. The classification of SGI and CGI according to ISO standards, their characteristics and the use of modern types such as ADI or Si–Mo were provided. The solidification path was shown, pointing to the important role of surface active elements in shaping the form of graphite. Models presenting eutectic grain growth in SGI and CGI were also described. It was also shown that in this connection, the main surface active elements (O and S) cause changes in the growth direction, and additionally, the so-called anti-spheroidizers, such as Ti, Bi, Zr, P and N, characterized by strong normal segregation, lower the liquidus temperature of the melt, thus creating the liquid channels that characterize CGI, which then stimulate the formation of compacted graphite. The issues of the number of eutectic grains, the cooling rate and the occurrence of defects in castings were raised. Finally the spheroidizing/compacting treatments have been shown along with the general scheme of the SGI/CGI preparation process.

Spheroidal graphite cast iron (SGI) and compacted graphite cast iron (CGI) belong to the group of high-quality cast iron, the production of which is continually increasing. The general classification of cast iron is shown in Fig. 6.1.

Currently, SGI and CGI, belongs to a group of the most important engineering materials, in view of its:

- high mechanical properties,
- significant savings in cost and weight (compared to equivalent steel and aluminum alloys),
- excellent combination of good castability and machinability,
- less sensitive to the cooling rate compared to cast iron (FGI),
- provides the starting material for the production of "high tech" austempered ductile iron (ADI) and austempered vermicular cast iron (AVCI),

© The Author(s) 2015

M. Holtzer et al., *Microstructure and Properties of Ductile Iron and Compacted Graphite Iron Castings*, SpringerBriefs in Materials,
DOI 10.1007/978-3-319-14583-9_6

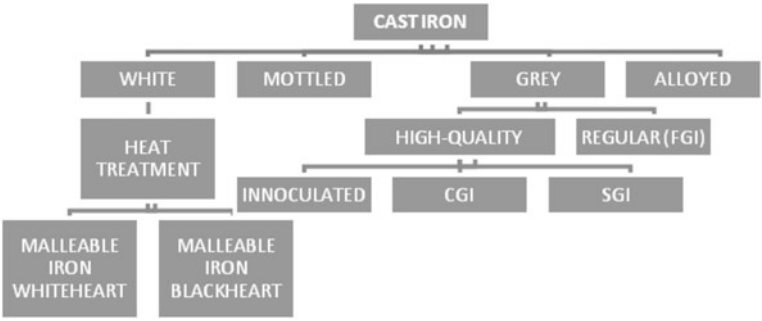

Fig. 6.1 General classification of cast iron

- presence of graphite which contributes directly to lubrication of rubbing surfaces and provides reservoirs to accommodate and hold lubricants.

The SGI and CGI castings can be tailored to fit an unusually broad diversity of needs, which remarkably, has opened new vistas for its application in the manufacture of automobile, construction, communication, transportation, agricultural, mining, heavy-machine, military and railroad components, which are traditionally produced by expensive forging and fabrication processes involving high grade alloy steels and other equivalent high performance materials [1–13].

6.1 Spheroidal Graphite Cast Iron (SGI)

The current ISO standard for SGI [14], ISO 1083-2004, specifies grades either by tensile strength, proof stress and elongation or Brinell hardness (HBW). Table 6.1 shows the range of grades available within the ISO Standard.

Table 6.1 Specifications for SGI castings according to ISO Standard 1083 (measured on test pieces machined from separately cast samples)

Grades	UTS (MPa min.)	YS (MPa min.)	A (% min.)	HBW
ISO1083/JS/350-22/S	350	220	22	<160
ISO1083/JS/400-18/S	400	250	18	130–175
ISO1083/JS/400-15/S	400	250	15	135–180
ISO1083/JS/450-10/S	450	310	10	160–210
ISO1083/JS/500-7/S	500	320	7	170–230
ISO1083/JS/550-5/S	550	350	5	180–250
ISO1083/JS/600-3/S	600	370	3	190–270
ISO1083/JS/700-2/S	700	420	2	225–305
ISO1083/JS/800-2/S	800	480	2	245–335
ISO1083/JS/900-2/S	900	600	2	270–360

SGI has graphite in the form of nodules. SGI has much higher mechanical properties, especially ductility compared to gray cast iron. Depending on the type of metal matrix (ferrite, pearlite), conventional ductile iron is able to exhibit mechanical properties similar to steel. The ISO Standard (Table 6.1), provides ten major grades of ductile iron; from cast iron (with the ferritic matrix) having a high plasticity (A > 22 %), tensile strength and impact strength exceeding UTS > 350 MPa, and K > 120 J respectively, to the cast iron of low plasticity (A > 2 %), characterized by tensile strength excessing UTS > 900 MPa. Significant improvement in the mechanical properties of ductile iron is obtained by heat treatment, involving austenitizing and austempering (ductile iron with ausferritic matrix (ADI: **ISO 17804:2005** Founding—spheroidal graphite cast Ausferritic irons—Classification)). The strength of this iron is comparable with the strength of processed and plastically heat-treated steel. ADI has a tensile strength from 800 to 1600 MPa. It also has excellent fatigue properties, good plasticity and high resistance to abrasion. Recently great interest has been taken in the types of alloyed SGI iron, known as "Si–Mo" (SAE Standard J2582) and "Ni-Resist" (ISO 2892:2007 Austenitic cast irons—Classification). Ductile iron type "Si–Mo" (containing 4–6 % Si and up to 2 % Mo) has a ferritic matrix and is designed to operate at high temperatures. Due to its excellent resistance to oxidation, stability of the structure, strength and resistance to cyclic thermal loading, and a good fluidity cast type "Si–Mo" is an ideal material for such items as exhaust manifolds and turbochargers. "Ni-Resist" type ductile iron contains 18–38 % Ni and up to 6 % Cr, has an austenitic matrix, has: a high corrosion resistance, high seal and creep resistance, as well as good load-bearing properties, is non-magnetic at low levels of chromium, and also has a very good castability and machinability. It is further characterized by very good properties of strength, wherein the tensile strength is in the range of 380–550 MPa and the elongation may be up to 45 %. This may also work in extremely negative temperature ranges.

6.2 Compacted Graphite Cast Iron (CGI)

According to ISO Standard [15], there are five defined standard grades of CGI, which are presented in Table 6.2.

Table 6.2 Specifications for compacted graphite cast iron according to ISO 16112 Standard

Grades	UTS (MPa min.)	YS (MPa min.)	A (% min.)	HBW
ISO 16112/JV/300/S	300	210	2.0	140–210
ISO 16112/JV/350/S	350	245	1.5	160–220
ISO 16112/JV/400/S	400	280	1.0	180–240
ISO 16112/JV/450/S	450	315	1.0	200–250
ISO 16112/JV/500/S	500	350	0.5	220–260

Compacted graphite in CGI is an intermediate form, in terms of compactness, between flake and nodular graphite. CGI properties at room temperature are intermediate between the respective properties of gray cast iron and ductile iron. CGI has better mechanical properties (including plasticity), stiffness, fatigue resistance than gray cast iron. Graphite particles in CGI cast iron interconnect, which results in higher properties such as thermal conductivity, the ability to suppress vibrations and machinability than in the case of SGI. As in the case of ductile iron—modern and perspective types of cast iron with compacted/vermicular graphite: ausferritic matrix (AVCI), with ferritic matrix (Si–Mo CGI), as well as an austenitic matrix, which have an excellent combination of mechanical properties (including work at high and low temperatures), and performance properties.

6.3 Solidification Path

The graphite morphology in SGI and CGI is influenced by a large number of factors during solidification [16–22]. Depending on the liquid composition, solidification starts with either primary precipitation followed by eutectic formation, or directly with an eutectic formation. Graphite precipitates during an eutectic reaction in eutectic compositions.

In the case of cast iron with a hypo-eutectic and eutectic composition, solidification involves the nucleation and growth of primary austenite dendrites, as well as the nucleation and growth of eutectic cells. The nucleation and growth of primary austenite dendrites is possible (when the liquid metal is undercooled below extrapolated liquidus line for austenite) even though the composition is eutectic or slightly hypereutectic, as cast irons solidify following an asymmetric phase diagram (Fig. 6.2).

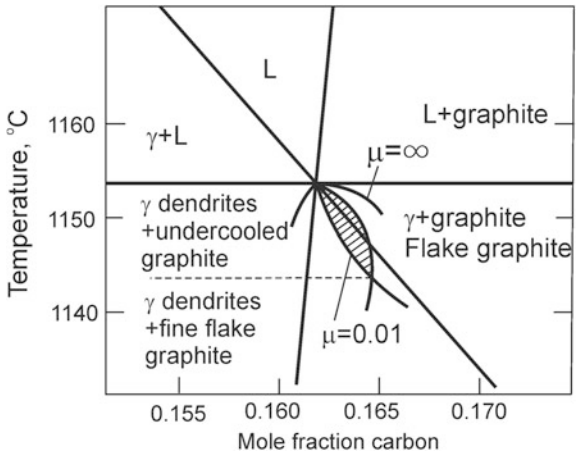

Fig. 6.2 The theoretically predicted coupled zone in the stable Fe–C phase diagram. γ—austenite [30]

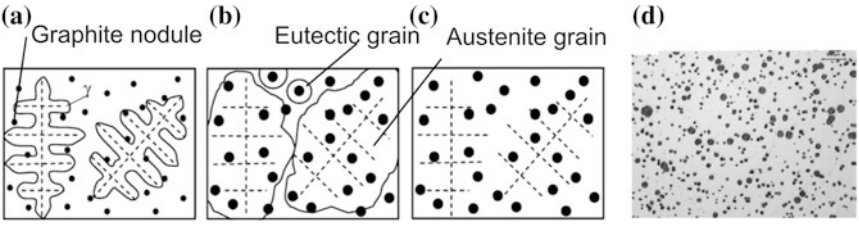

Fig. 6.3 Schematic description of **a** solidification of SGI, **b–c** austenite shells around graphite nodules and off-eutectic austenite dendrites, **d** the microstructure of ductile iron [49]

In accordance with conventional solidification theories, the austenite commonly nucleates on the mold wall resulting in columnar growth, and at a slightly lower temperature the austenite can nucleate on heterogeneities in the liquid metal leading to equiaxed growth [23, 24]. The primary austenite grows as rather thin dendrites with a high growth rate until they impinge. The thin dendrites grow rapidly and form a network of dendrites. Each dendrite forms a rather large austenite grain. After the impingement of the dendrites, growth will continue by dendrite arm coarsening [25].

Undercooling of the liquid metal below the eutectic equilibrium phase transformation temperature is followed by nucleation and growth of the eutectic cells (grains), which consist of graphite and austenite (Fig. 6.3). Eutectic cell (grain) is therefore a product of the spatial creation comprising of two or more interpenetrating crystals growing from a single nucleus during eutectic transformation. Accordingly, each graphite nucleus is expected to give rise to a single graphite nodule in ductile iron or to a single graphite "worm" in the compacted graphite cast iron. Since each eutectic cell is the product of a graphite nucleation event, eutectic cell count measurements can be used to establish the graphite nucleation susceptibility of a given cast iron.

Please note that while the compacted graphite particles appear vermicular when viewed in two dimensions, three dimension micrographs (after deep etching) show [17] that individual "worms" can be independent or connected to their nearest neighbours within the eutectic cell. Due to graphite particle-austenite dendrite interactions, several graphite particles may be incorporated into one austenite grain (Fig. 6.3). Stefanescu [26] considered that the substances which form the nuclei of graphite in CGI and SGI irons are not fundamentally different, but the nucleation substances of compacted graphite contain more complicated and a greater variety of compounds, as compacting agents (vermicularizers) contain many elements such as: Mg, Ce, N, Ca, Al and Ti.

Tartera et al. [27] reported that graphite nuclei in CGI contained MgS and CaS similar to nuclei found in SGI. In SGI, graphite nodules are nucleated which then freely grow in the liquid (Fig. 6.4a) for a relatively short time prior to being enveloped by austenite. The austenite shell nucleates directly on the graphite nodules. The austenite coating increases in the liquid metal in the spherical form until it collides with the adjacent grains. The effect of grain impingement is to

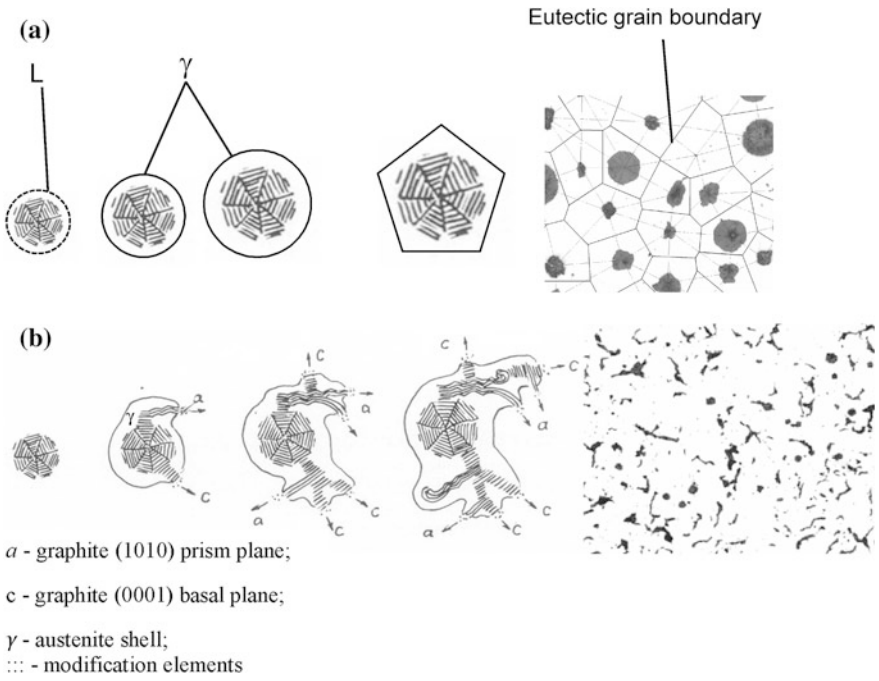

Fig. 6.4 **a** Growth of eutectic grains in ductile iron, **b** Transformation mechanism from a spheroidal to compacted graphite shape [32]

change the shape of (deformation) the austenite shell without changing the shape of the graphite. The numerical calculations used various kinds of assumption that the eutectic grains in such alloys are represented, by e.g. collection of polygons or by a Voronoi polyhedron (Fig. 6.4a) [28].

According to Lux [29], compacted graphite, contrary to spheroidal graphite, does not grow in isolation from liquid metal (Fig. 6.4b). During the growth of compacted graphite (CG), liquid channels (Fig. 6.4b) contacting the ends of compacted graphite and its remaining liquid exist. These liquid channels result from the enrichment of surface active elements, which change graphite growth conditions between the A axis and C axis [30]. Oxygen and sulfur are two surface-active elements, which lower the surface tension between the graphite and liquid. This affects the kinetic reaction and reduces the kinetic growth constant for graphite [31].

From the graphite growth analysis it can be stated that its morphology is not dependent on the structure of nuclei but on the local growth condition of the graphite particles. The main surface active elements (O and S) causing changes in the growth direction, but also so-called anti-spheroidizers, such as Ti, Bi, Zr, P and N, characterized by strong normal segregation [32], which lowers the liquidus

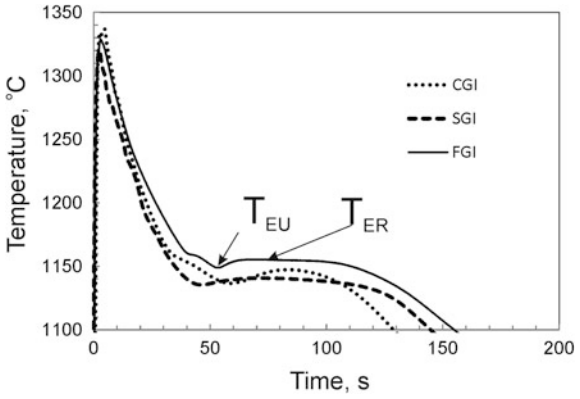

Fig. 6.5 Thermal analysis cooling curves of FGI, CGI and SGI for the same chemical composition

temperature of the melt [33], thus creating the liquid channels that characterize CGI, which then stimulate the formation of compacted graphite. Double and Hellawell [33] showed that the material will solidify as SGI in a pure cast iron melt, completely free from impurities. This indicates that the 'normal', i.e. preferred growth of graphite in a clean cast iron melt would result in SGI. However, since the amounts of surface active elements required to promote the formation of FGI are very small, the only commercially viable way to produce CGI and SGI is with the addition of an alloying element like Mg or RE metals (commonly Ce) that neutralize such elements, which are unavoidable in commercial casting operations [34]. As a consequence of the low amount of surface active elements needed to cause a transition to FGI, it is of great importance to have close control of the Mg or RE additions made.

The shape of a cooling curve from a thermal analysis reflects the solidification process of a liquid metal under a given solidification condition. Therefore, all types of factors influencing melt quality, such as chemical composition and trace elements, inclusions, inoculation and spheroidisation/vermicularization treatments and sampling temperature, will influence the solidification process of the melts and further the shape of its cooling curve [35]. According to the results of the research conducted by Jinhai et al. and Backerud [20, 34], the undercooling that initializes crystallization of austenite-compacted graphite eutectic is of the same order as in the case of ductile cast iron (curve 2 and 3 in Fig. 6.5).

Figure 6.5 shows that for the same chemical composition of cast iron, the lowest eutectic temperature (T_{EU}), the highest eutectic temperature (T_{ER}) and recalescence degree ($\Delta T_r = T_{ER} - T_{EU}$) of the FGI, CGI and SGI are significantly different. Podrzucki et al. and Jinhai et al. [18–20] concluded that during the eutectic growth of grey cast iron, the graphite tip always grows and extends into the liquid ahead of the austenite crystal frontier. Since the carbon diffusion rate in the liquid phase is about 20 times faster than that in solid austenite, graphite grows quickly and results in poor carbon distribution in the area surrounding the growing graphite tip. This contributes to the growth of austenite. Therefore, eutectic growth requires less

driving force and eutectic undercooling is small. It shows on the curve that T_{EU} is higher compared to those in SGI and CGI. Also, due to the higher T_{EU}, which is close to T_{ER}, the recalescence degree ΔT_r is also smaller. The spheroidal graphite in SGI grows by carbon diffusion through the austenite shell [21]. This causes a low diffusion speed of the carbon atom in austenite, which results in the rate of eutectic solidification being slow and the latent heat released per time unit also being small. As a result, the T_{ER} temperature is relatively low and recalescence is also small. The growth rate of compacted graphite in CGI is between those in LGI and SGI. Compacted graphite cast iron has the highest rate of recalescence. This results from the afore-mentioned thin liquid channels [36]. As the graphite is in contact with the melt, the diffusion process needed for the growth of the eutectic is not solely dependent on diffusion through the austenite envelope [37]. This implies that the eutectic interface of CGI can grow quickly and thus the latent heat release will be very fast, giving a high rate of recalescence [21].

6.4 Nodule Count and Cooling Rate

The importance of the exhibited number of eutectic grains (nodule/compacted graphite count) can be related to the graphite nucleation potential of the liquid metal. In general, increasing the number of eutectic grains in ductile or compacted graphite iron leads to [1–13]:

- a reduction in the chilling tendency of cast iron,
- an increase in the pre-shrinkage expansion,
- a reduction in segregation,
- changes in the usable properties.

Accordingly, it is evident that the eutectic grain count has a strong influence on the various technological factors used in the foundry practice.

A high cooling rate (Fig. 6.6) causes a significant increase in the number of graphite nodules [38] in the structure of cast iron.

Increasing the cooling rate increases the number of graphite nodules, reducing the distances between them. As a result of shortening the diffusion path of carbon the ferrite fraction in a matrix increases. On the other hand, increasing the cooling rate promotes the transformation of austenite into pearlite of increased dispersion. The cooling rate also affects the graphite morphology [29, 39]. With the decreasing wall thickness it is easier to obtain a higher degree of spheroidal graphite, and thus it may be necessary to limit the content of spheroidising elements.

The cooling rate is not only a function of the wall thickness (for a given pouring temperature and the type of molding sand), but also depends on the thickness of the neighboring parts of the casting, the charging method, or duration of the metal flow through the cross-section. These factors have a significant impact on the crystallization of castings and can be used to produce the desired structure and to eliminate casting defects.

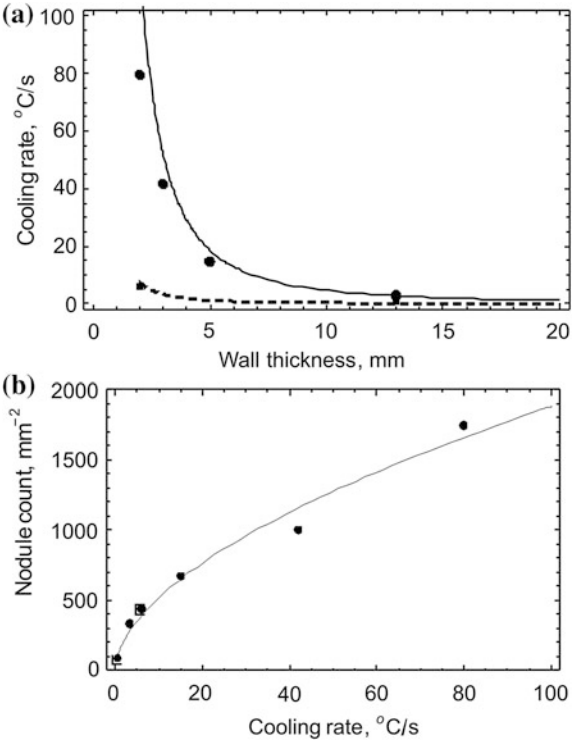

Fig. 6.6 Effect of wall thickness on the cooling rate of the casting: *solid curve* ●—experimental points for silica sand, ■—experimental points for LDASC (low-density alumina-silicate ceramic) insulation sand (**a**), effect of the cooling rate on the number of graphite nodules in SGI (**b**) [38]

As reported by Fraś and Lopez [40] a reduction in the size of eutectic grain (or an increase in eutectic grain count) lowers the plane of weakness within the compacted graphite cast iron. The interconnection between graphite particles edges can lead to an easy fracture, as well as areas of high stress concentrations. In the case of thin wall castings, compacted graphite iron microstructure can contain independent (not connected) graphite particles (due to the short crystallization time) which minimize the planes of easy fracture. From the tensile strength point of view, the microstructure that possesses a high graphite particle count is the most desirable. Hence, a high eutectic grain count is associated with a high tensile strength. This applies to SGI and CGI. In contrast, ductile iron contains not connected, nearly spheroidal graphite particles thus minimizing the planes of easy fracture. As it was mentioned, by reducing the wall thickness it is easier to obtain graphite of high degree of sphericity, which significantly improves the mechanical properties of the SGI.

According to the literature, a moderate increase in the nodule count in normal wall parts, from 100 to 250 mm^{-2} leads to this significant increase in strength and ductility, as a result of a uniform distribution of fine nodules and a homogeneous micro-structure obtained by austempering. In particular, it has been shown [13] that the rolling contact fatigue resistance of high nodule count austempered ductile iron (ADI) samples is over five times higher than in that obtained in the normal ADI

nodule count of a similar hardness. In contrast, it has been observed that under abrasive the wear rates condition increases as the nodule count increases [13].

6.5 Defects

Different defects may appear during the production of SGI castings, such as defects in the casting skin (flake graphite at the casting-mold interface), a grouping of graphite, exploded graphite, slag inclusions, shrinkage porosity, eutectic and secondary chills and cold shuts [22, 41–44]. These disadvantages are shown in Fig. 6.7, and potential causes [41] of their formation are shown in Table 6.3.

Depending on the technological factors affecting the cooling rate as well as on the physicochemical state, the thickness of the degenerated graphite layers in SGI and CGI castings is usually up to 3.0 mm [41]. High contaminant and/or low Mg

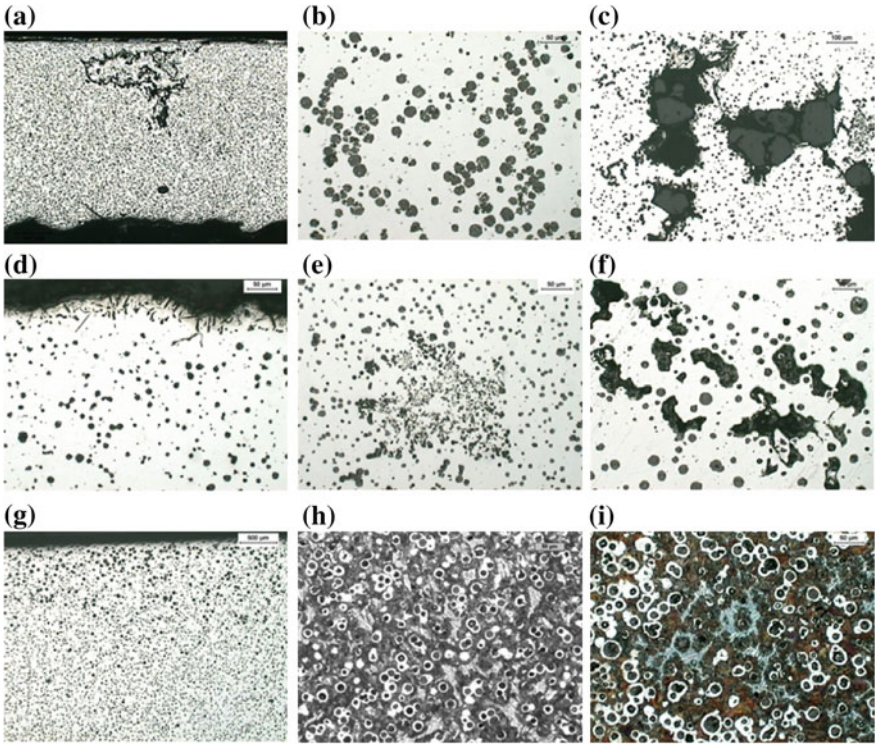

Fig. 6.7 Defects in the structure of ductile iron castings: **a** slag inclusions, **b** nodular grouping, **c** the undissolved particles of inoculant, **d** the skin of flake graphite, **e** highly dispersed graphite particles, **f** the shrinkage porosity, **g** grouping the graphite at a casting surface, **h** eutectic chills, **i** secondary chills. **a**–**g** no etched samples; **h**, **i** nital etched samples

Table 6.3 Defects in ductile iron castings

No	Defect	Potential causes
1	Flake graphite at the surface	Excessive S build-up
		Excessive Mg/RE oxidation
		Molding sand conditioners
		High pouring temperature
2	Graphite grouped on the surface of casting (flotation)	High carbon equivalent (CE)
		Excessive pouring temperature
		Slow cooling rate
		Insufficient inoculation
3	Slag inclusions	Inadequate slag control
		Excessive slag forming materials
		Turbulent mold filling
		Metal-mold reaction
4	Grouping graphite	High carbon equivalent (CE)
		Turbulent mold filling
		Excessive inoculation
5	Exploded graphite	Excessive rare earth (RE)
		Particularly high purity charge
		Normally in thick castings
		Usually for high CE
6	Shrinkage cavities	Insufficient power supply
		Lack of rigidity forms
		A high degree of inoculation
		A large number of CE
7	Primary and secondary chill	High-speed cooling
		Small CE values
		Insufficient degree of inoculation
		The presence of carbide forming elements
8	Cold shuts	Low temperature casting
		Inadequate venting forms
		Too slow or intermittent flooding forms
		Poorly designed gating system

residual produce relatively more graphite flakes surface layer. The presence of microporosity, degenerate graphite, dross stringers and other imperfections are at the surface, all properties are reduced, a situation observed in all tensile test bars exhibiting these defects [41]. As reported by Fallon [44] fatigue properties (by about 15 %) are significantly reduced. Moreover depending on the severity, the presence of slag reduces fatigue limit between 19 and 33 %; while pinholes have the greatest effect on the fatigue limit, causing a reduction of about 40 %. It is worth noting that in the thin wall castings made of SGI, these drawbacks have even greater influence on the mechanical properties. For example, the casting with a wall

thickness of 2 mm, and a slag inclusion of 1 mm reduces the active area of the cross section (carrying load) by 50 % (Fig. 6.7a). In contrast, the same inclusion in a wall having a thickness of, for example, 20 mm in the cross-sectional area is reduced by only 5 % and has a significantly lower impact on the mechanical properties. Slag inclusions can be eliminated by using gating system filters, among others.

6.6 Production

The production of high quality, defect-free SGI and CGI castings involves a series of stages, which need to be carefully controlled. The practice of obtaining SGI and CGI involves the same processes and procedures as shown in Fig. 6.8.

A number of spheroidizing/compacting treatments have been developed based on the use of:

In SGI

- Mg + the addition of such elements as: Si, Ca, Ni, Cu, Rare Earth (RE);
- treatment with cerium lub Rare Earth (RE)

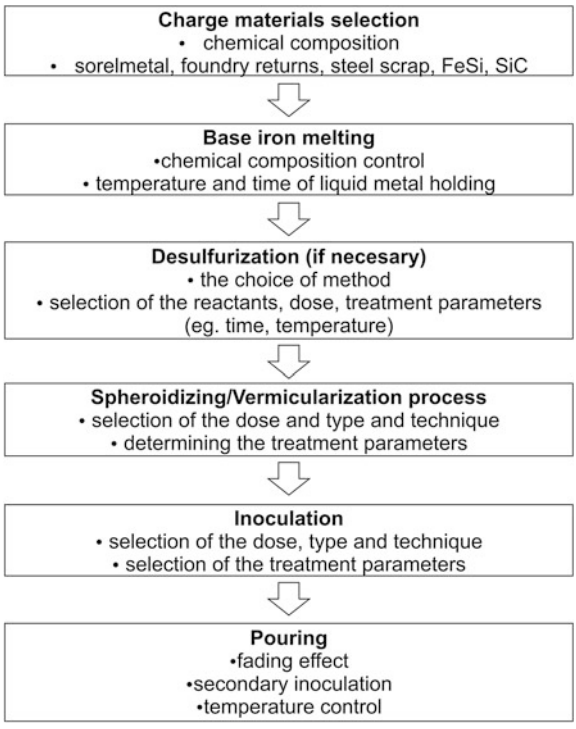

Fig. 6.8 The general scheme of the preparation process of SGI/CGI cast iron

In CGI

- under treatment with Mg where standard MgFeSi alloys can be used;
- Mg plus Ti treatments, where the Ti is added usually as an integral part of the MgFeSi;
- Mg + Rare Earth (RE) alloy usually containing 5.5–6.5 % RE in MgFeSi alloy;
- treatment with cerium or nitrogen [45–48].

Many technological solutions concerning spheroidisers/vermiculisers were developed over many years while producing SGI and CGI cast iron, and ways of implementing them into the liquid metal. Detailed discussion of such processes can be found elsewhere [18–22, 43–48]. The formation of nodular graphite in SGI and compacted/vermicular graphite in CGI is closely associated with a relevant physicochemical state of the liquid metal and control of the cooling rate. The holding time and temperature prior to the spheroidizing/vermicularization treatment must be limited to maintain a high nucleation potential of the melt and retain a high quality metallurgical factor of the liquid metal [22]. The chemical composition and pouring temperature, fading effect must also be taken into account to produce defect free castings.

References

1. Fraś E, Górny M, Lopez HF (2006) Chilling tendency and nodule count in ductile cast iron Part I—Theoretical background. AFS Trans 114:575–594
2. Fraś E, Górny M, Lopez HF (2006) Chilling tendency and nodule count in ductile cast iron Part II—Experimental verification. AFS Trans 114:595–603
3. Fraś E, Górny M, Lopez HF (2005) The transition from gray to white iron during solidification, Part I—Theoretical background. Metall Mater Trans A 36A:3075–3082
4. Fraś E, Górny M, Lopez HF (2007) Eutectic cell count, chilling tendency and chill in flake graphite iron, Part II—Experimental. AFS Trans 115:453–465
5. Nicholas KE (1961) Inoculation and casting expansion. Br Cast Iron Res Assoc J 1:103–116
6. Vondrak V (1971) Eeinfluss der vorschwidungsausdehnung aauf die lunkerbildung bei gusseisen mit kugelgraphit. Giesserei 4:84–88
7. Lesoult G, Castro M, Lacaze J (1999) Solidification of spheroidal graphite cast iron: III Microsegregation related effects. Acta Mater 47:3779–3792
8. Achmadabi MN, Niyama E, Ohide T (1994) Structural control of 1 % Mn ADI aided by modelling of microsegregation. AFS Trans 97:269–278
9. Ruff GF, Doshi BK (1980) Relation between mechanical properties and graphite structure in cast irons, Part I—Gray iron. Mod Cast 70:50–55
10. Soufe M, Okada S, Sasaki T (1978) High quality ductile cast iron with improved fatigue strength. AFS Trans 86:173–182
11. Ruff GF, Doshi BK (1980) Relation between mechanical properties and graphite structure in cast irons, Part II—Ductile iron. Mod Cast 70–74

12. Javaid A, Thompson J, Davis KG, Sahoo M (2001) Effect of microstructure on the mechanical properties thin-wall ductile iron castings. AFS Trans 109:1097–1114
13. Rebasa N, Dommarco R, Sikora J (2002) Wear resistance of high nodule count ductile iron. Wear 253:855–861
14. Spheroidal graphite cast irons—classification ISO 1083:2004(E)
15. Compacted (vermicular) graphite cast irons classification ISO 16112:2006
16. Konig M (2010) Literature review of microstructure formation in compacted graphite iron. Int J Cast Metal Res 23(3):185–192
17. Sofroni L, Riposan I, Chria I (1974) Some considerations on the crystallization features of cast irons with intermediate-shaped graphite (vermicular type). In: Proceedings of the 2nd international symposium on the metallurgy of cast iron, Geneva, Switzerland, Institute Battele, Georgi Pub. Co. pp 179–196, 29–31 May 1974
18. Podrzucki C, Wojtysiak A (1987) Unalloyed ductile iron. Part I—Cast iron with spheroidal graphite. AGH, Krakow
19. Podrzucki C, Wojtysiak A (1988) Unalloyed ductile iron. Part II—Cast iron with vermicular graphite. AGH, Krakow
20. Jinhai L, Litao Y, Guolu L et al (2011) Influence of fading on characteristics of analysis curve of compacted graphite iron. China Foundry 3:295–299
21. Fras E (2003) Solidification of metals and alloys. WNT, Warszawa
22. Labrecque C, Gagne M (1988) Review ductile iron 50 years of continuous development. Can Metall Q 26(4):343–378
23. Lesoult G, Castro M, Lacaze J (1998) Solidification of spheroidal graphite cast irons—I. Physical modelling. Acta Mater 46:983–995
24. Lacaze J, Castro M, Lesoult G (1998) Solidification of spheroidal graphite cast irons—II. Numerical simulation. Acta Mater 46:997–1010
25. Fraś E (2001) Solidification of alloys. WNT, Warszawa
26. Stefanescu DM, Martinez F, Chen IG (1983) Solidification behavior of hypoeutectic and eutectic compacted graphite cast irons: chilling tendency and eutectic cells. AFS Trans 91:205–216
27. Tartera J, Llorca-Isern N, Marsal M, Rojas JL (2003) Similarities of nucleation and growth of spheroidal and compacted graphite. Int J Cast Met Res 16:131–135
28. Burbelko A, Początek J (2013) Averaged Voronoi polyhedron in the diffusion controlled solidification modeling. In: TMS 2013 annual meeting supplemental proceedings. TMS (The Minerals, Metals & Materials Society), Wiley, pp 523–530
29. Showman RE, Aufderheide RC (2004) Controlling nodularity in thin-wall compacted graphite iron castings. AFS Trans 112:823–830
30. Fredriksson H (1975) The coupled zone in grey cast iron. Metall Trans 6A:1658–1659
31. Fredriksson H, Akerlind U (2012) Crystallization processing in metals and alloys. Wiley, London
32. Den X, Zhu P, Liu Q (1984) Structure and formation of vermicular graphite in the physical metallurgy of cast iron. In: Frederiksson H, Hillert M (eds) Proceedings of material research society, Stockholm, Sweden, pp 141–150
33. Double DD, Hellawell A (1995) The nucleation and growth of graphite: the modification of cast iron. Acta Metall Mater 43(6):2435–2442
34. Backerud L, Nilsson K, Stem H (1974) Study of nucleation and growth of graphite in magnesium-treated cast iron by means of thermal analysis. In: Proceedings of the 2nd international symposium on the metallurgy of cast iron, Geneva, Switzerland, Institute Battelle, Georgi Pub. Co., 29–31 May 1974, pp 625–637
35. Sun XJ, Li YX, Chen X (2008) Identification and evaluation of modification level for compacted graphite cast iron. J Mater Process Tech 200:471–480
36. Chen JY, Wu DH, Liu PC, Loper CR (1986) Liquid metal channel formation in compacted/vermicular graphite cast iron solidification. AFS Trans 94:537–544
37. Pan EN, Ogi K, Loper CR (1982) Analysis of the solidification process of compacted/vermicular graphite cast iron. AFS Trans 90:50–527

38. Górny M, Tyrała E (2013) Effect of cooling rate on microstructure and mechanical properties of thin-walled ductile iron castings. J Mater Eng Perform 22(1):300–305
39. Llorca-Isern N, Nesa D, Vicente M (2003) Thin wall compacted graphite cast iron for automotive applications. Int J Cast Metal Res 16(1–3):325–328
40. Fraś E, Lopez H (2010) Eutectic cells and nodule count-an index of molten iron quality. Int J Metalcast Summer 10:35–62
41. Riposan I, Chisamera M, Stan S, Skaland T (2006) Factors influencing the surface graphite degeneration in ductile iron castings in resin mold technology. In: Proceedings of the eighth international symposium on science and processing of cast iron, Beijing
42. Boeri R, Sikora J (2001) Solidification macrostructure of spheroidal graphite cast iron. Int J Cast Metal Res 13:307–313
43. Metal Handbook (1988) Volume 15: Casting. ASM International, Ohio
44. Fallon MJ (1995) Experiences in the manufacture of ductile irons. The Foundrymen 88 (9):308–318
45. Cornell HH, Loper CR (1985) Variable involved in producing compacted (vermicular) graphite cast iron using rare earth—containing alloys. AFS Trans 93:435–442
46. Campamanes E, Goller R (1976) Production of cast iron containing intermediate forms of graphite. Mod Cast 66(3):71–72
47. SinterCast (1994) Method for the production of compacted graphite cast iron. US Patent US no 5337799 A
48. Debabrata SG, Gray JM, Kay DA, Purdy GR, Subramanian SV (1980) Process for the production of vermicular cast iron. US Patent no 4227924 A
49. Fraś E, Górny M, Lopez HF (2007) Eutectic cell and nodule count in cast iron. Part 1—Theoretical background. ISIJ Int 47(2):259–268
50. Lux B, Vendl A, Hahn H (1980) Uber die Ausbildung eutektischer Gefuge in grau erstarrten Guβeisen. Radex-Rundschau (1/2):30–50

Chapter 7
Influence of the Technological Parameters on the Microstructure and Quality of the Casting Surface

Marcin Górny

Abstract This chapter presents the issue of the effect of technological parameters (impact on the cooling rate and the physicochemical state of liquid metal) on the microstructure and quality of the casting surface. A diagram of the impact of the technological factors on the parameters of the microstructure of cast iron SGI and CGI is presented. It is demonstrated that wall thickness of the casting and pouring temperature affect the initial temperature of the metal in the mold, which determines the thickness and the presence of flake graphite in the surface layer. Moreover, the issues is raised dealing with chemical composition, including despheroidising elements, metallurgical treatments, as well as changes in the cooling rate at the transition from conventional through thin up to the ultra-thin wall castings in terms of shaping defects and the casting surface. In addition to this, molding sand is also considered in this chapter. Special attention is paid to the molding sands containing reclaimed resin-bonded sand with *p*-toluenosulfonic acid as a hardening catalyst. Finally, a comparison between the effects of different types of molding sands with using fresh and reclaimed materials, protection atmosphere and coatings is shown.

The microstructure and with it the properties of spheroidal graphite cast iron (SGI) and compacted graphite cast iron (CGI) are formed in the process of solidification, especially eutectic. Here you can distinguish three basic parameters that are taken into account in the analysis of the solidification process, i.e. the degree of undercooling, the number of nuclei and eutectic grain growth rate. These factors determine the microstructure of the casting in terms of quality and quantity, i.e. the geometry of the crystallizing phases (graphite, austenite, cementite), their participation and the number of eutectic grains. Another factor in determining the microstructure of the volume is the chilling tendency, which is expressed as the width (or height) of chill or CT value, i.e. the absolute chilling tendency [1, 2]. These factors are related to each other's technological parameters, which are shown in Fig. 7.1.

© The Author(s) 2015

M. Holtzer et al., *Microstructure and Properties of Ductile Iron and Compacted Graphite Iron Castings*, SpringerBriefs in Materials,
DOI 10.1007/978-3-319-14583-9_7

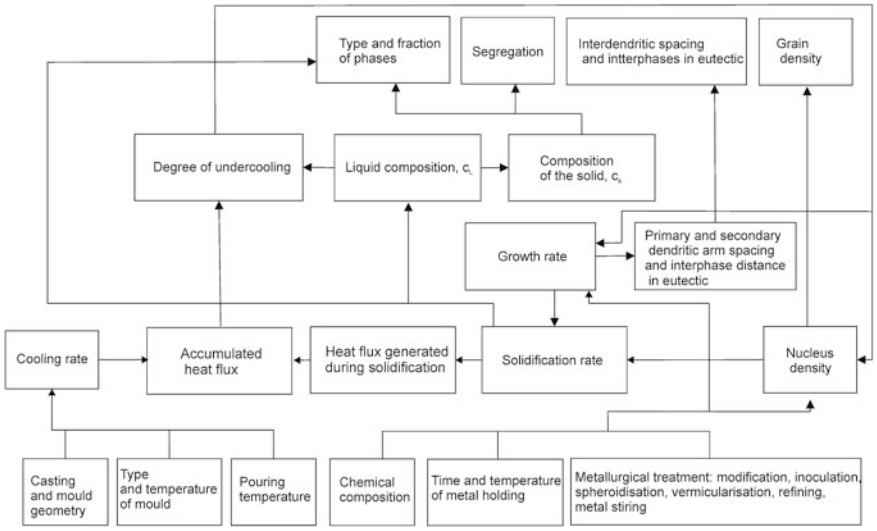

Fig. 7.1 A schematic representation of the effect of various factors on the microstructure of SGI and CGI [3]

Technological factors influence the physicochemical state and the cooling rate. Referred to in this way, such a change, e.g. eutectic grain growth conditions (graphitic) entails a change in the degree of deformation of the nodular (in SGI) or the degree of the graphite branching skeleton (in the case of FGI). Changing the cooling rate causes a concomitant change in the number of eutectic grains, their growth rate and the degree of undercooling of the corresponding consequences for the interfacial distance. The diagram of technological factors (Fig. 7.1) influencing the microstructure of cast iron generally relates to eutectic crystallization. In the case of cast iron in non-eutectic composition, the primary crystallization of austenite and primary graphite are additionally taken into account. The crystallization of pre-eutectic and eutectic phases determines the cast iron's basic microstructure. They determine the number, volume fraction, shape and size of primary austenite dendrites, eutectic and primary graphite, indicating the critical level and functional mechanical properties of cast iron. The final microstructure of the casting is formed as a result of eutectoid transformation, bainitic or martensitic. In this regard, the factors affecting the physicochemical state of the liquid metal have only an indirect influence through interaction with the microstructure during the primary and eutectic transformations. Another group of factors, i.e. influencing the cooling rate, plays an important role because it determines the undercooling related to the equilibrium temperature with respect to these changes.

7.1 Pouring Temperature

Górny et al. [4] demonstrated the effect of the wall thickness and the initial temperature of the metal in the mold cavity on the formation of the flake graphite in the surface layer of the ductile iron castings. Boonmee [5] have performed simulations (2-D thermal-diffusion model) connected with the thickness of flake graphite formation as a function of pouring temperature. The effect of the casting temperature on the formation of the flake graphite layer at the metal-mold interface is shown in Fig. 7.2.

The higher the pouring temperature the higher the thickness of the flake graphite layer at the metal-mold interface (see also Fig. 7.2). The higher liquid metal temperature primarily affects the timing and intensity of the diffusion reaction at the metal-mold interface. A higher temperature increases the contact time of molten metal with the mold. It should also be stressed that the variable conditions of heat

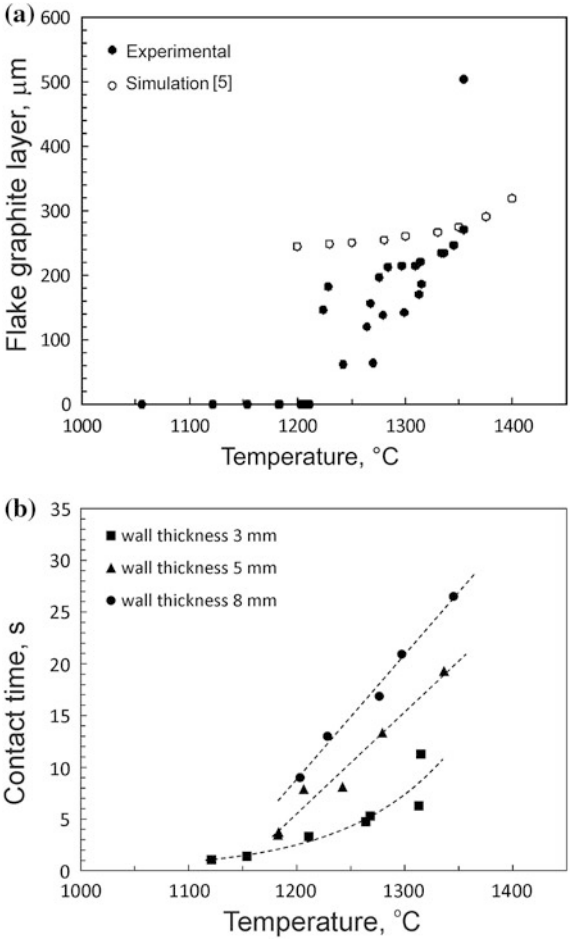

Fig. 7.2 Effect of temperature of the liquid metal on the layer thickness of flake graphite in the casting surface (**a**), the contact time of liquid metal mold with (**b**)

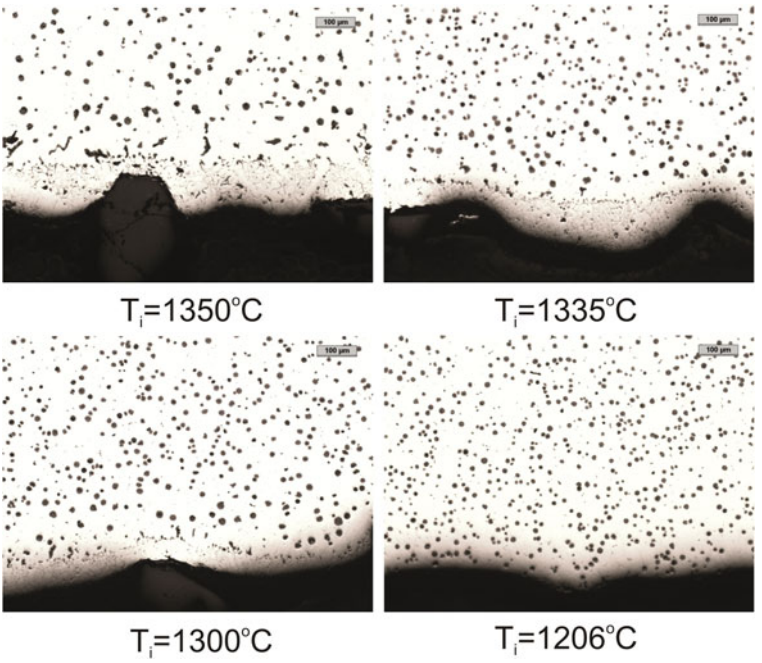

Fig. 7.3 Microstructure of SGI in castings at the metal-mold interface, for a different initial temperature in mold cavity T_i (castings with wall thickness of 5 mm), non-etched samples

exchange prolong the contact time with the increasing casting wall thickness. From the research [4] it can be concluded that the flake graphite layer on the metal-mold interface disappears when the casting temperature reaches 1200 °C (Fig. 7.3).

7.2 Composition of Alloy and Metallurgical Treatment

The proper selection of the chemical composition plays an important role in the production of SGI and CGI. The typical range of basic elements in SGI and CGI are within the range C = 3–4 %, Si = 2–3 %, Mn < 0.5 %, P < 0.05 %.

In the discussion on the possibility of degenerate or flake graphite in the surface layer of the casting, special attention should be paid to the elements, the so-called nodulizers and vermiculizers, despheroidizing elements, as well as inoculants.

In the group of spheroidizer/vermiculizers, the decisive role is played by magnesium and its alloys and rare earth elements, usually in the form of mischmetal, which includes elements such as Ce, Ne, Pr and La. SGI and CGI can be obtained when treating a base iron with a controlled magnesium (magnesium alloy) concentration. Better control of residual magnesium can be achieved in the production of SGI. This is due to the wide range of acceptable magnesium concentrations

(0.03–0.06 % mass) at which a nodular graphite is obtained in the cast iron microstructure. The amount of magnesium that should be in the iron depends upon the cooling rate of the casting. Its measurement is usually a casting module (i.e. V/A; V—casting volume, A—surface area of a casting), which is proportional to the magnesium content required for spheroidizing treatment. Cooling at high rates in thin-wall castings required the magnesium content might be even less than 0.02 %. You should also keep in mind the significant effect of treated cast iron temperature as during its nodularisation, higher magnesium evaporation levels reduces its yield. Using a lower dose of spheroidizer increases the danger of the occurrence of flake graphite or degenerated spheroids in the surface layer of the casting. In turn, when the magnesium content of the cast iron is too high, especially in thin castings, it can cause the formation of eutectic carbides (i.e. chills). CGI iron castings are much more endangered to the risk of the occurrence of flake graphite in the surface layer. The most important methods that can be used for CGI production can be classified as: the previously mentioned controlled undertreatment with magnesium-containing alloys, treatment with a rare-earth-base alloy, treatment with alloys containing both vermiculizer (magnesium or rare earth elements) and anticompactizing elements (aluminum or titanium and sulfur and aluminum). The preparation of compacted/vermicular graphite requires a very narrow range of concentration of magnesium in cast iron (in the vicinity of 0.02 % Mg mass), which may contribute to the risk of the degeneration of graphite in the casting surface layer. As reported by Sergeant and Evans [6] using a magnesium + titanium combination rather than magnesium alone dramatically increases the range of residual magnesium, over which compacted graphite can be obtained in the entire cast microstructure. The treatment of iron with rare earth alloys (mischmetal) is used for the production of medium and heavy section CG iron production. This is due to its strong effect on the tendency to chills and the creation of adverse inclusions, especially sulfides, the removal of which is much more difficult from the molten metal (due to of their higher density) compared to sulfides or magnesium oxides.

For the formation of degenerate graphite in the surface layer surface active elements are responsible, which include mainly sulfur and oxygen. The research [7, 8] shows that the S/Mg ratio increased fivefold from 0.5 in the center or body of the casting, up to more than a 2.5 ratio at the casting surface. Graphite degeneration in the near surface layer of SGI or CGI therefore occurs due to the magnesium (vermicularization element) concentration decrease (gradient). This decrease is caused by the reaction of magnesium with, firstly, sulfur or oxygen, which diffuse from molding sand into metal. The higher the concentration of these elements in the liquid metal and also in the molding sand, the higher the thickness of the degenerated graphite layer.

The surface layer on CGI castings can include a degeneration of different variants of graphite morphologies, from a mixture of various graphite shapes (flakes with different type of distribution and compacted with a different shape factor) with transitions, such as: type A flake → type D flake → Compacted → Spheroidal (Fig. 7.4). The degeneration of an A-type graphite into a D-type graphite in the surface layer is associated with a decrease in the concentration of active surface

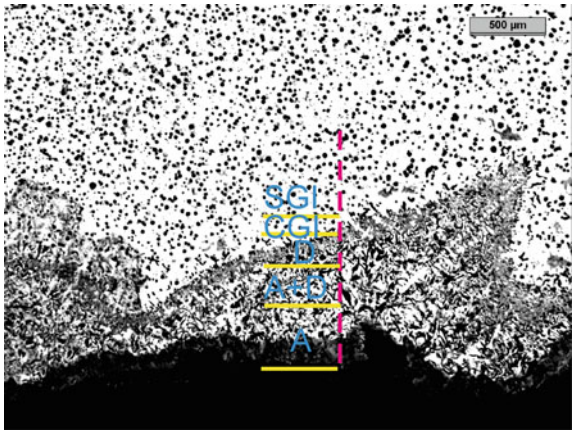

Fig. 7.4 Surface layer with the zone of transitions away from the surface A type flake → D type flake → Compacted → Spheroidal

elements (mainly sulfur). As mentioned above, the concentration of magnesium decreases in the near surface layer of SGI or CGI, up to the level where the compacted eutectic degenerates into a D-type flake eutectic. A further decrease of magnesium concentration degenerates a D-type eutectic into an A-type, which occurs at high concentrations of surface active elements in the molding sand. Graphite degeneration on the surface of the SGI is shown in Fig. 7.4.

7.3 Carbon Equivalent—CE

The effect of CE (Carbon Equivalent, $CE = C + 0.30 \cdot Si + 0.36 \cdot P$, where: Si and P are silicon and phosphorus, respectively) on the formation of flake graphite in surface layer as reported by Boonmee [5] is connected with the amount of the primary phase formed at the beginning of solidification. The formation of primary austenite dendrites in hypoeutectic iron produces Mg segregation as the Mg rejected by the solid is pushed by the solidification front, leaving an Mg depleted zone at the casting skin. This creates a highly oriented dendritic structure with fine flake graphite between the dendrites. As the CE increases, less austenite is produced, which results in a thinner flake graphite layer.

7.4 Cooling Rate

The work of Goodrich and Lobenhofer [9], and also Duncan and Kroker [10] highlights the significant impact of the cooling rate on the SGI structure and properties. They concluded that the flake graphite layer lowers elongation, tensile strength

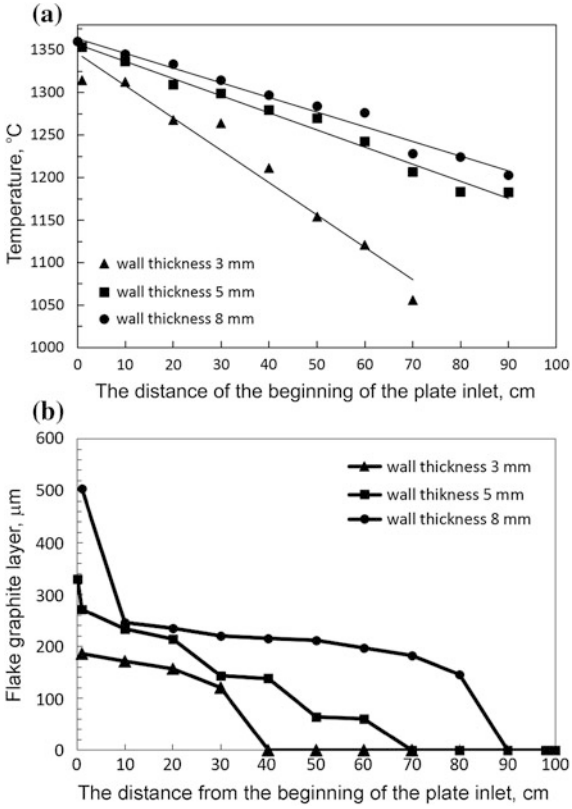

Fig. 7.5 Initial temperature of metal in the mold cavity during metal filling for castings with different wall thicknesses (**a**). Thickness of the flake graphite layer as a function of the distance from the beginning of the plate inlet (**b**) [4]

(UTS) and yield strength (YS) in a ferritic grade of a SGI. The effect of the graphite layer on ferritic SGI decreases as the wall thickness increases. As the cooling rate increases, both the yield strength and tensile strength increases linearly while elongation decreases linearly for ferritic grades of SGI [9]. Górny et al. [4] demonstrated the effect of the cooling rate, expressed with a variable wall thickness on the formation of the flake graphite in the surface layer of ductile iron castings (Fig. 7.5).

Figure 7.5 shows that the temperature of the liquid metal decreases approximately linearly with the distance from the entrance to the mold cavity and there is a large drop in temperature during the mold filling that strongly depends on the wall thickness. For casting with a higher wall thickness decrease of the temperature during mold filling is lower. The consequence of this is a higher temperature and a longer contact time of the liquid metal with the mold as compared to a casting with smaller wall thickness. A flowing metal stream through the mold cavity heats it up. As a consequence, the conditions of heat exchange along the flowing path change. With the increasing distance from the entrance to the mold cavity, there is a shorter contact time of the liquid metal with the mold, which results in decreasing temperatures and velocity profiles. From the research conducted, [4] it follows that the thickness of the flake graphite layer in SGI decreases with the distance from the

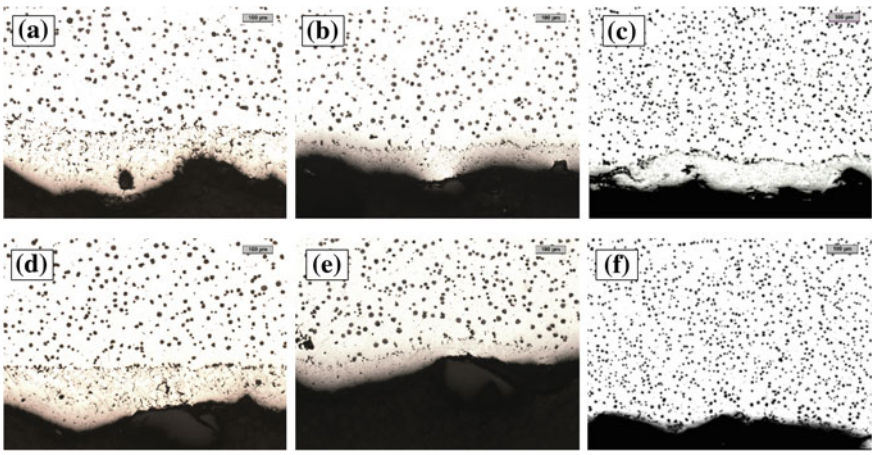

Fig. 7.6 Microstructure of ductile iron in plate shaped castings with different wall thicknesses (**a**, **b**, **c** plates with 8, 5 and 3 mm wall thickness, respectively and 30 cm distances from the beginning of the, **d**, **e**, and **f** plates with a 8, 5 and 3 mm wall thickness, respectively and 40 cm distances from the beginning of the plate

beginning of the plate inlet. At a distance 40 cm from the beginning of the plate shaped casting (with wall thickness of 3 mm), flake graphite is not present in the surface layer of a casting. It is worth noting that the thicknesses of flake graphite layer is much higher in castings with wall thickness of 5 and 8 mm and disappears after reaching 70 and 90 cm. respectively from the casting inlet. This demonstrates a significant influence of the wall thickness on the occurrence and the thickness of flake graphite in the surface layer. The smaller the wall thickness of the casting the higher temperature the drop of the flowing metal stream filling the mold cavity. Figures 7.6 shows the microstructure of ductile iron in the surface layer in plate shaped castings. As in the case of SGI it is obvious that in the case of CGI the thickness of flake graphite layer increases with increasing section thickness for all types of mold coatings (Fig. 7.7). As reported by Boonmee [5] the degraded graphite (flake graphite) becomes coarser as the section thickness increases.

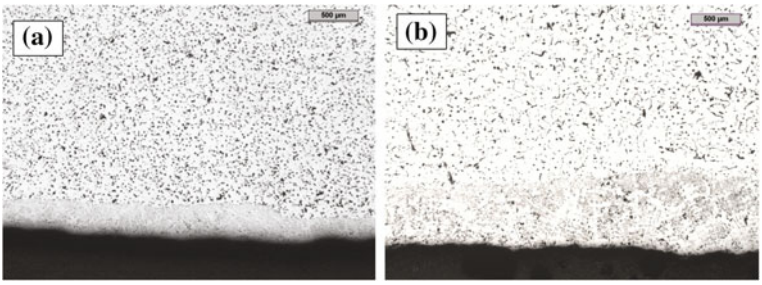

Fig. 7.7 Effect of wall thickness on the microstructure at the metal-mold interface for CGI: **a** wall thickness of 5 mm, **b** wall thickness of 13 mm

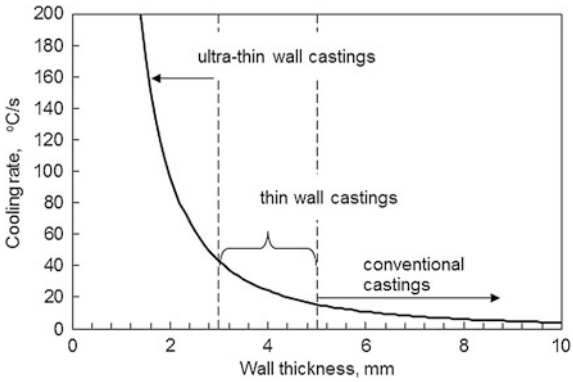

Fig. 7.8 Effect of casting wall thickness at the rate of cooling (typical molding sand on a silica sand base)

In the literature [11–13] the contractual allocation can be found on conventional castings, i.e. castings with wall thicknesses greater than 5 mm, and the thin-wall castings, i.e. castings with a wall thickness of less than 5 mm (Fig. 7.8). In the conducted research [14] taking the dependence of the cooling rate of the casting wall thickness into account (Fig. 7.8), the castings are divided into three groups, i.e. conventional castings with a wall thickness greater than 5 mm, thin-wall castings with a wall thickness in the range of 3–5 mm, and ultrathin-wall casting with wall thicknesses not exceeding 3 mm. The features of thin-wall and ultrathin-wall castings are large cooling rate changes and small changes of the wall thickness. This effect is shown in Fig. 7.8. The analysis shows that the change in the wall thickness of the casting, e.g. by 1 mm, causes almost negligible changes in the cooling rate of conventional castings (when changing the wall thickness, e.g. from 15 to 14 mm), but significant for thin-wall castings (from about 16 to 24 °C/s, the change in wall thickness of 5–4 mm) and essential for ultrathin-wall castings (from about 43 to 97 °C/s, and the change in wall thickness from 3 to 2 mm). The problem of obtaining ultrathin-wall castings is not easy, because this is associated with a large cooling rate range.

This contributes to a greater tendency for the formation of defects, in particular in the inhomogeneity structure and the occurrence of chills. Knowledge of the impact of technological factors on the cooling rate and physicochemical state of liquid metal is fundamental to obtain cooling castings at high speeds with good mechanical properties and performance, without, at the same time, casting defects.

7.5 Molding Sand

Molding sand is of high importance in SGI and CGI production. Bentonite and resin-bounded sands can usually be used for both SGI and CGI production. In general, all molding materials that can produce rigid molds may be used in the production of SGI and CGI casting iron. It has to be stressed that for production of CGI, liquid metal is more sensitive to sulfur pickup from the mold than for the production of SGI. This results from the fact that CGI has, as previously mentioned, a very narrow range of critical concentration of magnesium so that liquid metal

must not be overtreated. Special attention must be paid to the molding sands containing reclaimed resin-bonded sand with *p*-toluenesulfonic acid as a hardening catalyst. The reclaimed additive can significantly increase the sulfur concentration by weight of the molding sand to over 0.30 % mass. Such an amount can causes sulfur content increase up to over 0.05 % mass S in the surface area, resulting in a graphite degeneration up to several micrometers in thickness.

Figure 7.9 shows the effect of the type of molding sand and the application of protective coatings to the presence and the thickness of the plate graphite layers on the surface of the casting. The research used molding sands with furfuryl resin, which was hardened with an acid catalyst with a differing sulfur content. In each case, the composition of the molding sand was as follows:

- reclaimed used sand—98.5 % mass
- furfuryl resin—1 % mass relative to the reclaimed sand
- acid catalyst—0.5 % mass with respect to the re-claimed sand

The reclaimed material was used, recovered from the casting process from molding sand with furan resin and an appropriate hardener for the particular sample (high-sulfur, low-sulfur and sulfur-free). The following types of hardeners were used:

- high-sulfur hardener, characterized by a content of sulfur—12 % mass
- low-sulfur hardener, characterized by sulfur content of—6 % mass
- sulfur-free hardener—phosphoric acid, characterized by a content of sulfur—0 % mass

In all trials, the use of reclaimed sand of similar quality, characterized by loss on ignition (LOI) value of 1.00–1.10 % mass was sought. As a result, after the preparation of molding sands, the following LOI values were characterized:

- with a high sulfur hardener—2.56 % mass
- with a low sulfur hardener—2.63 % mass,
- molding sand with a sulfur-free hardener—2.69 % mass

Before performing the investigations, the sands were tested by means the sulfur content, the results of which were as follows:

- sulfur content in molding sand with a high sulfur hardener—0.18 % mass
- sulfur content in molding sand with a low sulfur hardener—0.10 % mass
- sulfur content in molding sand with a sulfur free hardener—0.00 % mass

A comparison between the effects of different types of molding sands and coatings shown and described in Fig. 7.9 is presented in Fig. 7.10.

As shown in Fig. 7.10 and also reported by Ivan et al. [15], the application of protecting mold coatings with lime, magnesia or talc is recommended or the substitution of sulfur-containing hardeners with phosphoric acid in molding sand with furan resin may completely eliminate the degenerated graphite layer. Coatings which enabled a desulfurizing reaction with sulfur migrating from the mold, such as CaO or MgO bearing material, eliminate or significant decrease the surface layer thickness and lead to the highest graphite nodularity.

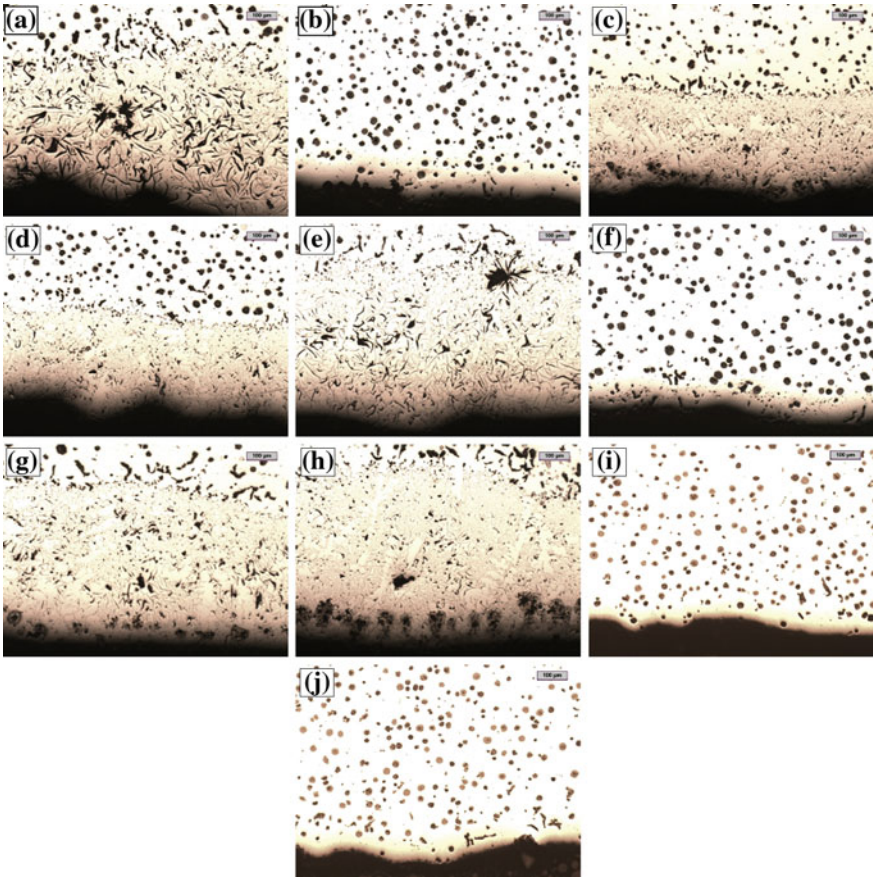

Fig. 7.9 Microstructure of the SGI castings in mold-metal-interface made in the silica sand mold: **a** low-sulfur resin-bonded sand, **b** low-sulfur resin-bonded sand with CaO protection layer, **c** low-sulfur resin-bonded sand with Fe–Si protection layer, **d** low-sulfur resin-bonded sand (helium atmosphere), **e** sulfur resin-bonded sand, **f** sulfur resin-bonded sand with CaO protection layer, **g** sulfur resin-bonded sand with Fe–Si protection layer, **h** sulfur resin-bonded sand (helium atmosphere), **i** sulfur free resin-bonded sand (helium atmosphere), **j** sulfur free resin-bonded sand

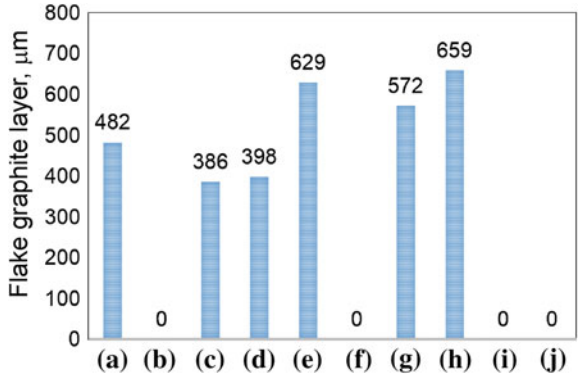

Fig. 7.10 The effect of the type of molding sand and the application of protective coatings on the thickness of the graphite flake layer

The use of sulfur-free hardener resulted in the complete elimination of flake graphite in the surface layer. From Figs. 7.9 and 7.10 we can conclude that the oxygen in the atmosphere does not significantly affect the formation of the said layer, as the use of sulfur-free molding sand eliminated it completely. The use of helium as a shield gas, to eliminate atmospheric oxygen from the surface layer of metal-mold was therefore not necessary in this case, but this factor may play a role in the formation of the degenerated graphite layers in the castings made in the molds made with sulfur-containing molding sand.

The presence of air (oxygen) in the mold cavity can play an important role in the graphite degradation in the case of large molds, poorly deaired and made of molding sand with a low permeability, which makes the process of removing the oxidizing atmosphere from the mold cavity during the pouring of the casting alloy occur too slowly and hence, Mg oxidation may occur.

Dańko et al. [16] reported that the mold production with the use of fresh and reclaimed materials of a higher LOI (meaning of larger amounts of spent binder left on matrix grains) results in the increase of the thickness of the flake graphite layer. During the research, four casts were made in different molding sands (sand 1–sand 4) of characteristics provided in Table 3.2. the average thickness of degenerated nodular graphite and pearlite layers—which are formed from the molding sand side—were estimated on the basis of casting microstructures investigations. The results are presented in Fig. 7.11.

It can be noticed that the thickness of these layers increases when the LOI of the molding sand, out of which the mold was produced, increases. The thickness of these layers is the smallest in the case of the casting produced of fresh molding sands (for which the sulfur and nitrogen content was determined as being 0.09 and 0.07 % mass, respectively, and loss of ignition of = 1.46 % mass). However, in this case, there is also a zone in which the nodular graphite, much desired from the casting point of view, was degenerated. In the case of the casting four microstructure (Fig. 7.10), for which the mold was produced of the molding sand containing 0.24 % mass of sulfur and 0.14 % mass of nitrogen (ignition loss = 4.26 % mass) the maximum thickness of the degenerated graphite layer was nearly 1500 µm.

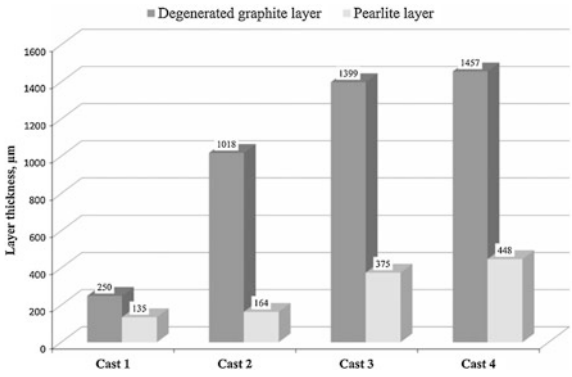

Fig. 7.11 Influence of the molding sand kind of which the mold was produced on the maximum thickness of the degenerated nodular graphite and pearlite layers

Dańko et al. [17] have shown that the LOI of the molding sand after three cycles of the reclamation treatment is nearly three times larger than that of the molding sand prepared on the fresh high silica sand. The matrix also indicates significant increases of ignition losses when the number of cycles increases, which indicates the accumulation of a spent binder—on matrix grains—not removed during the reclamation treatment preceding the molding sand preparation. Multiple reclamation treatments cause the accumulation of sulfur and nitrogen content in molding sands. Sulfur and nitrogen content in molding sands analyzed as a function of their LOI values indicates nearly linear character. Moreover they reported [17] that castings performed in the mold of the fresh molding sand indicate the best surface quality. When the number of the reclamation cycles was increased, the deterioration of casting surfaces occurred.

References

1. Fraś E, Górny M, Lopez HF (2007) Eutectic cell and nodule count in grey and nodular cast irons. Mater Sci Tech 23(9):1109–1117
2. Fraś E, Górny M, Kapturkiewicz W, Lopez HF (2008) Chilling tendency and chill of cast iron. Tsinghua Sci Technol 13(2):177–183
3. Fraś E (2003) Solidification of alloys, WNT, Warszawa
4. Górny M, Dańko R, Holtzer M (2015) The effects of the metal temperature and wall thickness on flake graphite layer in ductile iron. Metalurgija 54(1):11–14
5. Boonmee S (2013) Ductile and compacted graphite iron casting skin—evaluation, effect on fatigue strength and elimination. PhD Dissertation, The Ohio State University (https://etd.ohiolink.edu/!etd.send_file?accession=osu1364310320&disposition=inline)
6. Sergeant GF, Evans ER (1978) The production and properties of compacted graphite irons. Br Foundryman 71:115
7. Marti F, Karsay SI (1979) Localized flake graphite structure as a result of a reaction between molten ductile iron and some components of the mold. AFS Trans 87:221–226
8. Nechtelberger E, Puhr H, van Nesselrode JB, Nakayasu A (1982) Cast iron with vermicular/compacted graphite-state of the art. In: International Foundry Congress, Chicago, pp 1–39
9. Goodrich G, Lobenhofer R (2002) Effect of cooling rate on ductile iron mechanical properties. AFS Trans 110:1003–1032
10. Duncan FC, Kroker J (2010) A new test casting to evaluate skin formation in CGI. AFS Trans 118:10–023
11. Javaid A, Davis KG, Sahoo M (1999) Effect of chemistry and processing variables on the mechanical properties of thin wall ductile iron castings. Materials Technology Laboratory Report MTL
12. Borrajo JM, Martinez RA, Boeri RE, Sikora JA (2002) Shape and count of free graphite particles in thin wall ductile iron castings. ISIJ Int 42(3):257–263
13. Stefanescu DM (2005) Metal handbook, properties and selection: irons, steels and high-performance alloys, vol 1. ASM International, Russell
14. Górny M (2010) Structure formation of ultra-thin wall ductile iron castings. Akapit, Cracow
15. Ivan N, Chisamera M, Riposan I (2012) Mold coatings to reduce graphite degeneration in the surface layer of ductile iron castings. Int J Metal Cast, 61–70
16. Dańko R, Holtzer M, Górny M, Żymankowska-Kumon S (2013) Effect of reclamation on the skin layer of ductile iron cast in furan molds. J Mat Eng Perform 22(11):3592–3600
17. Dańko R, Holtzer M, Górny M, Żymankowska-Kumon S (2014) Effect of the quality of furan moulding sand on the skin layer of ductile iron castings. ISIJ Int 54(6):1288–1293

Chapter 8
Influence of the Metal/Mold Processes on the Casting Mechanical Parameters and Corrosion Resistance

Marcin Górny, Rafał Dańko, Halina Krawiec

Abstract This chapter presents the issue related to the morphology of graphite, namely, flake/compacted/spheroidal graphite that is the main controlling factor of the mechanical and physical properties of cast irons. It is presented that flake graphite in the surface layer can be regarded as a local source of stress concentration and thus the crack growth resistance of the cast iron with flake graphite is extremely poor. It has also been shown that the presence of flake graphite in the surface layer has a significant influence on the mechanical properties of spheroidal graphite cast iron (SGI) and compacted graphite cast iron (CGI), including firstly its plasticity, which decreases with the increasing thickness of the flake graphite layer. Moreover it was shown that the presence of flake graphite makes the surface layer brittle, non-plastic, which results in forming cracks. No flake graphite in the surface layer causes the specimen to deform uniformly, providing the most favorable combination of mechanical properties. Finally, the results of SGI iron corrosion resistance, performed in 0.1 M sodium chloride solution, are shown. It has been indicated that the presence of a thick layer of flake graphite in the surface layer of the castings significantly increases the cathode current, which stimulates the cathodic reaction and oxygen reduction.

8.1 Mechanical Properties of Cast Iron

The morphology of graphite in cast iron, namely, flake/compacted/spheroidal graphite, determines the types of cast irons to be gray iron (FGI), compacted graphite cast iron (CGI), or spheroidal graphite cast iron/ductile iron (SGI). It is the main controlling factor of the mechanical and physical properties of cast irons. Lee and Chang [1] reported that cast iron with compacted/vermicular graphite, as well as with flake graphite fractures in a brittle manner. He also concludes that graphite morphology (i.e., nodular, compacted, or flake) is the most dominant factor in controlling fracture toughness, then matrices and finally temperature. Flake graphite at the metal-mould interface with its sharp edges allows cracks to extend even more

© The Author(s) 2015

M. Holtzer et al., *Microstructure and Properties of Ductile Iron and Compacted Graphite Iron Castings*, SpringerBriefs in Materials,
DOI 10.1007/978-3-319-14583-9_8

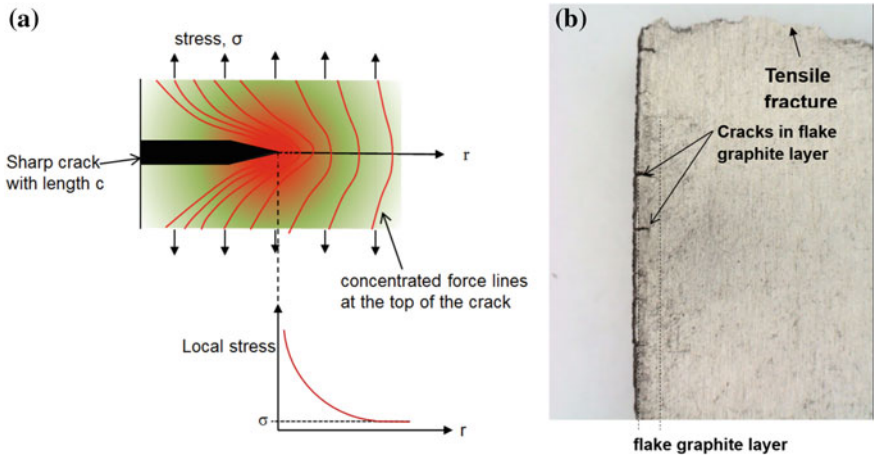

Fig. 8.1 The lines of force of the sample under load and the stress distribution as a function of the distance of the crack [3] (**a**) and the sample back to the static tensile test with cracks in the flake graphite layer in SGI casting (**b**)

easily along the direction of the flake and continue on to connect with other flakes [2]. They can therefore be regarded as a local source of stress concentration (Fig. 8.1).

Thus, the crack growth resistance of cast iron with flake graphite is extremely poor. Compacted graphite is an intermediate structure to that of flake and nodular graphite (Fig. 8.2). Hence, the crack growth resistance also lay between those for FGI and SGI.

The mechanical properties of alloys are generally measured on standard specimens that are machined. In fact number of castings retain its cast surface (without machining). This surface layer has a microstructure different from the bulk. The occurrence of a surface layer containing flake graphite results in its mechanical properties being radically different compared to those determined on samples after machining. In castings, the degenerated surface layer can cause increases in stress in the casting, similar to a notch, so all the useful properties are reduced, especially the

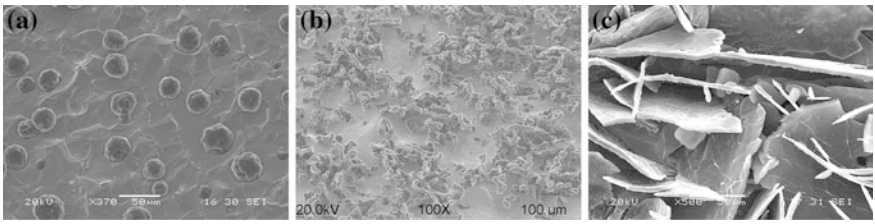

Fig. 8.2 Scanning electron micrographs (SEM) of graphite after deep-etched: **a** in SGI, **b** in CGI and **c** in FGI

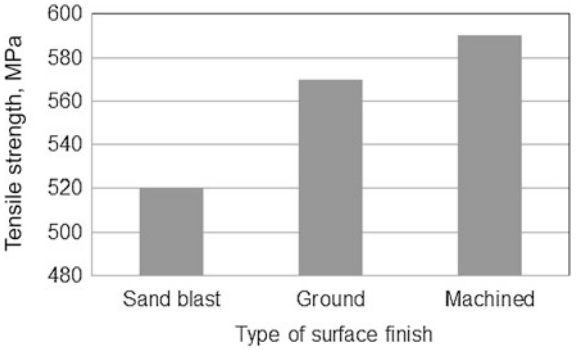

Fig. 8.3 Tensile strength as a function of surface finish [8]

fatigue limit and impact resistance. Goodrich and Lobenhofer [4], Mampaey et al. [5] and Torrance and Stefanescu [6] demonstrated that as the thickness of the casting decreases, the role of the flake graphite layer of the mechanical properties increases. The graphite degradation in the surface layer is most critical for thin wall castings, where it could become more than 10 % of the total section [7]. This also affects castings of thicker walls, due to the long solidification time providing an extended metal-mold interaction time.

Studies [8] showed that the tensile strength (UTS) of samples of thin-walled castings is significantly influenced by the way of finishing of their surface (Fig. 8.3), because the very small cross section of samples greatly enhances the role of surface roughness and the presence of a flake graphite layer, acting as notches.

In the work of Stefanescu et al. [7] and Boonmee and Stefanescu [8, 9] it was shown that fatigue properties are essentially decreased by the presence of a flake graphite layer. In Fig. 8.4, Stress-No of cycles (from a 4-point bending test) for machined and as cast samples for compacted graphite cast iron (CGI) are shown.

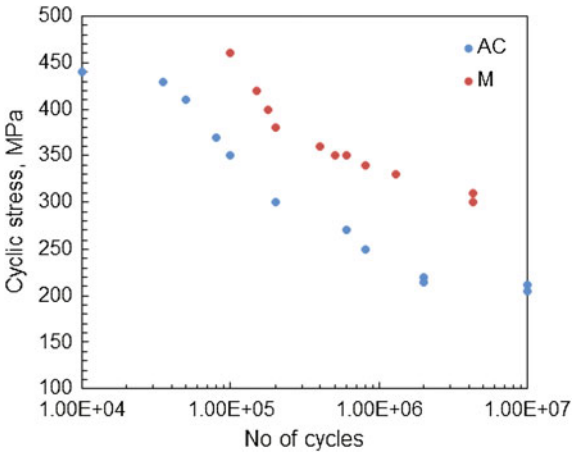

Fig. 8.4 S-N curves of as-cast (*AC*) and machined (*M*) sample for compacted graphite cast iron (σ_m = 250 MPa) [9]

From Fig. 8.4 it is evident that there is an essential difference between fatigue strength obtained in machined and as cast samples. The as cast samples shows a significant reduction in fatigue strength when comparing to those that were machined. Boonmee and Stefanescu [8] reported that the fatigue skin factor (SF) which is defined as the ratio in the as cast fatigue data (σ_{ac}) compared to the machined ones (σ_m) is 0.687 and 0.650 at the mean stress of 250 and 300 MPa, respectively:

$$SF = \frac{\sigma_{ac}}{\sigma_m} \tag{8.1}$$

where

σ_{ac} and σ_m are fatigue limits in as-cast and machined conditions, respectively.

The skin factor takes values ranging from zero to unity. The smaller value indicates the greater effect of the flake graphite layer.

During fatigue stress, cracks are initiated at the casting surface that acts as a stress raiser. A cleavage fracture occurs due to the lack of the ductility at this layer.

The negative effect of the thickness of the flake graphite layer on the mechanical properties is shown in Fig. 8.5.

It was demonstrated [9] that tensile strength and elongation are significantly decreased as the thickness of the flake graphite layer increases. An approximately 15 % reduction in tensile strength is observed [9] for the CGI with 0.4 mm flake graphite layer thickness. Due to the presence of the flake graphite, the average decrease in tensile strength was 9 % (skin factor of 0.91). The average tensile strength decreased from 355 MPa on the machined specimens to 300 MPa on plates with 0.4 mm skin [9]. This gives a skin factor of 0.845 (or 15 % decrease).

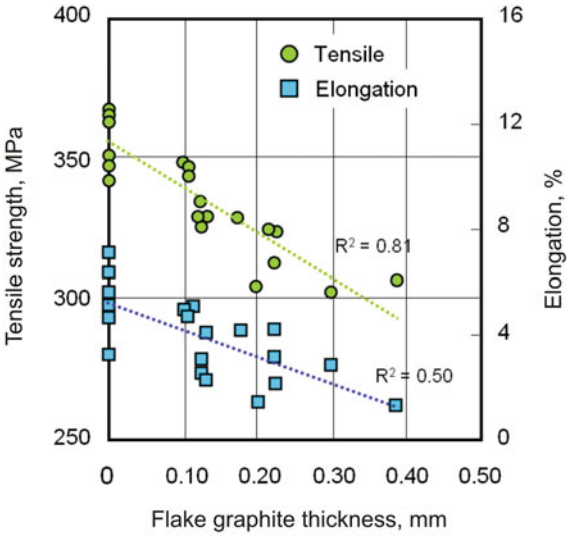

Fig. 8.5 Tensile strength and elongation as a function of the flake graphite layer thickness of CGI [8]

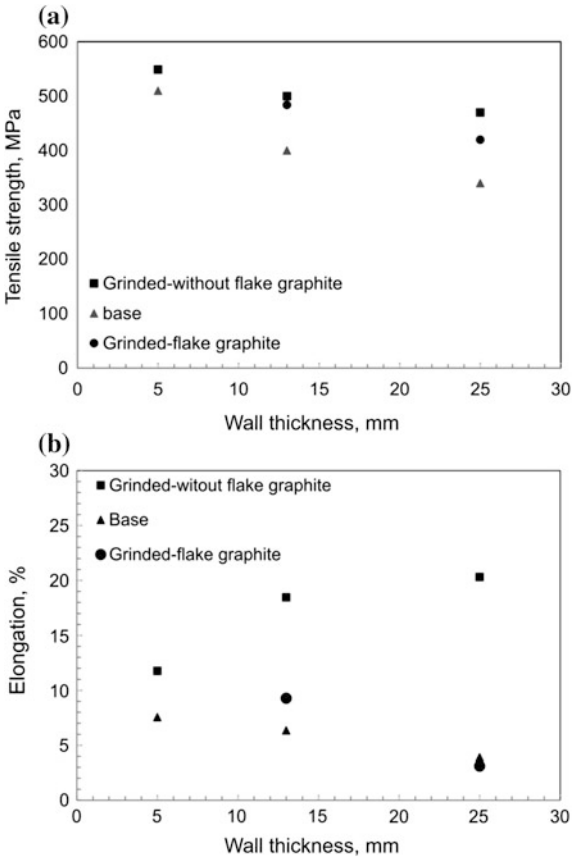

Fig. 8.6 Influence of the thickness of flake graphite layer on mechanical properties: **a** tensile strength (UTS), **b** elongation (A)

Figure 8.6 shows the results of the tensile properties, i.e. tensile strength (UTS) and elongation (A), taking the presence of flake graphite in the surface layer into account. Samples were tested in a polished state containing flake graphite in the surface layer and after its removal, as well as in the initial state, i.e. without machining.

From this figure, it is evident that the presence of flake graphite in the surface layer has a significant effect on the tensile properties, primarily including the plastic properties, which reduce with the increasing thickness of the graphite flake. The occurrence of the flake graphite surface layer makes it brittle, which resulted in a crack, which is shown in Fig. 8.7. The lack of flake graphite in the surface layer results in the sample becoming deformed uniformly, providing the most favorable combination of mechanical properties.

According to studies [8] shot blasting can effectively reduce the impact of flake graphite in the surface layer as shown in Fig. 8.8.

It was reported [9] that the flake graphite layer thickness can be decreased by almost 50 % after 1 min of shot blasting and by 80 % after 5 min of shot blasting

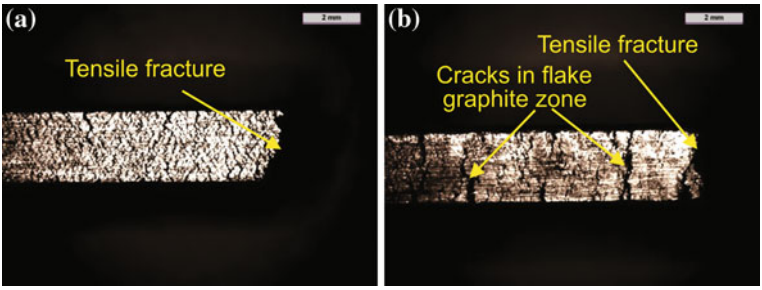

Fig. 8.7 The end face view of the sample after the static tensile test: **a** without the occurrence of flake graphite in the surface layer, **b** with the occurrence of flake graphite in the surface layer in SGI castings

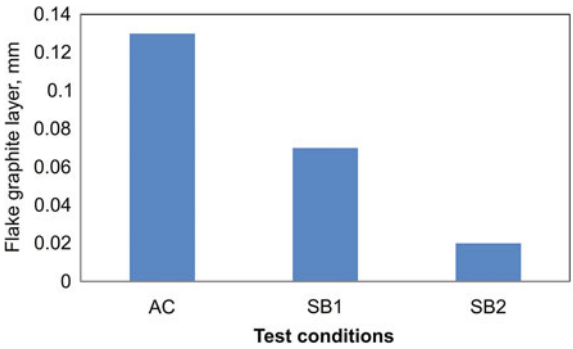

Fig. 8.8 Effect of shot blasting on visual flake graphite layer thickness; *AC* as-cast; *SB1* shot blasted after 1 min; *SB2* shot blasted after 5 min) [8]

(Fig. 8.8). The reduction in the flake graphite layer thickness resulted in both improved tensile strength and elongation as previously mentioned (Fig. 8.6).

The comparison of the color micrographs of the structure near the sample surface before and after shot blasting is shown in Fig. 8.9.

As reported by Boonmee et al. [10] shot blasting can be used to effectively reduce the negative impact on the casting flake graphite layer on the mechanical properties. The improvement of the tensile strength and fatigue limit was due to the generation of a compressive stress field on the sample surface and the partial removal of the casting flake graphite layer (Fig. 8.9b).

8.2 Corrosion Resistance of Cast Iron

The microstructures of the SGI samples, containing flake graphite in the surface layer with a thickness of 120 µm (sample A) and 700 µm (sample C) are shown in Fig. 8.10. A reference sample having the same chemical composition, however did

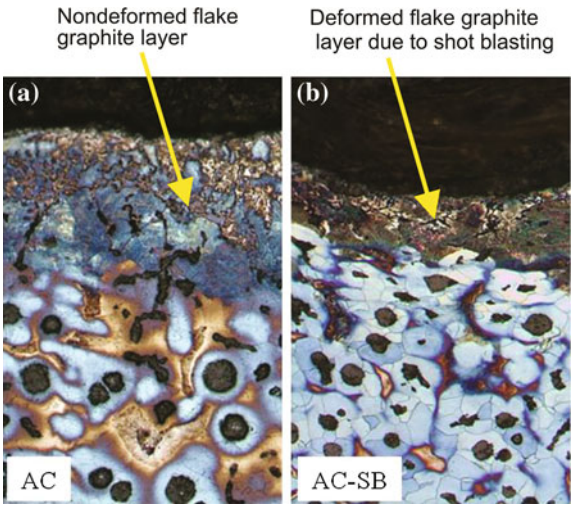

Fig. 8.9 Color micrographs of the casting skin before and after shot blasting; *AC* as-cast, *AC-SB* as-cast-shot-blasted: for 15 % nodularity CG iron [9]

not have the layer of flake graphite (sample B). In addition, samples A and B were tested after grinding marking them as A_g and B_g. In the case of both specimens, flake graphite was completely removed from the surface layer.

In order to determine the corrosion resistance of the tested alloys, corrosion potential measurements and potentiodynamic polarization curves in an aqueous solution of sodium chloride were carried out. Potentiodynamic curves were performed by means of the linear sweep voltammetry technique. The polarization curves were plotted from a cathodic potential of −1.0 V to anodic direction at a potential scan rate 1 mV s^{-1}. Electrochemical measurements were performed in the classical three-electrode system, where the working electrode was a studied sample (cast iron), the counter electrode is a platinum grid, and the silver-silver chloride electrode was used as a reference electrode Ag/AgCl (3 M KCl). Electrochemical measurements were performed by means of an AUTOLAB PGStat 302 N potentiostat.

Figure 8.11 shows changes in the corrosion potential of cast iron in an aqueous sodium chloride solution. As it can be seen, the corrosion potential for all the specimens reached a stable value after a period of about 3 h. Corrosion potential values for samples numbered A_g and B_g without skin were similar and were around −700 mV versus Ag/AgCl (black and gray dotted curves, Fig. 8.11). Much higher corrosion potentials were recorded for samples A and B, which consist of the skin. Corrosion potential of the samples with the skin after 10 h of exposure in the sodium chloride solution was respectively: −600 mV for sample A (gray curve, Fig. 8.11), and −610 mV for the sample B (black dotted line). This result clearly indicates that the form of graphite has a significant influence on the corrosion behavior of cast iron in a sodium chloride aqueous solution.

Polarization curves, Fig. 8.12 also confirms that the presence of the skin has an effect on the electrochemical behavior of cast iron. Cast iron samples with the skin

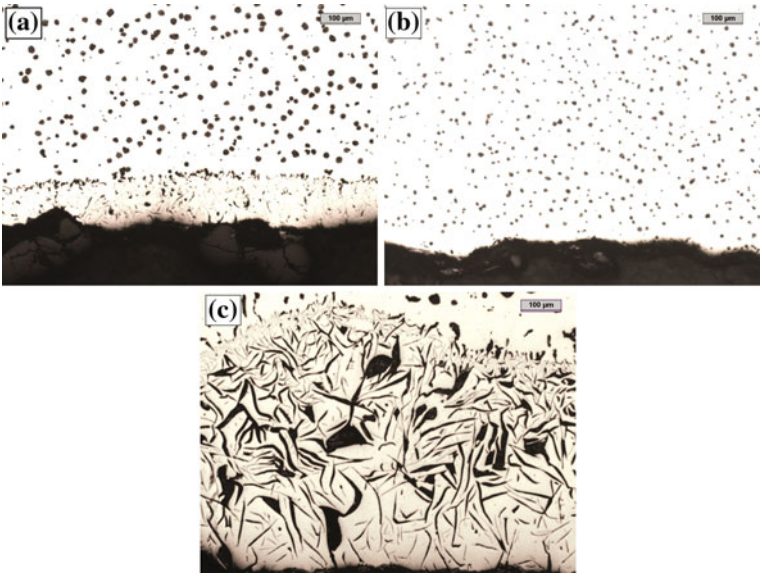

Fig. 8.10 Cast microstructure in the surface layer: **a** sample A, **b** sample B and **c** sample C

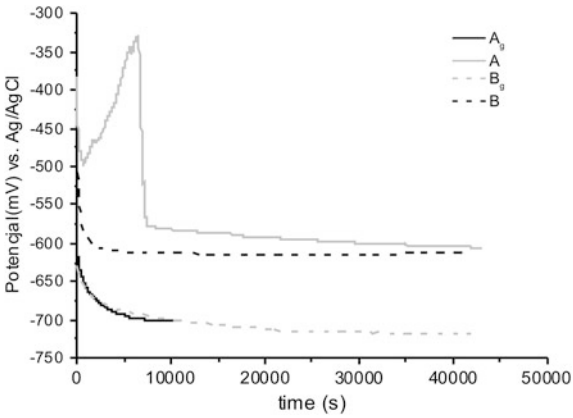

Fig. 8.11 Evolution of the corrosion potential versus time of cast iron in 0.1 M sodium chloride solution

showed a significantly higher current density in the cathodic domain (curves gray and black dotted, Fig. 8.12) than the sample without the skin (A_g and B_g). Furthermore, two stages in the anodic domain are observed on the polarization curves plotted on cast iron specimens with the skin as shown in Fig. 8.12 (A and B, Fig. 8.12):

Stage I—a clear current plateau was observed in the potentials range of about −800 to −550 mV, wherein the anodic current density is about 100 μA/cm^2. In this range of potentials cast iron samples with the skin were passived.

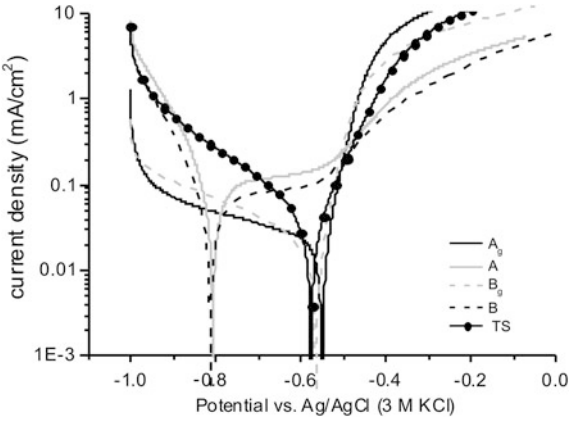

Fig. 8.12 Potentiodynamic polarization curves of cast iron plotted in 0.1 M NaCl solution with a potential scan rate of 1 mV/s

Stage II—potential greater than −550 mV a gradual increase in the anodic current density was observed, however the current density is much lower compared to the cast iron samples without skin.

Polarization curves obtained for the specimens of cast iron without skin, i.e. A_g and B_g (black and gray dotted curves, Fig. 8.12), indicate a very active behavior of the alloy in the sodium chloride solution. After reaching the steady state potential, a sharp increase in the anodic current density is observed (black and gray dotted curves, Fig. 8.12). Corrosion tests clearly show that the skin has a significant effect on the corrosion resistance of cast iron in a sodium chloride aqueous solution. Cast iron having a relatively small skin thickness of 120 μm (non-ground) exhibits better corrosion resistance than cast iron sample from which the skin has been removed. There is no significant difference in corrosion resistance between samples labeled A and B, both with skin and without it. The presence of a very thick skin—sample C (black curve with black circle, Fig. 8.12) with flake graphite (flake graphite layer thickness ≈700 μm) exhibits a corrosion resistance similar to a polished surface (sample A_g and B_g). The thick skin contains a lot of defects (cracks, holes), hence it does not protect ductile iron against corrosion as well as thin skin.

It is well know that the cast irons are prone to graphitic corrosion. It is selective leaching of iron from gray cast iron, which takes place because graphite is cathodic to iron, and gray iron's structure develops a galvanic cell. Hence, iron is dissolved and graphite grains remain intact. Ductile cast iron is less prone to graphitic corrosion than gray iron. Previous studies have revealed that the corrosion of ductile iron starts at the graphite/matrix interfaces and around oxide inclusions [11, 12]. The results presented above show that the skin containing flake graphite enhance the corrosion resistance of cast iron in the sodium chloride solution. First the surface layer undergoes corrosion, then the corrosion of cast iron with graphite spheres begins.

References

1. Lee S, Chang YB (1991) Fracture toughness and crack growth rate of ferritic and pearlitic compacted graphite cast irons at 25 °C and 150 °C. Metall Trans A 22A:2645–2653
2. Voigt RC, Eldoky LM, Chiou HS (1986) Fracture of ductile cast irons with dual matrix structure. AFS Trans 94:645–656
3. Asby M, Shercliff H, Ceboc C (2009) Materials engineering, science, processing and design. 2nd edn. Elsevier Ltd, New York
4. Goodrich GM, Lobenhofer RW (2002) Effect of cooling rate on pearlitic ductile iron mechanical properties. AFS Trans 110:1003–1032
5. Mampaey F, Li P, Wettinck E (2003) Variation of grey iron strength along the casting diameter. AFS Trans 111:03–056
6. Torrance JW, Stefanescu DM (2004) Investigation on the effect of surface roughness on the static mechanical properties of thin-wall ductile iron castings. AFS Trans 112:757–772
7. Stefanescu DM, Wills S, Massone J, Duncan F (2008) Quantification of casting skin in ductile and compacted graphite irons and its effect on tensile properties. Int J Metalcast 2(4):7–26
8. Boonmee S, Stefanescu DM (2011) The mechanism of formation of casting skin in CG iron and its effect, on tensile properties. Key Eng Mater 457:11–16
9. Boonmee S, Stefanescu DM (2014) The occurrence and the effect of casting skin in compacted graphite iron. In: Proceedings of 10th international symposium on the science and processing of cast iron—SPCI10, Mar del Plata, Argentina, paper no. 03
10. Boonmee S, Moran MK, Stefanescu DM (2011) On the effect of the casting skin on the fatigue properties of CG iron. AFS Trans 119:421–430
11. Krawiec H, Lelito J, Tyrała E, Banaś J (2009) Relationships between microstructure and pitting corrosion of ADI in sodium chloride solution. J Solid State Electrochem 13:935–942
12. Krawiec H, Vignal V, Banaś J (2006) Macroscopic and local electrochemical studies of austempered ductile iron in perchlorate solutions. J Electrochem Soc 153:B231–B237

Chapter 9
Phenomena Model on the Mold/Casting Interface

Mariusz Holtzer, Marcin Górny, Rafał Dańko

Abstract Good quality casting that meets the customer's requirements depends on many factors. Generally, these can be classified into two groups, related to metal and the casting mold. However, it may happen that the metal meets all the criteria and the mold is properly made but the quality of the casting can be unsatisfactory. The reason for this may be the phenomena on the interface mold/casting, which are not always taken into account. Processes taking place there are mainly due to the quality of the casting surface, which is very important; especially in the case of castings whose surface is exposed directly to adverse factors (wet corrosion, dry corrosion, wear, etc.). However, processes taking place on the interface mold/casting may also adversely affect the mechanical properties of the casting, e.g., tensile strength, fatigue limits, machinability. This is caused by the degeneration of nodular and compacted/vermicular graphite, or decarburization of the casting surface layer, or the appearance of areas of pearlitic/ferritic rim. Several mechanisms are responsible for the formation of abnormal surface layer on the CGI and SGI castings, which are associated with a reduction in the concentration of either Mg (reaction with S and/or O) or the cooling rate of the casting (formation of austenite layer).

In the process of casting in a sand mold at the mold/metal interface, after pouring the liquid metal until the shake-out of the mold, various physicochemical processes undergo, which may affect the structure of the casting surface layer, the chemical composition of an alloy, the useful properties of casting, the quality of the skin of raw casting. It is important that a casting meet the requirements from the user point of view. Therefore, any changes in that time, which may adversely affect the properties of the casting are undesirable. A special role is played here by the phenomena on the two phases of the mold/metal interface (both in the liquid state and after solidification). It is therefore important to choose the right matrix, bonding material, coating and the proper design of the casting. In many cases, this allows adverse processes occurring at the mold/metal interface to be prevented. However, this is not always technically possible, or we are not always aware of the phenomena taking place there and their influence on the properties of the cast [e.g. 1–4].

© The Author(s) 2015

M. Holtzer et al., *Microstructure and Properties of Ductile Iron and Compacted Graphite Iron Castings*, SpringerBriefs in Materials,
DOI 10.1007/978-3-319-14583-9_9

An example of this may be the processes occurring in the surface layer of SGI or CGI castings performed in the molds from molding sand, which contain sulfur components (such as furan resin hardened with compounds containing sulfur). As shown by numerous studies in this field, carried out mainly by Stefanescu et al. and Riposan et al. [e.g. 5–11], we are dealing with the formation of the surface layer, in which degeneration of nodular or compacted graphite to the flake graphite form occurs. In addition, the surface layer of castings from CGI and SGI—graphite depletion phenomenon may occur, and there may be areas of pearlitic/ferritic rim. This abnormal surface layer may be present in any casting section thickness. However, it becomes most critical for thin wall castings, where it can easily be more than 10 % of the total thickness, but is also a concern in heavy castings due to prolonged solidification time (long time of mold/casting exposure). The surface layer with degenerated graphite reduces many properties (see Chap. 8). It is responsible for the reduction of the tensile strength and fatigue limits of CGI and SGI. This is due to the surface roughness and graphite degradation layer. The surface roughness induces notch effects for crack initiation and tensile instability. The graphite degradation layer can be viewed as a layer of flake graphite which favors crack propagation. The ferritic rim decreases the abrasion resistance, while the pearlitic rim can decrease machinability.

The CGI is more susceptible to the casting skin effect than grey cast iron (FGI) and SGI. This is because CGI has relatively low Mg content that makes it more susceptible to Mg depletion. SGI has a higher magnesium level and a typically thinner graphite degradation layer. In FGI, there is only a small difference between the graphite degradation layer and the bulk structure, as graphite is flake, both at the surface and in the bulk.

Several mechanisms may be responsible for the formation of abnormal skin castings from CGI and SGI. The scheme of the formation of casting skin is shown in Fig. 9.1.

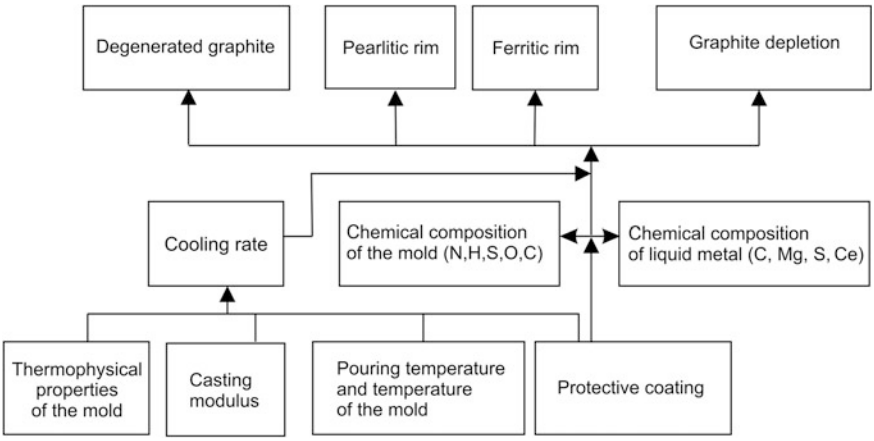

Fig. 9.1 Scheme of mold-metal interaction for the casting skin formation mechanism

Mg reacts with oxygen and/or sulfur, which reduces the concentration of magnesium in the surface layer of the casting, and consequently the degeneration of graphite. High undercooling on the mold/casting interface promotes crystallization of austenite dendrites, which results in the magnesium reject at the solidification front. Thus, areas with low Mg content and flake graphite structure are adjacent to the mold/casting interface. Mg depletion and solidification kinetics effects are suggested as the main formation mechanisms for graphite degradation [12–15].

It can be concluded that in order to minimize the formation of a surface layer with a degenerate form of graphite on the CGI and SGI castings, the possibility of Mg oxidation and the degree of undercooling on the mold/metal interface should be reduced.

Stefanescu et al. [8, 9] proposed two mechanisms leading to the degeneration of graphite in the skin of SGI and CGI casting, which are based on the assumption that the cause of this phenomenon is the reduction of the Mg concentration in the surface layer of the casting. The Mg depletion of this layer may occur as a result of two processes:

- the reaction of magnesium with sulfur and oxygen

  or

- increase in the primary austenite fraction, which depends on the crystallization kinetics of the alloy.

Two models were developed to clarify the mechanism associated with the oxidation of magnesium: 1D diffusion model [8], and thermal-diffusion model 2D [6, 9]. The 2D model well explained the experimental results obtained in this connection, among others, allowed to predict the thickness of the surface layer formed by Mg oxidation, although it did not take the influence of the kinetics of crystallization of the casting into account.

The increase of the primary austenite fraction on the mold/casting interface may be the result of undercooling and/or reduction of the eutectic carbon equivalent (CE). The use of further protective coating to the molds and cores (particularly with high thermal conductivity) will lead to an increase in undercooling, which increase the thickness of the surface layer of the casting and the chilling tendency. The use of such active protective coating, e.g. FeSi, due to its effect modifiers, reduces the undercooling and thus creates a smaller fraction of primary austenite, and consequently forms a thinner flake graphite layer.

Figure 9.2 shows a diagram [9] to clarify the scope of the mechanism of the action leading to the Mg depletion of the areas on the mold/metal interface, and thus the formation of flake graphite in the casting layer.

In general, it can be stated that the thicker sections in the casting produce larger thickness of the flake graphite layer. This is due to the longer solidification time that extends the reaction time for magnesium depletion. Therefore, Mg depletion is the predominated mechanism for the thicker sections. In general, the skin formation is controlled by Mg depletion at a low cooling rate, and by the austenite layer formation at the mold/metal interface at a high cooling rate.

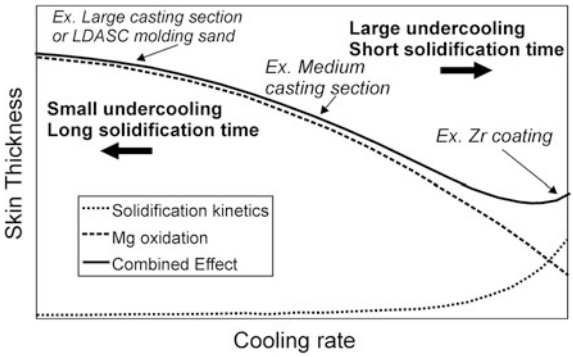

Fig. 9.2 Schematic diagram of the combined effect between two skin formation mechanisms (LDASC-low-density alumina-silicate ceramic) [9]

An important question remains: which of the surface-active elements—sulfur or oxygen—contribute more to the Mg depletion of the mold/metal interface.

As demonstrated by thermodynamic calculations made by the authors (see Chap. 1)—the reaction of magnesium with oxygen ($\Delta G_{1723\ MgO} = -315$ kJ) relative to the reaction of magnesium with sulfur ($\Delta G_{1723\ MgS} = -218$ kJ) is the more thermodynamically favored (has a higher affinity for oxygen than sulfur). Due to the greater affinity of magnesium to oxygen than sulfur, after the introduction of Mg to the molten iron oxides are formed first, and then sulfides.

However, apart from the thermodynamic condition which are the values of the Gibbs energy of MgO and MgS creation ($\Delta G_{1723\ MgO} < (\Delta G_{1723\ MgS})$ the kinetic parameter to have full information as to the course of the process, which may decide about the whole process (its effectiveness) must still be taken into account.

To demonstrate the validity of the above thermodynamic calculation the authors carried out a series of experiments varying the gas atmosphere in the mold cavity (oxygen, helium), different catalysts (in terms of sulfur content) to harden the molding sand with furan resin and the molding sand matrix with reclaimed sand (the impact of sulfur accumulation in the molding sand in the subsequent cycles of production) [16–20].

The use of a sulfur-free catalyst resulted in the complete elimination of flake graphite in the surface layer of the casting, even when the atmosphere in the mold contained oxygen. In contrast, a thick casting skin with flake graphite was obtained using an inert atmosphere (such as helium) in a mold cavity, through the use of a catalyst containing sulfur to harden the furfuryl resin (see Chap. 7). From the results it can be concluded that the magnesium reaction with sulfur plays a decisive role in the formation of CGI and SGI castings skin with flake graphite. Therefore, special attention should be paid to the possibility of the accumulation of sulfur in the molding sand subjected to the mechanical reclaiming process. It can be noticed that the thickness of the flake graphite layer increases when the LOI of molding sand increases. In the case of the casting produced of fresh molding sands (LOI = 1.46 % mass) the thickness of this layer is 250 μm. In the case of the casting for which the mold was produced of reclaimer after three cycles of reclamation (LOI = 4.26 % mass), the maximum thickness of the degenerated graphite layer was nearly

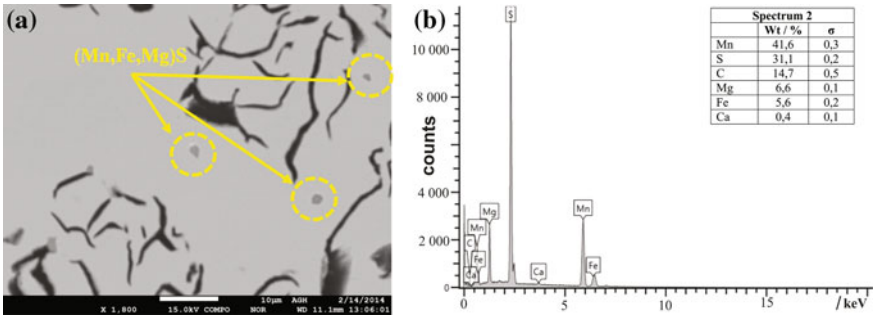

Fig. 9.3 SEM microstructure (**a**) and EDS spectrum (**b**) of complex sulfides (Mn, Fe, Mg)S [17]

1500 μm. The presence of air (oxygen) in the mold cavity can play an important role in the degradation of the graphite in the case of a large mold, slightly vented and made of low permeability molding sand, which makes the process of removing the oxidizing atmosphere of the mold cavity during the pouring of the casting alloy to be slow and Mg oxidation may appear, also with the oxygen from the air.

The research of casting microstructures in molds made of molding sand with different sulfur contents conducted by the authors is a confirmation of the decisive role of sulfur in the flake graphite formation process in the surface layer of SGI or CGI castings, through a reaction with Mg, [20]. The EDS (Energy-dispersive X-ray spectroscopy) analysis made for casting (for LOI = 3.86 % mass) shows that this occurs through the interaction of sulfur with magnesium, and also with, among others, manganese and iron through the creation of complex sulfides in the surface layer. EDS studies indicate that the number of such sulfides decreases as the distance from the casting surface increases. This decrease depends on the diffusion of sulfur from the molding sand into metal (Fig. 9.3).

WDS (Wavelength-dispersive X-ray spectroscopy) analyses were also made for this sample. As a result, sample maps, by means of WDS analysis of magnesium, sulfur and oxygen concentrations in different positions (from mold/metal interface to center) as well as the microstructure at a given position, are presented in Fig. 9.4. It can be stated that the concentration of measured elements decreases with the increasing distance from the metal-mold boundary.

WDS mapping analyses confirms the creation of complex sulfides of (Mn, Fe, Mg)S type. The number of these sulfides decreases with the growing distance from the metal-mold contact boundary. Moreover WDS mapping shows an increased level of oxygen in the vicinity of flake graphite particles. A sharp drop in the number of sulfides and oxygen concentration exists at the boundary of flake to nodular graphite transition zone. In summary, it can be stated that the higher the concentration of sulfur in the molding sand, the higher the thickness of the flake graphite layer in the casting surface.

The research [12] showed that the thickness of the flake graphite layer depends on the initial temperature of the metal in the mold cavity and on the contact time of the mold with the liquid metal. In the case of casting a wall thickness of 3 mm, flake

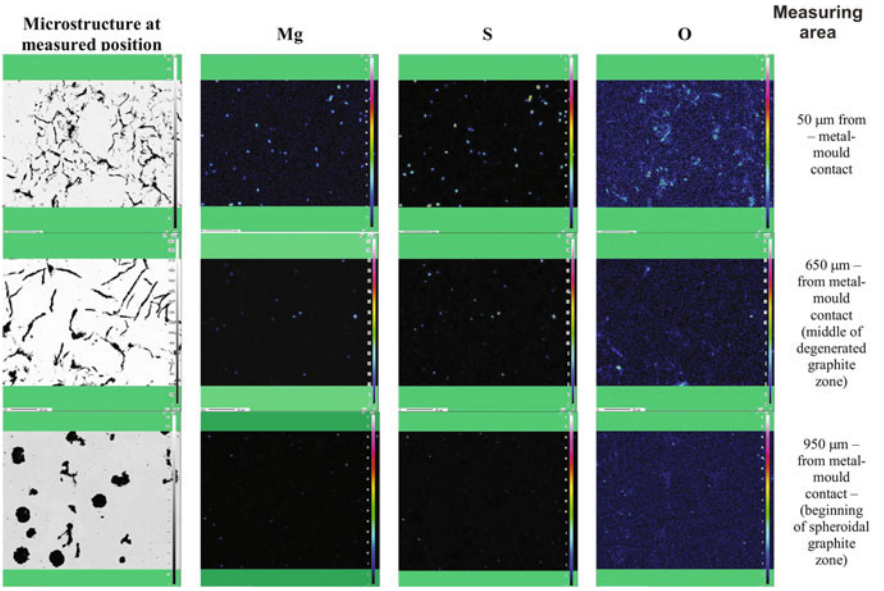

Fig. 9.4 Results of the WDS mapping analysis [20]

graphite in the surface layer does rise up to a distance of 40 cm. This corresponds to the minimal initial temperature of the metal in the mold of 1206 °C and the minimum contact time of about 3.5 s of the liquid metal with a mold. In the case of casting with a wall thickness of 8 mm, flake graphite in the surface layer does rise up to a distance of 90 cm. This corresponds to the minimal initial temperature of 1203 °C and the minimum contact time of about 9 s of the liquid metal with a mold. It is worth noting that the above-mentioned temperatures, for which there is a disappearance of flake graphite in a surface layer for casting with different wall thicknesses, are similar.

Wide studies have shown that the formation of flake graphite layer results in a clear deterioration of the mechanical properties of castings, such as: fatigue limit, tensile strength, elongation (see Chap. 8) [e.g. 7, 8, 11, 15, 21]. It should be noted that the castings with the casting skin may also have much worse properties, those in which the decisive role is played by the quality of the surface, e.g. resistance to corrosion. Corrosion resistance test in a NaCl solution showed that the form of graphite in the surface layer has a significant influence on the corrosion behavior of cast iron in a sodium chloride aqueous solution. Cast iron of a relatively small skin thickness of 120 µm (non-ground) exhibits better corrosion resistance than a cast iron sample from which the skin has been removed.

Shot blasting can be used to effectively reduce the negative impact on the casting skin on mechanical properties. The improvement of tensile strength and fatigue limit was due to the generation of a compressive stress field on the sample surface and the partially removal of the casting skin [9].

The use of appropriate protective coatings on the mold is one of the possible solutions to prevent degradation of the graphite surface layer in the cast. The protective coating minimizes mold/metal interaction by being a protective layer and providing a desulfurizing effect [5, 19, 20]. The application of a mold coating can significantly reduce the thickness, or even prevent the formation of the surface layer. If the coatings employed desulfurization materials, such as MgO, the following mixture (CaO + MgO + Talc) or Mg-bearing FeSi, they acted to remove any S-released by the mold media (such as furan resin and phenolic urethane bonded sands) and they protect the graphite shape, improving graphite nodularity, at the metal/mold interfaces. MgO and CaO will behave as inactive coatings when there is no sulfur in the binder. The best results, for both lowering the surface layer thickness and increasing the graphite nodularity in the casting center were obtained when coatings incorporated active Mg, either as a fine size FeSiCaMgRE alloy or as a mechanical mixture of Mg in a fine size FeSi75 alloy [6, 19]. Oxide type coating (MgO or MgO + CaO + Talc) acted mainly to neutralize sulfur migration from mold in a desulfurizing reaction, whereas the Mg–Fe–Si coatings performed a complementary role beyond desulfurization with supplementary magnesium regenerating the nodularizing potential prior to solidification.

References

1. Svoboda JM (1994) Mechanisms of metal penetration in foundry molds. AFS Trans. 102:461–473
2. Hayes KD et al (1998) Mechanical penetration of liquid steel in sand molds. AFS Trans 106:769–776
3. Lane AM et al (2001) Penetration of liquid steel in sand molds, part II: Chemical reactions at the mold/metal interface during casting of steel. AFS Transa. 109:1327–1345
4. Stefanescu DM el al (1996) Cast iron penetration in sand molds. Part I: Physics of penetration defects and penetration model. AFS Trans 104:1233–1248
5. Boonmee S, Stefanescu DM (2013) Casting skin management in compacted graphite iron. Part I: Effect of mold coating and section thickness. AFS Trans 121:435–448
6. Boonmee S (2013) Ductile and compacted graphite iron casting skin—evaluation, effect on fatigue strength and elimination. PhD Dissertation, The Ohio State University. https://etd.ohiolink.edu/!etd.send_file?accession=osu1364310320&disposition=inline
7. Stefanescu DM (2008) The effect of mould/metal interface phenomena on the surface quality of casting. 10th Asian Foundry Congress (AFC10), Nagoya, Japan, pp 21–24
8. Stefanescu DM, Wills S, Massone J, Duncan F (2008) Quantification of casting skin in ductile and compacted graphite irons and its effect on tensile properties. Int J Metalcast 2(4):7–26
9. Boonmee S, Stefanescu DM (2013) Casting skin management in compacted graphite iron. Part II: Mechanism of casting skin formation. AFS Trans 121:449–459
10. Boonmee S, Stefanescu DM (2014) The occurrence and the effect of casting skin in compacted graphite iron. In: Preceedings of 10th international symposium on the science and processing of cast iron—SPCI10, Mar del Plata, Argentina, paper No. 03
11. Boonmee S, Moran MK, Stefanescu DM (2011) On the effect of the casting skin on the fatigue properties of CG iron. AFS Trans 119:421–430

12. Górny M, Dańko R, Holtzer M (2015) The effects of the metal temperature and wall thickness on flake graphite layer in ductile iron. Metalurgija 54(1):11–14
13. Ruff GF, Doshi BK (1980) Relation between mechanical properties and graphite structure in cast irons, part I-gray iron. Modern Casting, pp 50–55
14. Javaid A, Thompson J, Davis KG, Sahoo M (2001) Effect of microstructure on the mechanical properties thin-wall ductile iron castings. AFS Trans 109:1097–1114
15. Goodrich GM, Lobenhofer RW (2002) Effect of cooling rate on pearlitic ductile iron mechanical properties. AFS Trans 110:1003–1032
16. Riposan I, Chisamera M, Stan S, Skaland T (2006) Factors influencing the surface graphite degeneration in ductile iron castings in resin mold technology. In: Proceedings of the 8th international symposium on science and processing of cast iron, Beijing, China
17. Dańko R, Holtzer M, Górny M, Żymankowska-Kumon S (2014) Effect of the quality of furan moulding sand on the skin layer of ductile iron castings. ISIJ Int 54(6):1288–1293
18. Dańko R, Holtzer M, Górny M, Żymankowska-Kumon S (2013) Effect of reclamation on the skin layer of ductile iron cast in furan molds. J Mat Eng Perform 22(11):3592–3600
19. Chrismera M. et al. (2014) Iron casting skin management in no-bake mould-effects of magnesium residual level and mould coating. In: 71th World Foundry Congress, Bilbao, pp 19–21
20. Holtzer M, Dańko R, Górny M (2014) Influence of the furfuryl moulding sand on the flake graphite formation in the surface layer of ductile iron castings. In: Preceedings of 10th international symposium on the science and processing of cast iron—SPCI10, Mar del Plata, Argentina, paper No. 41
21. Boonmee S, Stefanescu DM (2011) The mechanism of formation of casting skin in CG iron. Key Eng Mater 437:11–16

Index

© The Author(s) 2015
M. Holtzer et al., *Microstructure and Properties of Ductile Iron and Compacted Graphite Iron Castings*, SpringerBriefs in Materials,
DOI 10.1007/978-3-319-14583-9